AD

PARTICLE DYNAMICS AND GRAVEL-BED ADJUSTMENTS

Final Technical Report

by

Carling, PA, Williams, JJ, Glaister, MG, and Orr, HG

May 1993

United States Army

EUROPEAN RESEARCH OFFICE OF THE U.S. ARMY

London England

Contract Number DAJA45-90-C-0006

Freshwater Biological Association

DISCLAIMER NOTICE

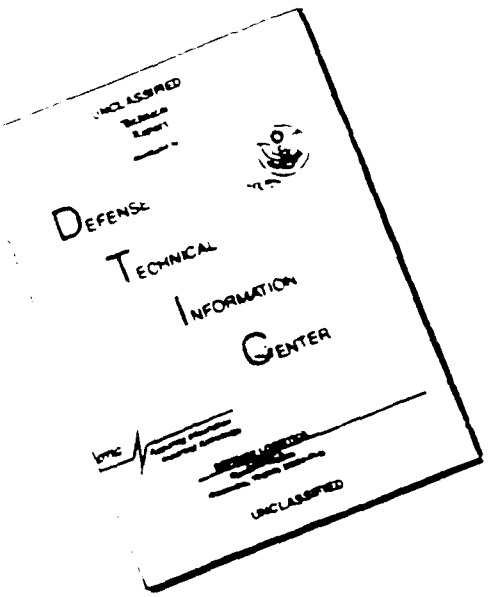

THIS DOCUMENT IS BEST QUALITY AVAILABLE. THE COPY FURNISHED TO DTIC CONTAINED A SIGNIFICANT NUMBER OF PAGES WHICH DO NOT REPRODUCE LEGIBLY.

REPORT DOCUMENTATION PAGE

Form Approved
OMB No. 0704-0188

1. AGENCY USE ONLY (Leave blank)	2. REPORT DATE	3. REPORT TYPE AND DATES COVERED
	MAY 1993	FINAL

4. TITLE AND SUBTITLE
PARTICLE DYNAMICS AND GRAVEL-BED ADJUSTMENTS

5. FUNDING NUMBERS

6. AUTHOR(S)
CARLING, P.A., WILLIAMS, J.J., GLAISTER, M.S. & ORR, H.G.

7. PERFORMING ORGANIZATION NAME(S) AND ADDRESS(ES)
FRESHWATER BIOLOGICAL ASSOCIATION
FERRY HOUSE, FAR SAWREY,
AMBLESIDE, CUMBRIA LA22 OLP

8. PERFORMING ORGANIZATION REPORT NUMBER
N/A

9. SPONSORING/MONITORING AGENCY NAME(S) AND ADDRESS(ES)
EUROPEAN RESEARCH OFFICE OF THE US ARMY
223-231 OLD MARYLEBONE ROAD
LONDON NW1 5TH, UK

10. SPONSORING/MONITORING AGENCY REPORT NUMBER

11. SUPPLEMENTARY NOTES

12a. DISTRIBUTION/AVAILABILITY STATEMENT

12b. DISTRIBUTION CODE

13. ABSTRACT *(Maximum 200 words)*

The purpose of the study was to further understanding of unsteady transport of coarse bedload. A particular focus was the interaction of the load with the river bed material and the effects of transport on stream hydraulics. It was anticipated that new methodology would be developed and that data sets suitable for further modelling would result. The nature of coarse gravel transport through a short reach of a mountain river was examined using novel methodology; primarily, magnetic particle detection; acoustic bedload detection, electromagnetic current meters and fine-resolution bed elevation surveys.

14. SUBJECT TERMS	15. NUMBER OF PAGES
	16. PRICE CODE

17. SECURITY CLASSIFICATION OF REPORT	18. SECURITY CLASSIFICATION OF THIS PAGE	19. SECURITY CLASSIFICATION OF ABSTRACT	20. LIMITATION OF ABSTRACT

DAJA45-90-C-0006
FINAL REPORT

ABSTRACT

The purpose of the study was to further understanding of unsteady transport of coarse bedload. A particular focus was the interaction of the load with the river bed material and the effects of transport on stream hydraulics. It was anticipated that new methodology would be developed and that data sets suitable for further modelling would result. The nature of coarse gravel transport through a short reach of a mountain river was examined using novel methodology; primarily, magnetic particle detection, acoustic bedload detection, electromagnetic current meters and fine-resolution bed elevation surveys.

For a wide range of flows, up to and including bankfull, the surface of an alternate bar and the neighbouring talweg channel remained essentially stable. At a critical in-bank discharge, bed sediment was transported from sources upstream through the study reach as a discrete slug of bedload. The interaction of this mobile 'sheet' with the coarse bed sediments led to selective deposition of fine bedload into the interstices of the static armour. This mechanism caused physical smoothing of the bed and concomitant reduction in hydraulic roughness during the passage of the sheet. Consequent energy slope adjustment caused water depths to drop and velocities to increase, leading to local readjustments in shear stress and streampower. As the tail of the sheet passed, the fine particles were reentrained from the armour; the bed roughened and hydraulic parameters adjusted again.

It is concluded that although exceeding an hydraulic threshold is required to initialize bedload transport, there are important mutual feedback mechanisms whereby the interactions of the mobile sediment and the bed, lead to further adjustment in the hydraulic climate which then further affect bedload transport.

KEYWORDS

Bedload Transport, Gravel Sheets, Gravel-Bar, Erosion, Unsteady-flow, Hydraulics, Velocity Profile, Turbulence, Shear Stress, Streampower, Initial Motion, Particle Entrainment, Bed-Roughness, Mountain Rivers, Montana.

Contents List

(contents continued overleaf)

List of Figures and Tables

INTRODUCTION

The process of bedload transport in gravel-bed streams is of practical interest to engineers and attracts considerable theoretical and empirical attention. One important focus has been the nature of particle interactions with the bed at the temporal-scale of turbulence measurements. At a larger scale, equivalent to the passage of an hydrograph, a second focus has been the hydraulic conditions necessary for initial transport and the relationship between flow and the total quantity of material in motion close to the bed. Recently limited field and laboratory data have indicated that bedload motion is distinctly unsteady even during hydrographs characterized by competent flow and is intimately related to turbulent flow structure at fine spatial and temporal resolution. Bedload may move as discrete pulses resulting in intense periods of transport and *vice versa*. Concomitant changes in bed elevation, bed grain-size, hydraulic roughness and near-bed velocity structure are expected. Until recently there were no comprehensive data sets that could be used to demonstrate the relationship of bedload pulses, channel boundary and hydraulic interactions in natural rivers. Data available relate almost exclusively to sand and fine gravel. Distinctly lacking are data pertinent to the motion of coarse gravel including pebbles and cobbles up to 200mm in size. The purpose of this study was to develop techniques which would provide comprehensive field data related to the passage of sheets of coarse bedload. At the same time it was anticipated that data sets would result which would be suitable for mathematical-modelling purposes.

Technical Objective

Rather than investigate initial motion, particle transport or bed level fluctuations in isolation in a natural stream, the present objective was to monitor the bedload phenomena and associated processes intensively over the full-width of a defined reach where the inputs and outputs of sediment were known. Linkages between hydraulics, initial motion criteria, transport mechanisms and bed-level fluctuations were to be established. A better understanding of the complex processes of sediment transport and river channel adjustment should ensue. Techniques developed and data acquired should have immediate relevance to defining theoretical bedload transport relationships and models of sediment sorting which have practical application to hydraulic engineering.

Statement of Programme

The methods are fully explained below but a brief synopsis at this point is useful. The program was conducted in the gravel-bed Squaw Creek in Montana, USA, near the city of Bozeman between 1990 and 1992. The river is ideal for study as it has a snow-melt regime in April and May each year. Steady changes in stage occur each day in response to diurnal changes in snowpack melt rates such that competent flows and bedload transport often occur at the study site in the evening. Individual naturally-magnetic particles and kinematic waves of particles were recorded passing into the experimental reach and exiting from the reach using two electromagnetic coils placed across the river bed. Within the reach a transect was established across a section which included the main talweg and an adjacent lateral bar. Detailed bed level fluctuations across this section were recorded and detailed velocity profiles taken, from which shear stress distributions across the bed were derived. Bedload samples obtained using a 3" Helley-Smith and a large net-sampler were used to calibrate the magnetic coil record. These methods had been developed at Squaw Creek prior to the present investigation and had yielded small amounts of useful data as techniques were refined. The three years of the present study were unusually dry and only

one season resulted in bedload motion. Despite this disappointment, equipment was installed and improved in the first year, four flood waves were monitored in the second year and in the final year turbulence data were obtained.

Historical Background

An important focal point to river research in recent years has been the nature of transport in gravel-bed rivers over time-scales comparable to the passage of an hydrograph and at length-scales equivalent to the channel-width. Answers to a variety of questions are currently being sought. For example, what are the hydraulic conditions necessary to initiate transport of natural bed mixtures and what is the nature of transport as an event begins and ends? Even during steady hydraulic conditions, it has long been known that gravel particles may move in groups, forming bedload pulses[1], so that the bedload transport rate is unsteady[2] and also may vary spatially across a section. As pulsing is associated with scour and fill[3], it follows that the passage of a large-scale pulse should be manifest as a change in the width or depth of the stored volume of bed sediment; inducing the development of dynamic bed-waves[2]. In addition segregation of particles by size within pulses may occur with coarse gravel at the leading edge and finer material in the tail[4].

The linkages between particle motion, bed elevation and hydraulics are most readily addressed in the laboratory flume[2,5,6], but it is evident that success in obtaining relevant data in the field is primarily constrained by technical difficulties. Most notable is the need to develop continuous automatic detection systems which will provide adequate temporal and spatial resolution.

In the past, a variety of devices and techniques have been developed to obtain suitable field data. Painted, tagged and radioactively- or magnetically-labelled clasts have been used as tracers[1,7,8,9,10,11]. Mechanical samplers, such as the Helley-Smith sampler, have also been used to measure coarse bedload transport[12,13]. Large-scale pit traps (of varying complexity) and vortex samplers have been installed in stream bottoms[14,15]. Instruments have been developed to monitor the motion of individual particles on the stream bottom as well. For example, in 1973 Tyoniuk and Warnock[16] used acoustic techniques to relate the sound of motion of individual particles on the stream bottom during transport to velocity and so isolate the locus of threads of high transport intensity.

The above methods have all suffered from various problems, including logistic and technical constraints as well as sampling efficiency and averaging problems. The list of techniques is not exhaustive, but does serve to point out the diversity of approaches used to investigate bedload transport in gravel-bed streams. The proliferation of techniques is related, in part, to the difficulties associated with monitoring transport[17,18]. Floodwaters can be turbid and damaging to sensitive equipment. Adequate sampling is often dangerous to the researcher because it must be done during peak stage. Natural events which must be sampled occur at times which may be unexpected and may occur at night. These problems make it essential that continuous robust automatic monitoring be developed with the time and spatial resolution necessary to advance bedload science.

In recent years, potentially suitable detector systems have been installed in stream beds to examine the temporal variation in (naturally-magnetic) bedload transport semi-continuously[11,19], whilst real-time acoustic tracing of individual particles is under development. The present generation of magnetic detector systems can only be used in those streams where the local geology provides a ready-source of naturally magnetic stones. However, in those situations it shows great potential for continuous detailed monitoring at a suitable time and spatial resolution.

Most alternative approaches average measurements or integrate over a discrete time period because of mechanical or other practical constraints . Such averaging can obscure the detail of transport patterns[20,21,22]. For example if 10 minute sediment transport averages are used, dynamic features with durations of less than 10 minutes are lost[22]. A device was introduced by Ergenzinger and Custer[19], which potentially reduces such problems and facilitates the investigation of detailed transport phenomena. The instrument is described below and is capable of counting the passage of individual naturally magnetic pebbles and cobbles. Consequently the device produces a real time record of sediment transport with minimal count-averaging. Such data, when combined with hydraulic data, make it possible to study the nature of transport as coarse particle motion begins and ends and to examine unsteady sediment transport.

Study Site

Squaw Creek is situated in the Northern Rocky Mountains of the USA and is a tributary of the Gallatin River which together with The Madison and Jefferson Rivers joins to form the Missouri approximately 65km downstream from the Squaw Creek confluence (Fig. 1). Squaw Creek drains an area of 106km^2 of andesitic volcanic terrain which comprises the Gallatin Range, Gallatin County, Montana. Originating below Hyalite Peak, Squaw Creek flows for approximately 22km through a forested catchment before joining the Gallatin. The climate of this area is characterised by long, cold winters and short, cool summers. The average annual precipitation of 813mm consists of a snowfall equivalent of 457mm and 356mm as rain. The snowpack in the mountains reaches its maximum water content in April or May and melting is usually completed by June or July[23]. Rapid melting has been observed in late May and early June in recent years (Fig. 2) and the river generally reaches its peak annual discharge at this time. Peak discharges are caused typically by snowmelt or more occasionally, and less predictably, as a result of convective rainstorms. As the lag time for snowmelt is about 8 hours, the peak diurnal stage is not reached until circa 2000 hr when discharge is typically <6 m^3 s^{-1}. Lag time for rain-induced hydrographs is less; typically 1.5 hours, commonly giving peak flows in the early afternoon. Bankfull discharge is about 7 m^3 s^{-1} with a fifty-year flood equal to 20 m^3 s^{-1} (Fig. 3). Further details of the hydrological conditions are given elsewhere[24,25,26,27].

The bedrock underlying the drainage basin of Squaw Creek (Fig. 4) is rich in magnetic minerals, composed of approximately 25% Archaen quartzo-feldspathic gneiss, 20% Palaeozoic and Mesozoic sediments and 50% Eocene andesitic and basaltic lava flows, mudflows and igneous intrusions[28]. Further details of the drainage basin characteristics are given by Ergenzinger and Custer[24].

The 30m long study reach is situated 100m upstream of the confluence with the Gallatin river, and consists of an alternate bar on the left bank with the main talweg channel against the right bank. Immediately upstream, but outwith the study reach, an alternate bar exists on the right bank. During very high flows (>7m^3 s^{-1}) a secondary channel is inundated on the right bank (Fig. 5). This channel was rarely active during the study period with negligible sediment transport and was not included in the present study. The bed slope of the river locally varies between 0.02 and 0.03, whilst the channel width varies between 8m and 20m. Through the study reach the bed-width is constant (10m). The channel has a width to depth ratio of about 6.7 at bankfull.

Median grain sizes (D_{50}) of the bulk bed material range from 19mm on the bar to 140mm in the channel, where more than 16% of the particles are larger than 200mm. According to analyses by Bunte[29] the majority of particles are ellipsoidal, falling in the central bladed-class of Sneed and Folk[30]. The bed

sediments (Table 1) are generally well armoured by material >D_{84} of bulk samples; that is 90mm on the bartop and 200mm in the base of the channel. This armour is rarely disrupted although flows up to 7 m^3 s^{-1} lead to slight disturbance[31] Bedload up to 180mm has been recorded for flows up to bankfull[31], indicating that the larger elements in the bed sediment remain as a stationary lag. These large particles, often stand proud of the bed level, are widely scattered over the bed, and may provide a second scale of flow resistance in addition to the grain resistance imparted by the periodically mobile finer bar-top sediments.

The study reach exhibits a number of attributes which contribute to it's suitability for research on coarse bedload transport dynamics. Most importantly Squaw Creek is an active gravel-bed stream whose banks are stable but whose bed can adjust to naturally occurring changes in sediment supply and stream discharge. The diurnal peak discharges in Spring are responsible for almost all annual bedload transport. The timing of these hydrographs are more or less predictable and commonly have similar durations and peak values. This allows the collection of replicate flood-event data during a defined sampling season.

In the early stages of the development of the magnetic pebble detector[24], the Squaw Creek catchment was identified as having a suitable proportion of magnetic bed material larger than 30mm[29] required for detection. Prior to the present study, a research project was conducted intermittently between 1981 and 1988 by the Free University of Berlin at the same site. These studies have provided background information on the fluvial geomorphology of Squaw Creek.

2. INSTRUMENTATION AND SAMPLING METHODS

In summary, the instrumentation consists of two magnetic detector logs (which are embedded flush with the river bed) at each end of the study reach and a measuring platform which was used to collect hydraulic data and information on bed level variations. Five stage recorders have been installed (Fig. 5) and a hut erected to protect instrumentation and provide shelter during fieldwork. Vehicular access is easy and, in addition, power, flood-lighting and a telephone were also installed.

a) Detection of bedload transport using the magnetic pebble detector system.

The particle movement detectors (Fig. 6) installed at Squaw Creek record the passage of individual magnetic particles both spatially and temporally. The method of detection of particle motion is based on the electromagnetic Faraday principle. If a naturally magnetic or artificially magnetized particle is moved over an electric coil the motion induces a voltage fluctuation in the coil. This voltage is produced by induction, and consequently no electrical power is supplied to the coil. However amplification of the signal is needed so that it may be recorded. During the development of the prototype system[23,32], cobbles either were implanted with magnets and then placed on the stream bed or naturally magnetic clasts were used. Owing to the reduced magnetism of the natural tracer compared to that of the artificial tracer it was necessary to place the detector coils flush with the stream bed surface rather than bury them. The use of the naturally magnetic tracer was superior to the artificially magnetized clast not only from a practical angle but their use also eliminates the logistic problems associated with seeding artificial tracers on, or in, the stream bed.

At Squaw Creek a magnetic particle motion detector had already been installed at the downstream end of the study reach by the Berlin team. During the present study period an additional detector was positioned at the upstream limit of the reach (Fig. 4). Each detector system has the capacity to detect motion at discrete 1.5m sections transverse to the flow. This configuration was devised so that input and

output of particle numbers to and from the reach could be determined. The detectors record the motion of particles in real-time and their signals presently are counted and logged at 10 minute intervals. The early system used by the Berlin team often was unreliable, with false signals induced by static electricity in the atmosphere, for example, or individual signals could not be isolated at high transport rates, when noise to signal ratios were high[26]. Logging consisted of a chart record which had to be manually analyzed. Technical information on this prototype detector is given elsewhere[33]. However, during this project, considerable technical improvements were made to the amplification/filter system. The electronics consisted of four main parts, a double auto zero amplifier and analogue multiplexer, a data acquisition controller with digital converter and some auxiliary electronics with a micro-controller. This meant that the signal to noise ratio was improved considerably. Data were recorded directly on a PC with visual output for monitoring the signals.

b) Detection of bedload transport using other samplers

Previous research at the site had made use of hand-held 3" or 6" Helley-Smith bedload samplers but these had proved to be inadequate in high flow and incapable of trapping the larger fraction of bedload in transport[28]. Latterly, a direct method of bedload measurement was used at the downstream limit of the study reach by trapping all gravel greater than 11mm in a specially designed net supported on a frame[31]. This large bedload sampler was deployed below a sill immediately downstream of the lower detector (Fig. 4). Although close in proximity, the two systems did not interfere with each other, and direct sampling allowed validation and calibration of the detector system[29,31]. The bedload net sampler was deployed for variable lengths of time dependant upon the prevailing transport conditions. In addition, in 1992 a vortex sampler[15] was constructed to obtain bedload bulk samples every 5 minutes, but no significant transport occurred during the sampling campaign.

A hydrophone[34] was calibrated to record the sediment generated noise (SGN) arising from inter-particle collisions during transport of bedload material. Unfortunately, and unusually, no bedload transport occurred in the 1992 season owing to inadequate snow-pack. However, the system was calibrated through artificial production of SGN. This passive acoustic method provides an opportunity to obtain continuous high temporal-resolution records of mass transport rates with negligible interference with the state of the bed or the flow.

The idea of utilizing noise generated by bedload to quantify transport appears to have originated with Mühlhoffer[35]. Previous attempts to apply SGN to monitor bedload transport[16,35,36,37,38,39,40,41,42,43,44,45] have met with only limited success. Using a combined theoretical and experimental approach Thorne[46] showed the SGN spectrum to be composed of band-limited noise, with a frequency range inversely proportional to the mass of mobile material. The origins of SGN have subsequently been explained theoretically through application of rigid body acoustic radiation theory[47].

Improved understanding of marine bedload transport processes has resulted through combined measurements of flow turbulence and SGN. In recent studies conducted in the west Solent, UK, quasi-fluid bursting events analogous to sweeps were found to be correlated strongly with intermittent bedload transport events[34,48,49] and improved description of mobilization threshold and transport rates have resulted. More recently, attempts have been made to monitor mobilization and transport of gravel under

combined wave and current conditions (Hardisty, *personal communication*) and statistical simulation studies of acoustic bedload data have been reported by Williams and Tawn[50].

Given the success in utilizing SGN and EMCM turbulence measurements in past marine studies, in the present study, an attempt was made to apply similar techniques. This is the first attempt to deploy the instrumentation in shallow, fast-flowing rivers.

c) Hydraulic measurements

i) Water depth: Five temporary float-operated water-level recorders were deployed in stilling wells positioned in the stream against the stream banks (Fig. 5). The chart records from these proved useful for routine assessment of the direction of changes in discharge during individual hydrographs. However, as the mechanisms were not damped, considerable fluctuations and shifts in the ratings were noted owing to pulsating flow into and out of the float chambers. In particular the development of standing waves of varying intensity at differing stages around the stilling tubes meant that only local water level and spurious water slope variations were indicated. Instead water depth was measured directly at half meter intervals every half hour across the section beneath the measuring platform. Meaningful depth-discharge relationships were then devised for individual hydrographs by integrating depth-averaged velocity across the section in relation to the actual wetted area.

ii) Velocity: The downstream component of velocity in the vertical was measured primarily using an array of six OTT c2 velocity meters. Vertical spacings could be altered with a minimum of 50mm and the voltage output from each instrument was logged simultaneously and converted to calibrated velocity on a Hunter micro-computer. Velocity profiles were taken at 0.5m intervals across the channel from the measuring platform every hour.

A single head OTT electromagnetic miniature current meter was also used to obtain detailed velocity readings at centimetre intervals in the vertical. This instrument has the advantage of determining the velocity closer to the bed than the c2 impeller and senses the flow over a surface rather than integrating over the area of a rotor. This meter could be moved in the vertical without altering the positioning of the wading rod with a precision of 1mm. Data were stored directly on a Hunter micro-computer or latterly on a Toshiba T3100SX PC for immediate pre-processing in the field.

The turbulence measuring system employed was supplied by VALEPORT Instruments, Dartmouth, UK, and consisted of a pair of 17cm annular open head EMCM's and associated electronics. Using a "Y" shape mounting spar, the coil axis of each EMCM head is fixed at 45° to the principal flow streamline and at 90° to the other (Fig. 21a). Prior to fieldwork, calibration was undertaken in a large recirculating flume in the Mechanical Engineering Department at Liverpool University, UK. In all cases, EMCM sensitivity was approximately the same (ie., 1 Volt m^{-1} s^{-1}), the relationship between EMCM output and flow velocity was linear and the standard deviation of the measurements at a given velocity was very

low (Fig. 21b).

Measurements of orthogonal turbulent flow components (u, v and w) were made using the EMCM positioned at 24cm above the bed. A sensitive Hydrophone was attached close to the current meter heads on the EMCM spar at approximately 23cm above the bed (Fig. 21a). Following laboratory tests, unwanted EMCM "noise" was reduced by passing output signals through a 15Hz low-pass filter. A smoothing envelope placed around the output from the log amplifier effectively increased the signal to noise ratio of the hydrophone without compromising the sensitivity to SGN.

Data from the five output channels were sampled at 30Hz using a data logging system and software developed at the Proudman Oceanographic Laboratory, UK, and stored directly to hard disk on a portable PC. Following each measurement campaign, raw data were screened for unwanted noise spikes. In all cases, data quality was high and little editing was required. Figure 22 illustrates schematically the instrumentation and data acquisition system used.

Measurements of flow turbulence and SGN were conducted during the period 4 to 8 June 1992. As stage remained low during this period it was necessary to deepen artificially the stream channel and to divert all available flow through the modified section. Following an adjustment period of several hours, the bed appeared to re-armour, relatively natural conditions were re-established and measurements could proceed in a flow depth of approximately 150cm.

Using a purpose-built mounting bracket securely attached to the large timbers of the bridge spanning the upstream portion of the test site (Fig. 5) it was possible to position the EMCM and hydrophone system at a fixed and stable position above the irregular stream bed (Fig. 21a). Despite efforts to ensure the system was rigid, slight vibration was noted on the EMCM mounting spar due to sensor and support oscillation in the fast flow. Possible leakage of this motion into EMCM signals is discussed below. As this campaign is the first to deploy this assemblage of instrumentation the full details of signal preprocessing are given in Annex 1.

iii) Measurement of bed elevation and water surface elevation: Variation in the bed and water surface elevations were recorded using a system of vertical rods spaced at 0.10m intervals across the measuring platform. This apparatus allows a manual traverse of the stream taking readings of the bed and water surface elevation relative to a fixed datum at half or hourly intervals. The sampling error was determined to be +/- 1.0cm (De Jong pers comm, 1992).

d) <u>Processing of hydraulic data.</u>

For brevity here, the preprocessing of the turbulence records is detailed in Annex 1. However, the near-bed shear stress (τ), was calculated using the Reynolds stress (RS) approximation:

$$\tau = -\rho\overline{uw} \quad (1)$$

or obtained using the Turbulent Kinetic Energy (TKE) approximation:

$$\tau = 0.19\rho E \quad (2)$$

where ρ is the density of water and E is defined in Annex 1.

The bed shear velocity (u_*) is given by:

$$u_* = (\tau/\rho)^{0.5} \quad (3)$$

Roughness length (z_o) and drag coefficient (C_d) were calculated from the following approximations:

$$z_o = z\, e^{(-\kappa/C_d(z)^{0.5})} \quad (4)$$

and;

$$C_{d(z)} = 1/2((u_{*TKE})^2 + (u_{*RS})^2)/\overline{U} \quad (5)$$

where κ is von Kármán's constant (0.40).

For those near-bed profiles which were logarithmic (see below) the near-bed shear velocity and roughness length were also calculated from the equation:

$$u_z = \frac{u_*}{K} \ln\left(\frac{z-z_r}{z_0}\right) \tag{6}$$

where u_z is the velocity at a height z above the bed, z_r is the reference height (typically $0.7D_{84}$) and the roughness length is the intercept of the regression function.

The approximate relationship between the roughness length obtained from equation 6, Nikuradse's equivalent roughness and the grain-size of the bed material was considered using the general scaling relationship;

$$30z_0 = k_s = \alpha D_i \tag{7}$$

In many gravel-bed rivers the constant α is often considered to be equal to 3.5[51] when the representative grain-size (D_i) is set equal to D_{84}.

The local shear stress ($\tau = \rho u_*^2$) was determined from individual profile data and the Darcy-Weisbach hydraulic roughness coefficient (f) from:

$$f = 8\left(\frac{u_*}{U}\right)^2 \tag{8}$$

where U is the velocity averaged over the boundary-layer. Alternatively, section-averaged values of all parameters (eg. τ') were obtained from data integrated across the section as appropriate.

Total streampower (Ω) and the energy slope (S) of the study reach were calculated from:

$$\Omega = U\tau' = \gamma QS \tag{9}$$

where γ is the specific weight of water and Q is the discharge.

RESULTS

Unsteady Transport

Spectral Analysis

Preliminary consideration of the original detector-log signals showed that at time-scales < ca 300 seconds no temporal structure in the disposition of signals was evident. It follows that there can be no correlation to bulk flow parameters at this scale. The lack of correlation to bulk flow, and scale considerations, imply that individual particle movement at the sub-minute scale is related to detailed turbulent flow structure[50], as well as to the vagaries of individual particle entrainment and the random break-up of discrete clusters[11,52]. At scales greater than a few minutes (Fig. 7), apparent temporally-coherent structures can be detected visually although stochastic inputs are still strongly in evidence. Manipulation of such data is appropriately viewed as a problem in *time series analysis*. Sediment transport data cannot be expected to show strong periodicity[53,54,55], in part because the duration of the hydrograph limits record length. Nevertheless the raw spectra, and a series of smoothed variance spectra, were calculated for the records from each detector block, using the Parzen window and 10% taper[56]. Also calculated were the cross-correlations between series although not all details are reported here. A typical spectrum is shown in Fig. 8. A number of observations may be made. Firstly, all locations across the channel width had broadly similar spectra indicating a similar dynamic response irrespective of position across the channel; this was confirmed by high cross-correlations and near negligible phase shift between series. Secondly the spectra are somewhat flat indicating that variance is spread relatively evenly across all frequencies. An occasional significant peak may occur at an approximately half-hour period but the confidence level is not high. No statistically significant peaks occur in the records at the high frequency end of the spectra. A significant peak at the low frequency end of all spectra (<0.01) is associated with the diurnal periodicity of the hydrographs as has been noted before[30]. Further spectral-analysis is not warranted, being impeded by the length of record. However, it is possible that particle-count records with a longer time-base, might demonstrate other significant frequencies. Bunte[30] for example detected a frequency at 0.033 (5 hour period) from visual inspection of a bedload record from Squaw Creek but this was not tested statistically. Nonetheless, in the present case we can conclude that no periodic pulsing occurred during the sampled events; rather after excluding the significant correlation with the period of the hydrograph, unsteadiness in transport was statistically random. However, the similarity of spectra, the strong cross-correlation between locations and the negligible phase shift indicates that the dynamic response of the bar-top environment essentially is contemporaneous with the talweg locations. Notably, bar-top dynamics are not driven by sediment moving slowly from the channel onto the bar top. This is an important observation in-as-much as it indicates a forcing function operative at span-widths equivalent to the channel breadth and reach length.

Statistical Distribution Of Transport Rate

The final proposition in the last section was further tested by considering the statistical distribution of the ten minute sampling-period data. A number of laboratory data sets, representing bedload sampled over 0.5 to 1 minute periods, have been shown to broadly compare with a normal distribution[21,57];

$$f(t) = \frac{1}{\sqrt{2\pi}} e^{-t^2/2} \qquad (10)$$

The normalized transport rates (t) are given as;

$$t = \frac{q_b - \bar{q}_b}{\sigma} \qquad (11)$$

where q_b and $\bar{q}_b$ are the individual bedload count rates and the average rate, and σ is the standard deviation.

In contrast, data sets for instantaneous sampling, such as raw particle-count data should include an infinitely large number of zero or near-zero counts. In the latter case a Hamamori[58] distribution might be appropriate[59,60]. Time-averaging is usually an essential element of sampling bedload and consequently, positively-skewed normal distributions should be common with a tail of large transport rates. Laboratory data presented by Kuhnle and Southard[21] in fact show weak positive skewness probably induced by the sampling strategy. The present field data are also well described by skewed normal distributions (Fig. 9). The distributions when comparing both upstream and downstream records and between events broadly are similar in peakedness and degree of skew; implying comparable generating mechanisms are involved. The minor differences in the distributions are more likely associated with inadequacies in sample size than process differences. An example is the weak development of polymodality towards the right-hand side of the distributions. However strong bi- or poly-modality would be significant for the following reason. If distinct pulsing occurred in the temporal distribution of time-averaged bedload records, then bimodal histograms might occur. This is because very low-rates and high transport pulses would be well represented whilst few data would exist for medium transport rates. The data from individual sections across the river are also skewed, but interestingly, in the case of the 23/24th May data, the bar and interface data have a greater weighting to smaller transport events than is observed for the channel sections; this is especially marked in the case of the interface (Figs. 10,11 & 12). The data for the 5/6th June demonstrate changes in the grain count distributions induced by transport between

upstream and downstream detectors. Distributions become increasingly peaked and less skewed; especially over the bar-top (eg Fig. 12). Although substantial variation exists in the transport rates across the sections, there is no evidence that the coarse bedload moves in distinct bands with near zero-transport in between (cf. [61,62]). Although maximum transport is associated with the talweg location the whole stream-width is active once bedload motion begins (Figs. 7 & 13).

General Transfer Function

Viewing the transport event as a whole, continuity in the mass of sediment transported as a sheet may be maintained such that as many particles may exit the reach as enter. The dynamic of the particles within a sheet may be seen as analogous to the passage of a tracked-vehicle, whereby individual plates are laid-down at the front subsequently to be picked-up again at the rear. A comparison of the upstream particle count (17479) for the whole event with the downstream count (16319) can be used as a measure of continuity and indicates that some deposition occurs within the reach. However, in this example, the difference of only 7% could be owing to instrument error.

If continuity of transport is maintained over the short study reach, it follows that the upstream count series should be capable of generating the downstream series. Visual inspection of the stream-wide series for the 23/24th event shows an initial in-phase correlation of transport peaks which later become lagged with the downstream detector peaks occurring up to ten minutes later. By treating both upstream and downstream data series as an input-output model using recursive iteration[63,64], in principle, general sediment transfer functions can be defined wherein stable model structure might elucidate the physical nature of sheet dynamics. The statistical analysis was implemented using a computer package called microCAPTAIN[65], in an attempt to find a black-box transfer function capable of generating the downstream record from the upstream series. The results for the whole event were poor, mainly because for this particular data set it proved difficult to model the initial spike in both records (Fig. 14). However, consideration of sub-sets (Fig. 15) proved more successful (Fig. 16). For example, modelling from the 55th to 99 points (ie from 1638hr to 2302hr), where a lag of approximately one time-step is evident, gave a significant coefficient of determination of 0.61 (Young Information Content = -4.627). A useful introduction to the statistical treatment of similar data sets is given by Young and Wallis[66]. The appropriate function in this example is:

$$l_k - 1.11583 l_{k-1} + 0.4750 l_{k-2} = 0.2504 u_{k-1} \qquad (12)$$

where

$$l_k = \frac{0.2504u_{k-1}}{1-1.11583z^{-1}+0.47503z^{-2}} \quad (13)$$

Where u_{k-1}, is the lagged input, l_k is the prediction at time k and z is an operator.

With only the one data set available at this time it is not possible to say whether the behaviour noted is characteristic. Clearly the lag identified is dictated in part by the averaging period used in pre-processing the count data. However, the procedures adopted above serve to establish a framework within which similar records usefully can be examined once these become available. The coherent structure of the dynamic sheet moving through the reach does tend to indicate, however, that there is little significant exchange of material between the sheet and the bed material. This observation is explored more fully below.

Bed Level Dynamics

The movement of bedload sheets through the study reach may be reflected in bed level fluctuations if exchange of sediment occurs in the vertical. Otherwise the relationship of the sheet and the bed would be passive, with bedload transport taking place over a static surface. Analysis of the topographic data showed that slight fluctuations in bed level did occur so that the sheets interacted with the bed material. Such a situation is superficially akin to the *Phase I* transport described by Jackson and Beschta[3], where fine sediment is entrained from and over-passes an intact armour layer and only local readjustment takes place, but differs in-as-much as here coarse bedload (up to 127mm) over-passes a largely static armour and, as will be shown below, fine sediment is deposited into the armour.

At each sample point, the minimum bed-level elevations for each event were subtracted from the maxima (Fig. 17a) to provide a measure of the thickness of the active layer. Interestingly the coarse-bedded talweg changed little whilst the bar top changed only markedly in the vicinity of the 2m mark where a slight topographic low already existed at the beginning of the event. Maximum change in elevation occurred along the interface between the bar and the talweg channel (Fig. 17b) and is equivalent to the disturbance of one or two armour-particle diameters. Elsewhere changes are attributable to isolated exposed particles being mobilized. The spatial distribution of these changes through time are illustrated in Fig. 18. However, following Hoey and Sutherland[2], the main temporal changes are illustrated well by considering the standard deviation of the bed-level records (Figs. 19 & 20). In both examples, the interface area is more dynamic than bar-top or channel talweg, but it is notable that as the interface roughens, the bar top is smoothed and *vice versa*. The variance in the data declines slightly as bedload transport commences and is then especially great in the period *following* the passage of a bedload sheet through the reach (Fig. 20). Consequently, the bed becomes rougher once

bedload transport ceases. Such physical adjustments are explained by the initial infilling of the interstices of a largely static cobble surface with finer pebble-sized material; material in particular being exchanged between interface and the bar-top area. As noted above, this fine bedload is derived from up-stream of the study reach and transported into the reach. Subsequently, once the peak of the bedload wave passes, the flow is still competent to transport more particles than it now contains and the recently deposited material is reentrained resulting in a coarsening of the bed. The infilling process however is very dynamic in-as-much-as many individual pebbles are probably deposited, reentrained, and then replaced by others constantly. The temporal changes in bed roughness will have an effect on turbulence intensity over the bar-top and concomitant changes should be expected in bulk flow parameters. The latter proposition is explored below.

Hydraulics

Turbulence

Statistical Aspects:

In Figures 23 to 27, for clarity, time series plots for the first 0.55 minutes of runs 4 to 8 show speed, u, v, w, uw, vw, stress magnitude (τ), stress direction (Ψ) and SGN. In addition power spectra and cospectra obtained using 8192 data values for u, v, w, uw and vw are also shown. A summary of average current speed, RMS turbulence intensity for u, v, and w, bed shear velocity obtained using turbulent kinetic energy (TKE) and Reynolds stress (RS) approximations, drag coefficient (C_d) and roughness length (z_o) values are given in Table 2.

As expected, the statistical distribution of instantaneous u, v and w values are found to be Gaussian (Fig. 28). In contrast, uw and vw and SGN series are found to be positively skewed and are characterized by a long tailed distribution (Fig. 29a & b). Although not demonstrated here, previous studies indicate that the high stress values associated with infrequent "events" shown in Fig. 29a are likely to be positively correlated with sediment mobilization[34]. Further discussion and statistical analysis of these distributions is given by Williams and Tawn[50]. The high frequency, low magnitude SGN events illustrated in Fig. 29b are considered to be associated primarily with flow "noise" rather than with sediment transport. In contrast, high magnitude, low frequency events are considered to originate through grain impacts or other acoustic sources at distances away from the hydrophone and show little correlation with local hydrodynamic conditions. Further consideration of these observations is given below.

The standard deviation for individual 10 minute blocks of EMCM data from a continuous measurement period of 1.5 hours showed no significant variation (< 1cm s^{-1}) through time. Further, although spectra obtained for the whole record indicated small rises or declines in stream stage, they did not exhibit low frequency energy peaks (5-10 minutes) as noted in other geophysical flows[67,68]. In general, as the typical

turbulent eddy sizes scale with flow depth (see below), fluid motions with a period of this order probably originate through a mechanism unassociated with normal production and dissipation processes for turbulent eddies. Whilst not yet confirmed, it has been suggested by Lapointe[68] and others that low frequency turbulent motions in marine, estuarine and large river situations may be associated in some way with bedform interactions with flow during active sediment transport. Although differing in flow Reynolds number by a factor of approximately 10 from the shallow marine situation (z = 20m; $\bar{U}$ = 1 m s^{-1}) and with turbulent eddies scaling more appropriately with flow depth than with grain size (see below), failure to detect these motions in Squaw Creek, where sediment transportation was negligible and recognizable bedforms were absent, would appear to support this suggestion.

In common with u, v and w time series, instantaneous velocity changes recorded by the EMCM system are found to be Gaussian and indicate that particles on the bed are likely to be subjected to rapid, high magnitude flow accelerations and de-accelerations through time (Fig. 30). Defining the period of an "event" as being the time during which the velocity of a given flow component continues to rise or fall, Fig. 31 shows that short duration events (<2.5 sec) give rise to the largest acceleration/de-acceleration terms and exhibit an approximately exponential decay with event length.

When normalizing using U_{*RS} values (Table 2) RMS turbulence intensity values show a high degree of consistency and range between 1.9 - 2.3, 2.2 - 2.3 and 1.0 - 1.6 for u, v and w respectively. These values are in good agreement with those obtained in other geophysical flows[69]. RMS turbulence intensity values normalized using U_{*TKE}, however, are consistently lower. Relatively steady flows during the measurement periods prevented study of the RMS turbulence levels over a range of flow conditions.

As time series obtained in this study correspond more closely to spatial than temporal variations in velocity[34], power spectra obtained using a fast Fourier transform (FFT) were converted to wavenumber spectra (not illustrated) by the transform:

$$E(k) = \{\bar{U}(z)/2\pi\}S(f) \qquad (14)$$

where E(k) is the wavenumber spectrum, $k = 2\pi f/U(z)$, z is the sensor height above the bed and S(f) is the power spectrum at frequency f. As frequency is the reciprocal of period (T), the resulting spectra plotted in a normalized form can be used to estimate typical eddy length scale L by;

$$k = 2\pi/\bar{U}T = 2\pi/L \qquad (15)$$

Thus

$$L = 2\pi z/k \qquad (16)$$

At peak spectral values, typical turbulent eddy length scales for u, v and w were found to be approximately 0.52, 0.54, and 0.11m respectively. Similar results were also obtained through autocorrelation analysis of the time series, (not illustrated here), and indicate clearly that typical eddies scale with flow depth in Squaw Creek.

Spectra plotted in Figures 23 to 27 exhibit spectral slope values ranging between -1.85 and 2.58 and deviate from the expected value of -5/3. These results demonstrate that fully isotropic conditions do not occur at the maximum spectral wavenumbers in this study. These discrepancies are considered to arise owing to the physical size of the EMCM heads and to sampling interval whereby the small scale turbulent motions responsible for energy dissipation are not recorded. This is a common problem with all current measurement devices employed in field studies of turbulence and can lead to underestimation of shear stresses when employing TKE and RS methods[70].

Evident on all spectra obtained in Squaw Creek are small peaks at frequency values of approximately 5 Hz. As these are absent in calibration spectra their presence may be attributable to the combined offset of EMCM head vibration in the relatively fast flow and to regular eddy shedding phenomena upstream of the test section. Although subject to rapid oscillation in the calibration flume, the narrow frequency band associated with the present spikes, however, suggests vibration of EMCM's is the primary cause. At worst, presence of these spurious "turbulence" signals results in an over estimation of bed shear stress of < 2% and can be ignored for the purposes of the present study.

Hydraulic parameters derived from turbulence data:

It is generally accepted that the "constant stress layer" of a turbulent boundary layer over an hydraulically smooth surface occupies approximately the first 10-15% of the total layer thickness and measurements of Reynolds stresses within this region yield an approximation to bed shear stress. Given a flow depth at the present study site of approximately 150cm, Reynolds stress approximations are only likely to be valid for z up to 15cm if the conditions of hydraulic smoothness can be met. Clearly given the nature and arrangement of the coarse particles comprising the bed, this assumption is likely to be misleading owing to the presence of an internal boundary layer with turbulence characteristics probably scaling with a bed roughness parameter. It would not be expected, therefore, that the present measurements obtained at z = 24cm using relatively large EMCM heads will give results that relate to bed shear stresses directly. In combination with sampling errors associated with the present EMCM system, it would not be surprising, therefore to find that u. values in Table 2 differ from those obtained

using a log-profile fitting technique.

Values of u. in Table 2 obtained using TKE and RS methods, however, are not only very consistent during measurement runs 4 to 8, but also agree well with some u. values obtained using the log-profile (Fig. 36). On the basis of these results it would appear that the present EMCM system provides a realistic estimation of bed shear stress in highly turbulent flow conditions encountered in Squaw Creek.

Also shown in Table 2 are drag coefficient (C_d) and roughness length (z_o) values obtained using equations 4 and 5. In common with u. values, C_d and z_o values are generally consistent over runs 4 to 8 and are generally lower than would normally be expected given the grain size distribution of the bed sediments. In contrast z_o values obtained from velocity profile data (reported below) are consistent with expectations based on a consideration of bed grain size and equation 7. The unusually low values of z_o obtained from the turbulence data series will require further investigation. One possible explanation is that in high velocity flow over rough beds, skimming flow develops such that roughness lengths obtained using outer-layer turbulence measurements are related to the interface between the outer-layer and the near-bed boundary-layer. Consequently, no direct relationship should then be expected between z_o and the bed material characteristics.

SGN measurements:

Time series plots of SGN in Figs. 23 to 27 show little visual correspondence with any flow parameter obtained using the EMCM measurements. This has been confirmed from cross-correlation analyses using 30 minute time series. Further, the spectrum of SGN is closely similar to that for u (Fig. 32), and for SGN output in flows without sediment transport. This suggests strongly that the hydrophone is only recording flow "noise". Attempts to seed Squaw Creek with copious amounts of mixed grain size particles on a number of experimental runs failed to produce correlation between SGN and bedload transport (Fig. 32). These results were recognized in the field during preliminary data analysis and thus an alternative experimental technique was sought.

Selected particles from the bed were collected and sorted by size. By gently knocking particles together underwater at a distance of 0.5m away from the hydrophone it was possible to detect and record SGN signal for a range of sizes and positions from the sensor. During experimental runs over approximately one minute, attempts were made to reproduce regular collisions between the test particles in order that they may be more clearly identified in the hydrophone record. In the event this proved to be unnecessary as the resulting SGN level was found to be significantly above the background acoustic noise of Squaw Creek.

SGN data typifying an impact test at 1.0m from the hydrophone using well- rounded particles with a diameter in the range 32 to 64mm is shown in Fig. 33. In common with previous plots, SGN is shown on a logarithmic scale. The near regular peaks present in Fig. 33 rise by at least two orders of

magnitude above the "background" level and thereby provide convincing evidence that SGN can be detected in Squaw Creek. This is illustrated further in Fig. 34 which shows SGN and u spectra on the same axes. Here, in contrast with Fig. 32, the spectral characteristics of u and SGN differ significantly over the range of frequencies shown. Given these clear results and the lack of natural bedload transport, no further analysis of SGN data was attempted.

Depth-integrated parameters

Shallow flow over large bed roughness may be associated with local flow accelerations and velocity profile distortion such that uniform flow assumptions are violated. The effect of large relative-depth ratios on the velocity distribution throughout the section is examined for data sets obtained at half-hourly intervals throughout the hydrographs (eg. Fig. 35). Water surface elevation closely matches variation in the topography across the section and isovels are distorted and close together in the vicinity of topographic high points. These high points were often isolated blocks around and over which the flow is forced to deviate. Although this induces strong secondary currents in the immediate vicinity to the blocks, there was no indication that such coherent secondary flow cells were persistent stream-wise. Such effects tended to reduce as water depth increased and the flow became more two-dimensional with a water surface less distorted. Variations on this theme occurred owing to the local development of standing waves out-of-phase with the bed topography, but owing to low Froude numbers, this was exceptional.

It has been established that if strongly local flow effects are avoided, then with care, results obtained from log-profile analysis can be representative of the bulk flow hydraulics[71,72]. Before calculating parameter values from velocity profile data obtained using the array of six impellers, a careful examination of the vertical flow structure was undertaken using a vertical deployment of the electromagnetic sensor. With this instrument velocity was measured at half to one centimetre intervals in the vertical (Fig. 36) with the lowest reading taken by nestling the sensor between surface bed particles such that the zero datum was ca $0.7D_{84}$. A number of observations may be made. The profile extending to ca 25% of the depth often is close to logarithmic. The point of inflection from this log-profile is representative of the thickness of the constant stress boundary-layer associated with the grain roughness, whilst the velocity readings above this point are representative of an outer-layer associated with both grain and form roughness. In this outer layer the vertical velocity structure demonstrated greater variance about respective trend-lines than was noted within the boundary-layer. Following Wilkinson[73], only those points representative of the lower 15% of the depth and within a few centimetres of the bed were used to calculate near-bed parameters. This procedure generally gave profiles close to logarithmic with little data scatter about the regression-line (r values >0.95). Following Jackson[74] consideration was given to adjusting the zero datum, but this was usually found to be inappropriate because the goodness-of-fit of data to a log-profile was excellent without any adjustment and it was concluded that the zero-plane was well represented by the mode of deployment (see also Soulsby[68]). There is no objective method available for making an adjustment in shallow flow over coarse gravel and instead, those near-

bed profiles (eg Profile 7) which did not meet the log-normal criteria were not analyzed further. Inflected profiles are common in the fluvial environment and often may be related to flow over surface-roughness changes[75], where concave-up profiles reflect a rapid transition in the development of the thickness of the boundary-layer as flow traverses from smooth to rough beds and *vice versa*[69]. Of the non-logarithmic distributions, convex-up profiles were more common than concave-up profiles but no evident downstream change in surface roughness was present. In addition it was noted that the log-layer is often well developed to circa 25% of the depth which mitigates against an explanation based on invoking rapidly reforming boundary-layers in response to stream-wise variation in roughness. Instead, these profiles are superficially similar to those compound profiles described for developed flow over coarse gravel[76,77,78] and by Dyer[79] , amongst others, for flow over dune fields. Consequently, such profiles can be attributed to flow over composite roughness; ie grain roughness and additional form roughness, where the latter is owing to isolated large blocks[80], or other large bedforms where the characteristic outer-region roughness lengths are greater than the grain roughness[81]. A particularly valuable mathematical derivation of the velocity profile in this environment is given by Jackson[74]. Immediately above the reference plane the flow structure depends primarily upon grain roughness and only weakly upon the geometry of large-scale roughness elements. In the outer layer, in contrast, the flow structure depends to a greater part on the presence of large-scale roughness. Visual inspection of the bed in Squaw Creek at the time indicated that the compound profiles could be ascribed to wake effects induced by larger than average bed-elements distributed randomly across the section. The sheltering effect of upstream blocks lead to a flow structure near the gravel-bed distinct from that above the block height. The values of z_o obtained from profiles taken within a few centimetres of the bed (Fig. 36) are typically of an order of 0.55cm; which from Equation 7 indicates that k_s for the cobble bed is circa 16cm or $1.8D_{84}$ of the bar-top gravels. This value for k_s compares favourably with experimental data[82] obtained over similar-sized cobbles in a laboratory flume. Profile data taken at greater heights above the bed, which may include outer-layer observations gave a median z_o value of 1.6cm (event of 23/24th May) and 1.8cm (event of 5/6th June) which indicates that k_s for the large scale roughness is of the order of half a meter or $2.5D_{84}$ of the channel armour. It has already been noted above that these z_o data obtained from log-profiles are at variance with the z_o data obtained from analysis of the turbulence record.

The vertical structure of air-flow over and through vegetation canopies[83] also is qualitatively similar to the form of profiles described above. This analogy between flow over blocks on a gravel-bed, dunes and through vegetation may provide further insight into the quantitative description of compound profiles within coarse-gravel rivers. It is the authors intention to consider this further when additional data are available.

Interaction of bed material and hydraulics

The relationship of hydraulic parameters to bed elevation and bedload data was considered both in terms of the spatial variance considering the individual data points across the section and for section-integrated

data. The variation in shear velocity for example across the section and through time is shown in Fig. 37. Correlation matrices were calculated relating; (i) adjacent bed elevation data, (ii) adjacent shear stress data and, (iii) bed elevation data with shear stress data. These however are not presented here as they showed little evidence of a consistent response of the bed surface to local variation in the shear velocity, although there was weak evidence for correlation of parameters, and hence a dynamic response, at the bar interface.

Negligible entrainment of bar and channel gravels in the study reach is further indicated by a consideration of theoretical thresholds for particle entrainment. Carling and others[82] provide an entrainment function for coarse ellipsoidal gravel in shallow streams such as Squaw Creek:

$$\tau_c = \frac{2V(\rho_s-\rho)g}{\psi C_d \pi(a_2 b_2 c_2)} \frac{\sin(\phi-\beta)}{\cos(\phi)} \frac{1}{[5.75\log(30z_p/k_s)]^2} \qquad (17)$$

For conciseness notation is given by Carling and others[82] but here appropriate values are: C_d = 1.25, ϕ = 53°, β = 2°, $(\rho_s-\rho)$ = 1.65g cm^{-3}, g = 981cm s^{-2}, z_p= 3.9cm and k_s = 15cm. V = $4/3\pi a_2 b_2 c_2$ (where a_2 = $D_s/2$ the short semi-axis of the ellipsoid and b and c represent the other major semi-axes). Entering these data into equation 17 and solving for τ_c, the critical shear stress for entrainment for a variety of grain-sizes can be ascertained. The bed armour over the bar top can be characterized by a D_{84} of at least 90mm (Table 1). A shear stress of circa 75 N m^{-2} is required to entrain any exposed armour particles seated on shallow cols between coplanar particles (exposure parameter Ψ = 0.84). Near coplanar particles (embedded, Ψ = 0.5) which form the bulk of the armour-layer require at least 150 N m^{-2} for entrainment. In contrast the gravel in the sheet moving over the bar in exposed locations (Ψ = 0.99) can be typified by a D_{84} of between 60 and 80mm (Fig. 38) which requires between 40 and 65 N m^{-2} to maintain mobility. A sensitivity analysis, varying parameters between known limits, readily shows that although threshold values change slightly, the bed armour would remain intact (eg for the event of 23/24 May the measured shear stress varied between 80 and 130 N m^{-2}). Consequently all grain-sizes within the sheet should pass rapidly through the reach with little entrainment of the compact bed armour.

Section-integrated data (Figs. 39 & 40) showed conclusively, that the passage of bedload sheets through the reach is indeed poorly correlated to bed elevation but has aneffect on bulk hydraulic parameters. This is best illustrated by the event of 23rd/24th May 1991. Although discharge tended to increase after 2000 hrs, the arrival and passage of a bedload sheet through the reach led to smoothing of the bed surface in the talweg and bar-interface (Figs. 19 & 40) such that velocity increased, water depth reduced and the shear velocity and streampower fell as the hydraulic roughness was reduced (Fig. 41). Similar reductions in bed roughness were associated with bedload transport during the event of 21st May and 5th/6th of June 1991 and reflect sudden changes in the energy slope as bedload sheets pass through the

reach. Following the passage of the sheets, the bed physically and hydraulically roughened (Fig. 20 and 41) with a concomitant adjustment of other hydraulic parameters including depth.

Owing to the coarse nature of the bedload and the inability of the net sampler to collect efficiently the fractions finer than 11mm, the bedload grain-size curves do not show well the changes in the finest fractions as material is exchanged with the bar top (Fig. 38). The D_{50} in fact changes little (Fig. 42) but there is some indication that between 1500hr and 0600hr the sheet at first is dominated by finer gravels (1600hr) with a negligible percentage coarser than 84mm. The distribution then coarsens slightly as it enters the reach and loses fines to the surface armour (1800hr) after which there is little change in the distribution until 0200hr, following which, the tail of the sheet passes over the bar and finer gravels increasingly dominate the distributions. Consequently, the coarse end member declines steadily from <127mm to <45mm (Figs. 38 & 42) with only sporadic examples of cobbles in transport after 0900hr. The main sheet had passed by 0800hr and transport rates dropped rapidly. Occasional bedload samples taken subsequently showed variable grain-size distributions. These latter samples reflect the random passage of a few cobbles and fines.

The variation in bed roughness and consequent changes in hydraulic parameters during the passage of bedload sheets demonstrates that even when the intensity of transport is only low, and the armour is largely intact, uniform-flow resistance equations are unlikely to be applicable. This notion was tested by applying Hey's[51] flow resistance equation to the data for the 23/24th of May and 5/6th June when transport was relatively weak.

$$\left(\frac{8}{f}\right)^{1/2} = 5.75\log\left(\frac{aR}{3.5D_{84}}\right) \qquad (18)$$

Hey's equation is currently the most satisfactory for gravel-bed rivers giving acceptable results when compared with measured flow resistance over stable beds[72]. In using equation 18, it was assumed that for a broad shallow channel[51], a = 11.1; whilst the fixed bed D_{84} should be optimized. This latter objective was achieved by first substituting observed values of R and f into the equation to produce a range of values for D_{84}. For example, the average for the event of 5/6th June equalled 197mm (sd 33.91mm for 9 observations). These values are consistent with variability in the armour-layer grain-size. However, when $(8/f)^{0.5}$ is calculated assuming this constant value of D_{84}, for observed variation in flow depth, the inadequacy of the function becomes apparent. Sediment transport commenced between the first and second observations smoothing the bed such that the second observed value of $(8/f)^{0.5}$ is much larger than predicted (Fig. 43). As bedload transport ceased the discrepancy declines, only to begin increasing again when transport starts again after 2100hr.

4.0 CONCLUDING DISCUSSION

■ During the relatively low flows encountered in 1991 and 1992 it has proven possible to obtain good quality measurements of flow turbulence and weak transport of bedload sheets. Further, through the local generation of SGN and magnetic induction it has been shown that acoustic and magnetic detection of bedload in fast flowing, gravel bed streams is possible using the present detection systems.

■ With appropriate scaling, the statistical properties of u, v and w time series were found to be consistent with measurements obtained in other geophysical flows.

■ In common with other natural flows over rough boundaries, the bulk of Reynolds stress production in Squaw Creek is associated with infrequent "events". In general "events" have a duration greater than 1.5 seconds and a return period greater than 10 seconds.

■ Typical eddy length scales determined using wavenumber spectra and autocorrelation functions were found to be 0.52, 0.54 and 0.11m for u, v and w respectively.

■ Spectral slope values in the range -1.85 to -2.58 demonstrate that fully isotropic conditions were not detected using the present sensors. This is considered to arise through a combination of circumstances including: selection of record length; digitization rate; low-pass filter cut-off; and the physical size of the EMCM heads. The individual significance of any single factor could not be determined.

■ Bed shear stress values obtained from EMCM measurements using TKE methods were found to be consistently lower than those determined using RS method. Further, location of the EMCM sensors well outside the "law of the wall" region, high bed roughness values and factors outlined above probably contribute to the disparity between u_* values obtained using these methods and some of those obtained using the profile method. In general, however, u_* values obtained here are in good agreement and are thought to be reliable indicators of bed shear stress in Squaw Creek.

■ The drag coefficients and roughness length values obtained using the present measurements of bed shear stress and flow speed are found to be consistent within data series; whether calculated from the turbulence data series or from the velocity profiles. However, bed roughness lengths estimated from turbulence data differ from those estimated from profile data.

■ Roughness length values obtained from near-bed velocity profile data scale with the grain size of the bed material, whilst roughness length values obtained from profile data which includes some outer-layer observations scale with the dimensions of largest elements of the bed armour.

■ Detailed velocity profiles taken through the constant stress layer and the outer-layer indicate the possible presence of an inflection above the near-bed layer. The presence of these compound velocity

profiles may indicate the presence of two scales of bed roughness and account in part for the discrepancies noted in estimated z_o values obtained using different instrumentation systems and procedures.

■ Manual generation of SGN at 0.5m from the hydrophone using a range of selected pebble sizes produced acoustic energy significantly higher than background in Squaw Creek. SGN generated in this way is easily detected and, based upon past experience, is considered to be typical of SGN arising during natural bedload transport.

■ The spectra for the bedload detector count data have no distinct peaks. Variance in contrast is spread fairly evenly across all the frequencies shown. Consequently, there is no periodic pulsing during the passage of the sheets; rather transport is statistically unsteady.

■ The statistical distributions of width-summed count data and for individual sections, at both the upstream and downstream detectors, conform closely to positively-skewed normal distributions. The positive skew may originate primarily from sampling constraints but this needs further investigation. The similarity between sections in the nature of the distributions and, in particular, the lack of bi-modality adds weight to the conclusion that there is no pulsing of transport and no movement of bedload in distinct and spatially discrete bands.

■ The spectral similarity and lack of phase shift between upstream and downstream series and between adjacent sections indicates that the dynamic response of the bar-top and channel talweg are in all probability contemporaneous and driven by a forcing function which operates at span-widths equivalent to the channel breadth (10m) and the reach length (30m).

■ The successful application of a general statistical transfer function to sub-sets of the upstream and downstream detector count data indicates that coherent sheet structure is maintained over length scales equivalent to the experimental reach (30m). In other words the sheet retains some memory of upstream behaviour as it translates downstream.

■ General transfer functions may be suitable to model sheet dynamics over similar length scales in other gravel bed rivers other than Squaw Creek.

■ The finer grain sizes from the mobile sheet are trapped in the interstices of the bed armour as the sheet arrives in the study reach. This deposition process leads to physical and hydraulic smoothing of the bed. Towards the tail-end of the sheets passage, the finer material is re-entrained which leads to roughening of the bed. This process induces a response in hydraulic parameters.

■ In any modelling exercise the effect of weak bedload transport on bed resistance cannot be ignored, as the passage of discrete bed load sheets induces strong hysteretic effects in hydraulic parameters;

including water level. The inapplicability of stable-bed equations, such as Hey's, during weak bedload transport has important repercussions for the use of general flow routing models for shallow mountain rivers.

■ If the observations and conclusions reported here also apply to larger gravel-bed rivers, then there are non-trivial implications for calculations required for engineering management. For example maintaining adequate freeboard along flood defence dykes, positioning of water abstraction intakes, and navigation depths depend on calculated water depths being accurate.

4.1 *Recommendations for further research*

Field Based Research

Additional field data would be valuable to clarify the grain-sorting mechanisms as bedload sheets pass and the interaction with the bed. In particular additional data at higher flow levels (than are reported here) are desirable. These data can be obtained, for example, using a vortex sampler or Helley-Smith type sampler, together with fine-resolution profiling of the bed elevations. These grain-sorting data need relating to hydraulic parameters calculated from detailed near-bed velocity profiles obtained using electromagnetic current meters as well as near-bed turbulence data.

The magnetic detector system and the acoustic detection system provide an opportunity to obtain long-runs of data on bedload transport at a temporal resolution necessary to relate particle dynamics to the scale of turbulent fluctuations. Not only does this have an important research context, but also offers the possibility of routine monitoring of bedload in remote locations.

The installations at Squaw Creek are unique and provide an opportunity to obtain the integrated data-sets required to elucidate the mechanisms of coarse bedload sheet dynamics and to develop further automated bedload monitoring. *It is recommended that consideration should be given to developing a further research and technical development programme at Squaw Creek.*

Modelling Unsteady Bedload Transport

The particle interactions with the flow and the bed material can be modelled using parallel processing techniques[84]. The existing detailed comprehensive hydraulic, channel geometry and bedload data could be used to construct a bedload transport model mimicking unsteady behaviour based upon fundamental physical principles. The implications for future generations of engineering models such as HEC-2 should be a key focus of the investigation. *It is recommended that a computer-based mathematical model should be developed which simulates the passage of coarse bedload in gravel rivers as unsteady waves of material.*

ACKNOWLEDGEMENTS

Prof P. Ergenzinger and various students of the Freien Universität of Berlin are thanked for valuable discussion and pre-processing of bed level and particle count data. Dr K. Bunte (University of Colorado) is thanked for discussion and preprocessing bedload data. Big Timber Works Incorporated and Hogin Machine and Welding, Bozeman, Montana provided a friendly construction service without which this project could not have been completed. Prof. S. Custer (Montana State University) provided unstinting assistance and advice. Prof. G. Christaller and the students of the Technisc[illegible] Fachhochschule, Berlin improved the electronics of the detector system. Mr A. Kelsey assi[illegible] in data analysis. All the above and many other individuals provided help in fieldwork often during u[illegible]sociable hours for which we are very grateful.

BIBLIOGRAPHY

1. Langbein, W.B. and Leopold, L.B. (1968) *River channel bars and dunes-theory of kinematic waves.* U.S. Geological Survey Professional Paper. L1-L20p. 422-L

2. Hoey, T.B. and Sutherland, A.J. (1991) Channel morphology and bedload pulses in braided rivers: a laboratory study. *Earth Surface Processes and Landfroms*, **16**, 447-462.

3. Jackson, W.L. and Beschta, R.L. (1982) A model of two-phase bedload transport in an Oregon coast range stream. *Earth Surface Processes and Landforms*, **7**, 517-527.

4. Whiting, P.J., Dietrich, W.E., Leopold, L.B., Drake, T.G. and Shreve, R.L. (1988) Bedload sheets in heterogeneous sediment. *Geology*, **16**, 105-108.

5. White, W.R. and Day, T.J. (1982) Transport of graded gravel bed material. In: Hey, R.D., Bathurst, J.C. and Thorne, C.R. (Eds.) *Gravel bed rivers*. John Wiley & Sons. Chichester. pp 181- 223.

6. Kuhnle, R.A. and Southard, J.B. Sediemnt transport fluctuations in a gravel bed laboratory channel. *Third International Fluvial Sedimentology Conference*. pp 25.

7. Ramette and Heuzel (1962) A study of pebble movement in the Rhone by means of radioactive tracers. *Houille Blanche A*, 389- 399.

8. Hubbell, D.W. and Sayre, W.W. (1964) Sand transport studies with radioactive tracers. *Journal of the Hydraulics Division*, **90**, 39-68.

9. Butler, P.R. (1977) Movement of cobbles in a gravel-bed stream. *Geological Society of America Bulletin*, **88**, 1072-1234.

10. Oldfield, F., Thompson, R. and Dickson, D.P.E. (1981) Artificial magnetic enhancement of stream bedload: A hydrological application of supermagnetism. *Physics of the Earth and Planetary Interiors*, **26**, 107-124.

11. Reid, I., Brayshaw, A.C. and Frostick, L.E. (1984) An electromagnetic device for automatic detection of bedload motion and its field applications. *Sedimentology*, **31**, 269-276.

12. Hubbell, D.W. (1964) *Apparatus and techniques for measuring bedload.* U.S. Geological Survey Water Supply Paper. 74p. no.1748

13. Emmett, W.W. (1980) *A field calibration of the sediment- trapping characteristics of the Helley-Smith bedload sampler.* United States Government Printing Office. pp44p.

14. Leopold, L.B. and Emmett, W.W. (1976) Bedload measuremnets, East Fork River, Wyoming. *Proceedings of the National Academy of Science.* pp 1000-1004.

15. Hayward, J.A. and Sutherland, A.J. (1974) The Torlesse tream vortex-tube sediment trap. *Journal of Hydrology*, 13, 41-53.

16. Tywoniuk, N. and Warnock, R.G. Acoustic detection of bedload transport. *Proceedings of Hydrologic Symposium at University of Alberta.* DoE, Natural Resource Council, Canada. Canada. pp 728- 743.

17. Reid, I., Frostick, L.E. and Layman, J.T. (1985) The incidence and nature of bedload transport during flood flows in coarse grained alluvial channels. *Earth Surface Processes and Landforms*, 10, 33-44.

18. Raemy, F. and Jaeggi, M. (1981) Some problems related to sediment transport measuremnet in steep mountain streams in erosion and sediment transport measurement. *Proceedings of the Florence Symposium.* International Association of Hydrologic Science. pp 231-239.

19. Ergenzinger, P. and Custer, S. (1982) First experiences measuring coarse material bedload transport with a magnetic device. In: Euromech 156 *Mechanics of Sediment Transport.* pp 223- 227.

20. Hubbell, D.W. and Stevens, H.H.Jr. (1986) Factors affecting accuracy of bedload sampling. *Proceedings of the 4th Federal Interagency Sedimentation Conference.* pp 4-20 - 4-29.

21. McClean, D.G. and Tassone, B. (1987) Discussion of bed load sampling and analysis. In: Thorne, C.R., Bathurst, J.C. and Hey, R.D. (Eds.) *Sediment transport in gravel bed rivers.* John Wiley & Sons. Chichester, UK. pp 109-113.

22. Kuhnle, R.A. and Southard, J.B. (1988) Bedload transport fluctuations in a gravel bed laboratory channel. *Water Resources Research*, 24, 247-260.

23. Klages, M.G., Logan, L.D. and Hsieh, Y.P. (1973) Suspended solids carried by the Gallatin River of South West Montana I. Amounts carried during spring run off. *NorthWest Science*, 47, 203-212.

24. Ergenzinger, P.J. and Custer, S.G. (1983) Determination of bedload transport using naturally magnetic tracers: first experiences at Squaw Creek, Gallatin County, Montana. *Water Resources Research*, **19**, 187-193.

25. Bunte, K., Custer, S.G., Ergenzinger, P. and Spieker, R. (1987) Measurement of course bed-load transport by means of the magnetic tracer technique. *Deutsche Gewasserkundliche Mitteilungen*, **31**, 60-67.

26. Custer, S.G., Bugosh, N., Ergenzinger, P.E. and Anderson, B.C. (1987) Electromagnetic detection of pebble transport in streams: A method for measurment of sediment-transport waves. In: Etheridge/Flores (Eds.) *Recent Developments in Fluvial Sedimentology*. Society of Paleontologists and Mineralogists. pp 21-26.

27. Bugosh, N. and Custer, S.G. (1989) The effect of a log-jam burst on bedload transport and channel characteristics in a headwaters stream. In: Woessner, W.W. and Potts, D.F. (Eds.) *Proceedings of a symposium on headwater hydrology*. American Water Resources Association Technical Publication Series. pp 203- 211.

28. McMannis, W.J. and Chadwick, R.A. (1964) Geology of the Garnet Mountain Quadrangle, Gallatin County, Montana. *Montana Bureau of Mines and Geology Bulletin*, **43**, 47.

29. Bunte, K. (1991) Untersuchungen zur zeitlichen variation des grobgeschiebetransportes und seiner korngroBenzusammensetzung(Squaw Creek, Montana, USA). PhD thesis, Freie Univ. Berlin.

30. Sneed, E.D. and Folk, R.L. (1958) Pebbles in the lower Colorado River, Texas a study in particle morphogenesis. *J. Geology*, **66**, 114-150.

31. Bunte, K. (1992) Particle number grain-size composition of bedload in a mountain stream. In: Billi, P., Hey, R.D., Thorne, C.R. and Tacconi, P. (Eds.) *Dynamics of gravel bed rivers*. John Wiley & Sons. Chichester. pp 55-68.

32. Ergenzinger, P. and Conrady, J. (1982) A new tracer technique for measuring bedload in natural channels. *CATENA*, **9**, 77-80.

33. Spieker, R. and Ergenzinger, P. (1990) New developments in measuring bedload by the magnetic tracer technique. *Erosion, transport and deposition processes*. IAHS Publication number 189. pp 169-178.

34. Williams, J.J., Thorne, T.D. and Heathershaw, A.D. (1989) Comparison between acoustic measurements and predictions of the bedload transport of marine gravel. *Sedimentology*, 36, 973-979.

35. Muhlhofer, L. (1993) Untersuchungen uber die Schwebstoff-und Geschiebefuhrung des inn nachst Kirchbichl (Tirol). *Die Wasserwirtschaft*, No 1, pp43.

36. Bradeau, G. (1951) Quelques techniques pour l'etde et la mesure du debit solide. *La Houille Blanche*, Spec. No A, 54.

37. Juniet, M. (1952) *L'Arenophone, un appareil detecteur des movement des sediments fins*. Societe hydrotechnique de France. Transport Hydraulique et Decantation des Materiaux Solides. pp39p.

38. Smoltczyk, H.V. (1955) *Beitrag zur Ermittung der Feingeschiebe Menganglinie*. Tech. Univ. (Berlin-Charlottenburg). 56p. VWS, Rept. 43

39. Bedeus, K. and Ivicsics, L. (1963) Observations of the noise of bedload. *Proc. of the Int.Assoc.Sci.Hydrol.* Publ. No. 65.

40. Johnson, P. and Muir, T.C. (1969) Acoustic detection of sediment movement. *J. Hydraulics Res.*, 7,

41. Hollingshead, A.B. (1969) *Sediment transport measurements in the Elbow River at Bragg Creek*. Report to Coop. Agencies, Res. Concil Alberta. pp67p.

42. Hollingshead, A.B. (1971) Sediment transport measurements in a gravel river. *J. Hydraulics Res.*, 97, 235-247.

43. Samide, G.W. (1971) Sediment transport measurement. Univ. Alberta. *MSc Thesis*.

44. Jonys, C.K. (1976) *Acoustic measurement of sediment transport*. Burlington, Ontario. Inland Water Directorate, CCIW Branch. pp118p. Scientific Ser. No. 66

45. Banzinger, R. and Burch, H. (1990) *Acoustic sensors (hydrophones) as indicators for bedload transport in a mountain torrent.* IAHS Publ. 207-214p. Hydrology in Mountainous Regions, 1 - Hydrological Measurements; the Water Cycle. No.193

46. Thorne, P.D. (1986) An intercomparison between visual and acoustic detection of seabed gravel movement. *Mar. Geol.*, **72**, 11- 31.

47. Thorne, P.D. (1987) The acoustic measurement of gravel transport. *5th Int. Conf. for Ocean Tech.* Inst. Electronic & Radio Engrs. pp 63-70.

48. Heathershaw, A.D. and Thorne, P.D. (1985) Sea-bed noises reveal role of turbulent bursting phenomenon in sediment transport by tidal currents. *Nature*, **316**, 339-342.

49. Thorne, P.D., Williams, J.J. and Heathershaw, A.D. (1989) In situ acoustic measurements of marine gravel threshold and transport. *Sedimentology*, **36**, 61-74.

50. Williams, J.J. and Tawn, J.A. (1991) Simulation of bedload transport of marine gravel. In: Speciality Conference, W.R.D.A. *Coastal Sediments 1991 Proceedings.* pp 703-716.

51. Hey, R.D. (1979) Flow resistance in gravel bed rivers. *Proc. Am. Soc. Civ. Engrs, J. Hydraul. Div.*, **105(HY4)**, 365-379.

52. Kang, S. (1982) Sediment transport in a small glacial stream: Hilda Creek, Alberta. University of Illinois, Chicago. *unpublished M.S. thesis.*

53. Rodriguez-Iturbe, I. and Nordin, C.F. (1968) Time-series analysis of water and sediment discharges. *Bull.Int.Ass.Scient.Hydrol.*, **31**, 69-84.

54. Dowling, J.M. (1974) A note on the use of spectral analysis to detect leads and lags in annual cycles of water quality. *Water Resources Research*, **10**, 343-344.

55. Thornes, J. (1982) Problems in the identification of stability and structure from temporal data series. In: Thorn, C.E. (Ed.) *Space and time in geomorphology.* Allen & Unwin. London. pp 327-354.

56. Bloomfield, P. (1976) Fourier analysis of time-series: an introduction. John Wiley & Sons, N.Y.

57. Gomez, B., Naff, R.L. and Hubbell, D.W. (1989) Temporal variations in bedload transport rates associated with the migration of bedforms. *Earth Surface Processes and Landforms*, **14**, 135-156.

58. Hamamori, A. (1962) *A theoretical investigation on the fluctuations of bedload transport*. Delft Hydraulics Laboratory Report. R4

59. Carey, W.P. (1985) Variability in measured bedload-transport rates. *Water Resources Bulletin*, **21**, 39-48.

60. Carey, W.P. and Hubbell, D.W. (1986) Probability distributions for bedload transport. *Proceedings of the 4th Federal Interagency Sedimentation Conference*. pp 4-131 - 4-140.

61. Bathurst, J.C., Leeks, G.J.L. and Newson, M.D. (1986) Field measurements for hydraulic and geomorphological studies of sediment transport - the special problems of mountain streams. In: Wessels, A.C.E. (Ed.) *Measurement Techniques in Hydraulic Research*. Balkema. Rotterdam. pp 137-151.

62. Warburton, J. (1992) Observations of bedload transport and channel bed changes in a proglacial mountain stream. *Arctic and Alpine Research*, **24**, 195-203.

63. Young, P.C. (1984) Recursive Estimation and time series analysis: an introduction. Springer-Verlag, Berlin.

64. Young, P.C. (1986) Time-series methods and recursive estimation in hydrological systems analysis. In: Kraijenhoff, D.A. and Moll, J.R. (Eds.) *River flow modelling and forecasting*. Dortrecht, Reidel. pp 129-180.

65. Young, P.C. and Benner, S. (1990) microCAPTAIN handbook version 2.0. Centre for Research on Environmental Systems, Institute of Environmental and Biological Sciences.

66. Young, P.C. and Wallis, S.G. (1993) Solute transport and dispersion in channels. In: Beven, K. and Kirkby, M.J. (Eds.) *Channel Network Hydrology*. Wiley. Chichester. pp 129-173.

67. Lapointe, M.F. (1992) Burst-like sediment suspension events in a sand bed river. *Earth Surface Processes & Landforms*, **17**, 253-270.

68. Lapointe, M.F. (1993) Monitoring alluvial sand suspension by eddy correlation. *Earth Surface Processes & Landforms*, **18**, (in press).

69. Soulsby, R.L. (1983) The bottom boundary layer of shelf seas. In: Johns, B. (Ed.) *Physical Oceanography of Coastal and Shelf Seas*. Elsevier. pp 189-266.

70. Soulsby, R.L. (1980) Selecting record length and digitizing rate for near-bed turbulence measurments. *J. Phys. Oceanography*, **10**, 208-219.

71. Thorne, C.R. and Zevenbergen, L.W. (1985) Estimating mean velocity in mountain rivers. *Pro. Am. Soc. Civ. Engrs, J. Hydraul. Engng.*, **111**, 612-624.

72. Bathurst, J.C. (1993) Flow resistance through the channel network. In: Beven, K. and Kirkby, M.J. (Eds.) *Channel Network Hydrology*. John Wiley & Sons. Chichester.

73. Wilkinson, R.H. (1983) A method for evaluating statistical errors associated with logarithmic velocity profiles. *Geomarine Letters*,

74. Jackson, P.S. (1981) On the displacement height in the logarithmic velocity profile. *J. Fluid Mech.*, **111**, 15-25.

75. Robert, A., Roy, A.G. and De Serres, B. (1992) Changes in velocity profiles at roughness transitions in coarse grained channels. *Sedimentology*, **39**, 725-735.

76. Aguirre Pe, J. (1975) Incipient erosion in high gradient open channel flow with artificial roughness elements. *Proc. 16th Congress Intl. Ass. Hydraul. Res.* pp 173-80.

77. Nowell, A.R.M. and Church, M. (1979) Turbulent flow in a depth-limited boundary layer. *J. Geophys. Res.*, **84**, 4816-24.

78. Marchand, J.P., Jarrett, R.D. and Jones, L.L. (1984) *Velocity profile, water surface slope, and bed-material size for selected streams in Colorado*. Lakewood, Colorado. US Geol. Surv. Open-File Rep. 84-733

79. Dyer, K.R. (1970) Current velocity profiles in a [illegible] channel. *Geophysical Journal of the Royal Astronomical Society*, **22**, 153-161.

80. Jarrett, R.D. (1984) Hydraulics of high-gradient streams. *Proc. Am. Soc. Civ. Engrs., J. Hydrul. Engng.*, **110**, 1519-39.

81. Smith, J.D. and McLean, S.R. (1977) Spatially averaged flow over a wavy surface. *J. Geophysics Res.*, **82**, 1735-1746.

82. Carling, P.A., Kelsey, A. and Glaister, M.S. (1992) Effect of bed roughness, particle shape and orientation on initial motion criteria. In: Billi P., Hey, R.D., Thorne, C.R. and Tacconi, P (Eds) *Dynamics of gravel-bed rivers*. John Wiley & Sons Ltd. Chichester. pp 23-40.

83. Raupach, M.R. (1991) Interaction between saltating particles and the airflow. *Acta Mechanica Supplementum*, **1**, 83-96.

84. Kelsey, A., Beven, K.J., Allen, C.M. and Carling, P.A. (1993, in press) Practical tracking model of sediment transport. In: Beven K. J., Chatwin, P.C. and Millbank, J.H. (Eds.) *Mixing and transport in the environment*. John Wiley & Sons. Chichester.

ANNEX 1: TURBULENCE DATA PREPROCESSING AND ANALYSIS.

1.0 *Scope of the work*

In this section the methodology used to analyze the EMCM data is detailed and problems likely to affect data quality and interpretation are highlighted. In general, data processing aims to quantify flow turbulence and Reynolds stresses and to relate these properties to bedload dynamics.

2.0 *Data Screening*

All data from the data logger are downloaded via a PC to a work-station. Single files containing EMCM and SGN data are prepared for each measurement run and channel numbers are assigned for each data set. Raw, uncalibrated data are then plotted and, in order to assess data quality, the mean and standard deviation for each data channel are calculated.

3.0 *Data editing*

In order to screen and edit data sets, files are processed using interactive software, (SERPLO4). This procedure involves the identification of infrequent data spikes by eye and subsequent "flagging" of all suspect points in a given time series. These flags are easily picked up in later processing and are removed using linear interpolations between adjacent data points. Use of SERPLO4 also facilitates first look inter-comparisons between data channels and a rapid "zoom-in", "zoom-out" and scan option enables rapid assessment of data quality.

4.0 *Offsets and trend removal*

Zero offset errors were present on all channels. These were measured carefully in the field before and after individual test runs. The resulting flume calibrations and offsets are applied to the appropriate data channels in each burst record.

A common problem with output from all EMCM systems is a tendency for the zero level to drift through time. However, in the case of data described here, the zero drift was very low during test runs and could be removed effectively using a least squares trend removal technique.

5.0 *EMCM axis rotation*

When deployed, great care was taken to ensure the EMCM axis was in line with the principle streamline of Squaw Creek. However, as accuracy of this technique is subjective, it was necessary to calculate EMCM head rotation angles for perfect alignment with the flow. This is achieved by plotting the apparent vertical mean velocity versus the mean horizontal velocity for successive blocks in a given record. Each plot shows a general trend corresponding to the mean tilt angle throughout the deployment, (correlation coefficients > 95% significant). Uncertainties in zero drift removal, variations in sensor attitude relative to the flow and bed through time and calibration errors combine to give rise to the scatter of data values in such plots. Following the present configuration of the EMCM heads, application of a horizontal rotation through 45_o (Φ) is also required for the channels containing the U and V flow components. This procedure gives time series of the turbulent flow components aligned along the fore/aft and transverse axes of the current meters. Rotation procedures are described in **6.3**.

6.3 *Data Analysis*

6.3.1 Summary of EMCM data

In the processing of EMCM data, both time series and summary statistics are generated in a form which facilitates direct comparison between experiments. In the description of calculated quantities given below the following notation is used:

z	Height of instrument above the bed, (no correction for local scour applied).
$\bar{U}$	Mean velocity along the fore/aft EMCM axis, (positive for downstream flow).
$\bar{v}$	Mean velocity along the transverse EMCM axis, (positive for flow from port to starboard ie; right bank to left bank looking downstream).
u	Horizontal turbulent velocity component.
v	Transverse " " "
w	Vertical " " "
ρ	Fluid density

6.3.2 Spectra

Energy spectra of u, v and w are obtained from the 9.1 minute runs (16 384 data values) using the fast Fourier transform (FFT) routine. The raw spectral estimates are smoothed using a weighted averaging scheme and plotted against frequency on log axes (a form generally used for turbulence spectra). The cospectra uw and vw are obtained by combining raw spectral estimates and subsequently smoothed using a weighted scheme. Cospectra are plotted in the conventional "equal area-equal energy form".

6.3.3 Time series and statistics

As described above, EMCM data requires suitable rotation in both the horizontal and vertical planes. These operations are defined below where the subscripts p and s indicate port and starboard EMCM heads respectively.

vertical rotation angle,	$\theta_1 = \tan^{-1}(\bar{w}_p/\bar{u}_p)$;
" " "	$\theta_2 = \tan^{-1}(\bar{w}_s/\bar{u}_s)$;
applying vertical rotation,	$w_p = w_p\cos\theta_1 - u_p\sin\theta_1$;
" " "	$u_p = w_p\sin\theta_1 - u_p\cos\theta_1$;
" " "	$w_s = w_s\cos\theta_2 - u_s\sin\theta_2$;
" " "	$u_s = w_s\sin\theta_2 - u_s\cos\theta_2$;
applying horizontal rotation,	$U = (u_s\sin\Phi) + (u_b\cos\Phi)$;
" " "	$V = (u_s\sin\Phi) - (u_b\cos\Phi)$:

Following rotation, software analyzing EMCM data produces useful summary statistics (see examples in Table 3). In addition, the following 30 Hz time series are calculated.

current speed, $S = (\bar{U}^2+\bar{V}^2)^{1/2}$;

current direction $\Psi_c = \tan^{-1}(\bar{V}/\bar{U})$, degrees anti-clockwise of the fore/aft axis ;

fore/aft Reynolds stresses,

$$Re_1 = \overline{-vw},$$

transverse Reynolds stresses,

$$Re_2 = -\overline{vw},$$

stress direction,

$$\psi_s = \tan^{-1}((\overline{-vw}/(\overline{-uw}));$$

stress direction re. current,

$$\phi_s = \psi_s - \psi_c ;$$

stress magnitude,

$$\tau/\rho = ((\overline{-uw^2}) + (\overline{-vw^2})^{1/2};$$

and, turbulent kinetic energy,

$$E = 1/2(\overline{u_t^2} + \overline{v_t^2} + \overline{w_t^2}).$$

6.3.4 Errors

Whilst every precaution is made to exclude errors from the processed data some unwanted "noise" must be tolerated. Error in EMCM rotation angle give rise to large errors in Reynolds stress values. Using the criteria outlined by Soulsby[70], it is considered that although suffering from the same minor imperfections, the processed data are acceptably accurate and are representative of turbulent flow conditions in Squaw Creek.

Table 1

Example of particle size distribution of bed material (mm).

	d_5	d_{16}	d_{25}	d_{50}	d_{75}	d_{84}	d_{95}
Bar	0.4	1.8	5	24	60	90	200
Channel	0.5	2.8	18	140	190	200	220

after Bunte[29]

Table 2

Summary of $\bar{U}$, RMS values for u, v and w, u_* values from TKE and RS measurements and C_d and z_o values during runs 4 to 8 in Squaw Creek, June 1992.

Run	U	√u'	√v'	√w'	u_{*TKE}	u_{*RS}	C_d	z_o
4	133.1	10.6	11.6	6.0	5.2	7.9	2.5	0.8
5	131.0	11.3	12.6	5.7	5.6	7.9	2.7	1.0
6	131.2	11.1	12.2	6.0	5.4	8.1	2.8	1.0
7	125.8	12.3	11.9	5.3	5.5	7.8	2.9	1.3
8	127.6	10.6	11.6	9.0	5.6	9.9	3.9	3.9

Table 3

Useful data summary statistics output for Run 4, Squaw Creek data.

Measurement period	≈ 30 minutes
Logging period	≈ 30Hz
Average current speed	≈ 133.1 cm s^{-1}
RMS u	≈ 10.6 cm s^{-1}
RMS v	≈ 11.6 cm s^{-1}
RMS w	≈ 6.0 cm s^{-1}
u_{*TKE}	≈ 5.2 cm s^{-1}
u_{*RS}	≈ 7.9 cm s^{-1}
C_d	≈ 0.0025
z_o	≈ 0.0081 cm.

Figure 1.

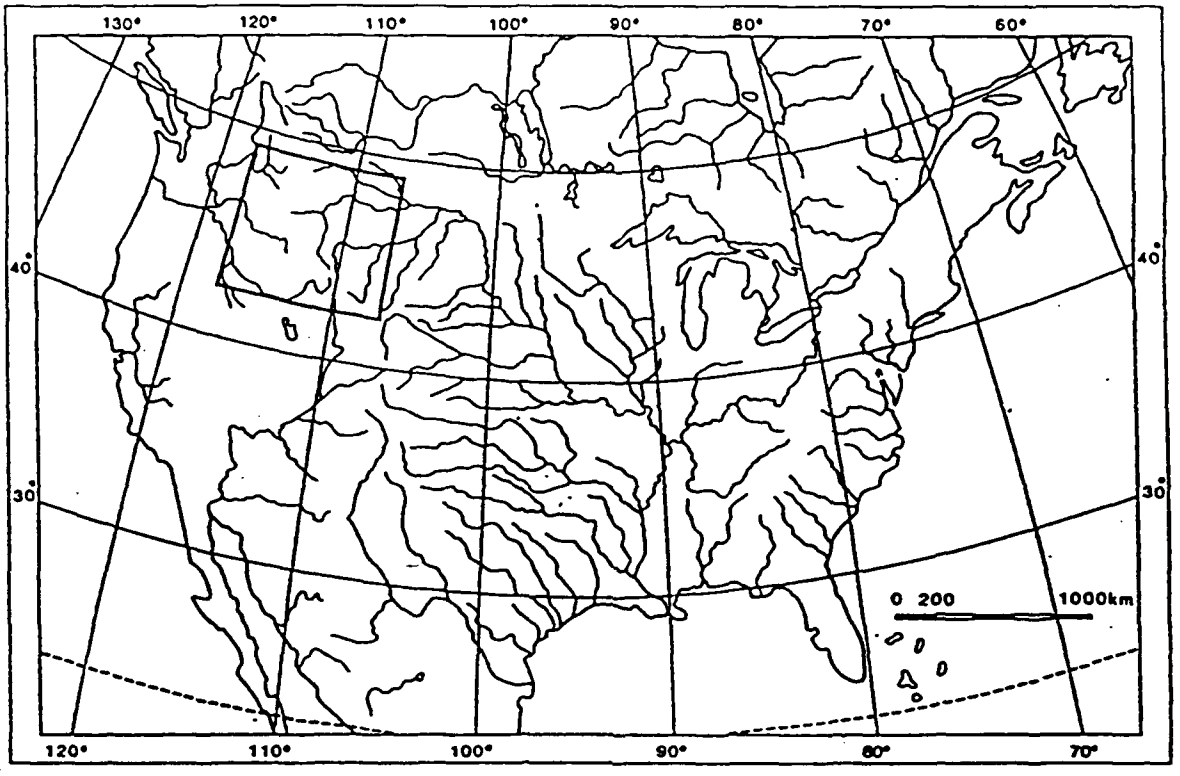
130°
120°
110°
100°
90°
80°
70°
60°
40°
30°
0 200 1000km

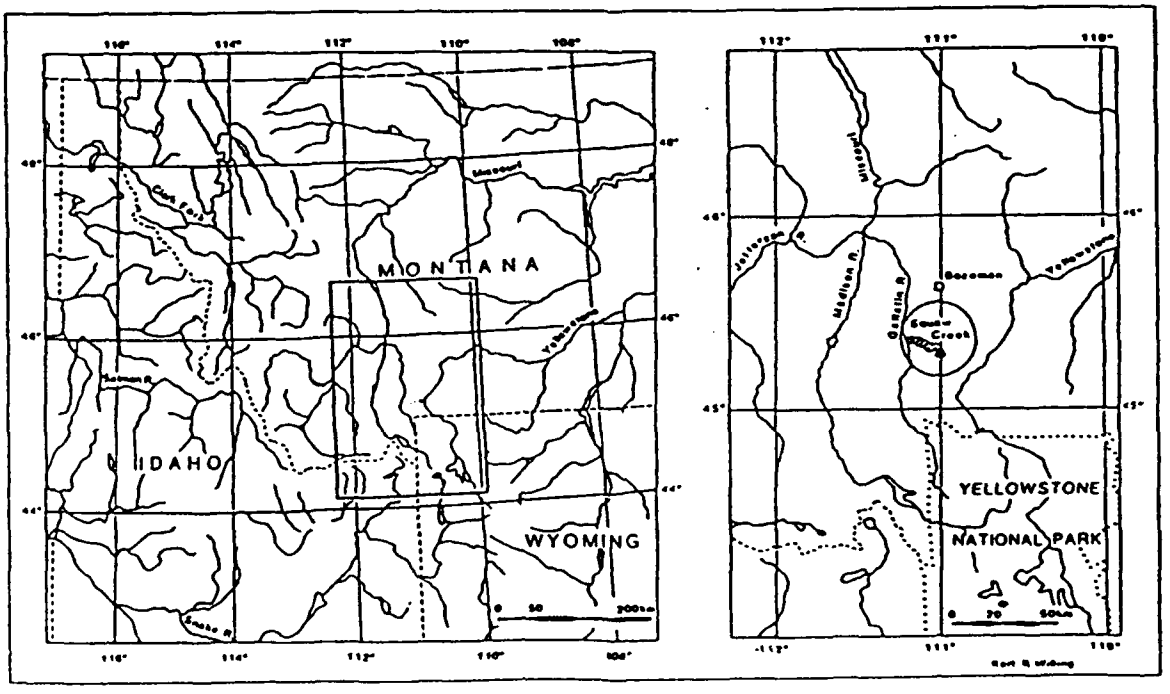
MONTANA
IDAHO
WYOMING
YELLOWSTONE
NATIONAL PARK

Figure 2.

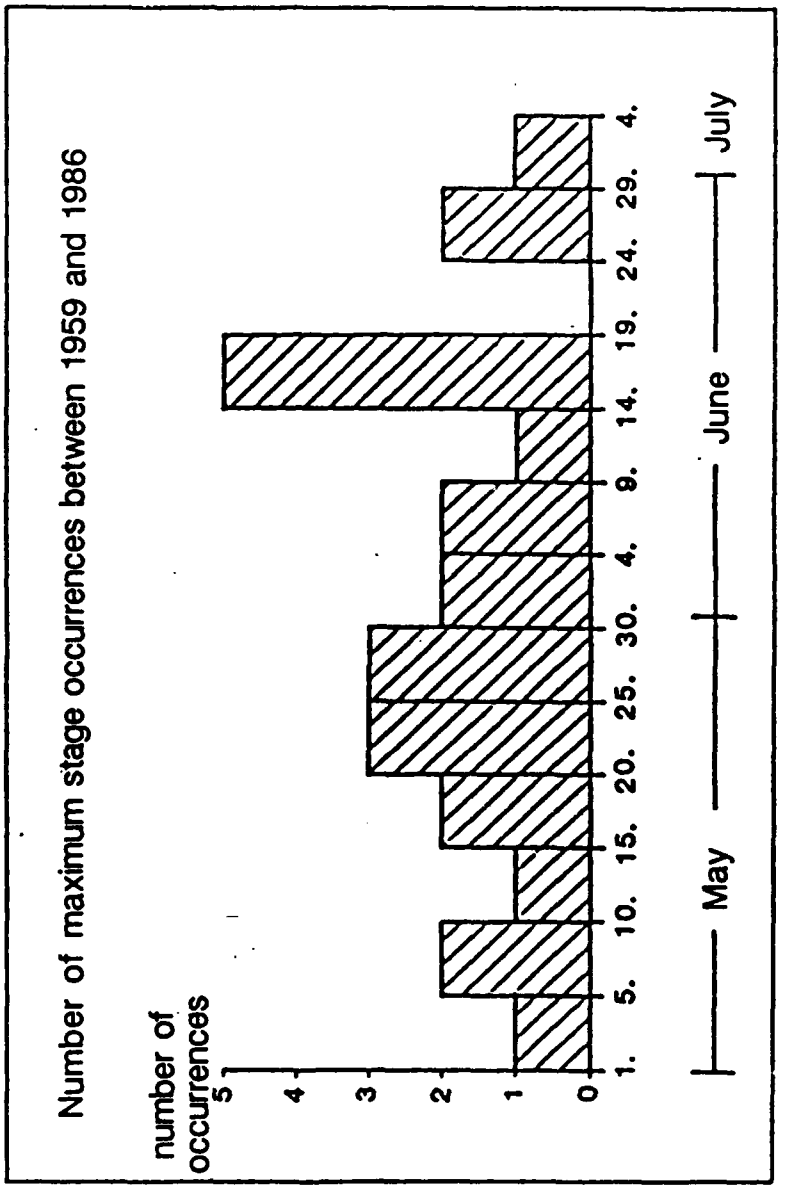
Number of maximum stage occurrences between 1959 and 1986
number of occurrences
5
4
3
2
1
0
1.
5.
10.
15.
20.
25.
30.
4.
9.
14.
19.
24.
29.
4.
May
June
July

Figure 3.

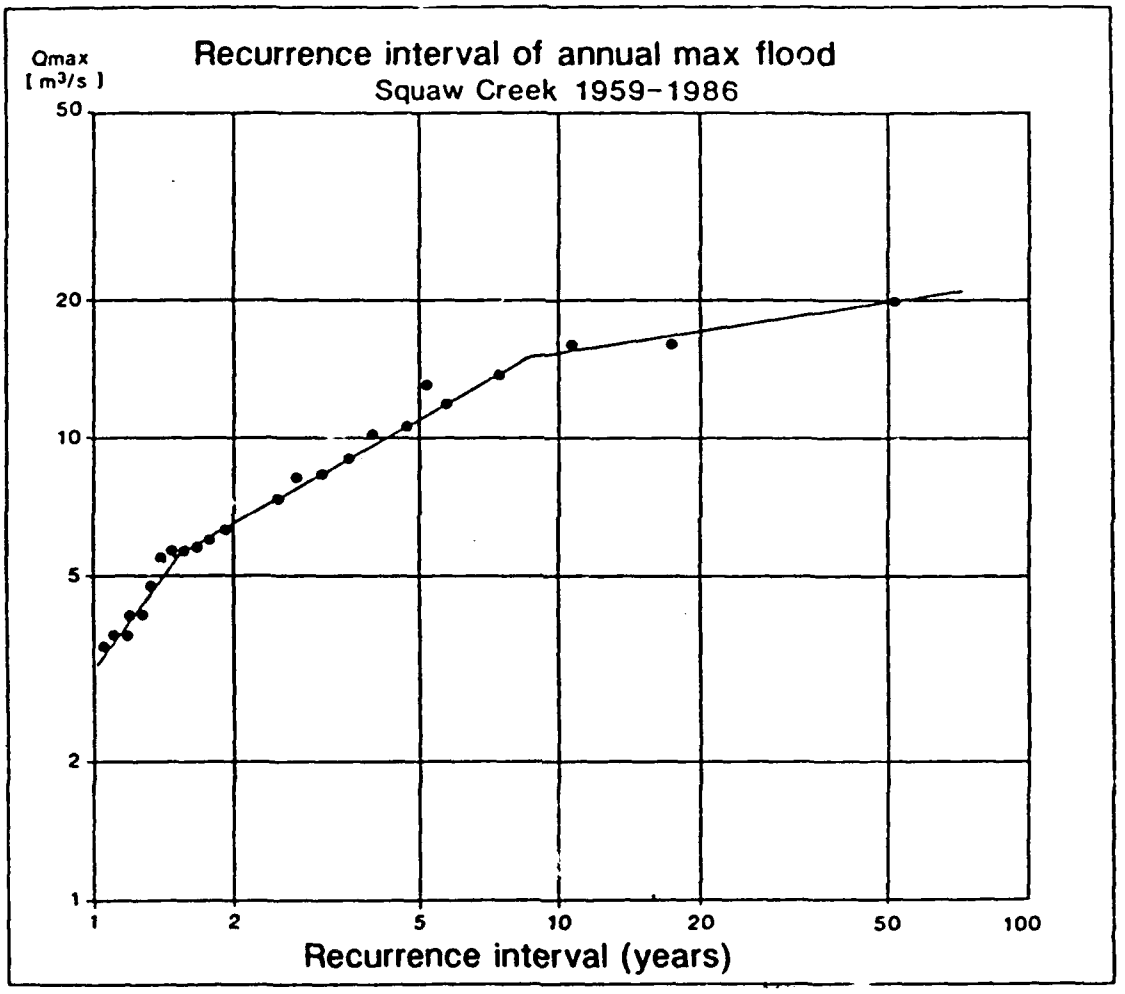
Qmax
[m³/s]
Recurrence interval of annual max flood
Squaw Creek 1959-1986
50
20
10
5
2
1
1
2
5
10
20
50
100
Recurrence interval (years)

SQUAW CREEK BASIN, GALLATIN COUNTY, MONTANA : GENERAL GEOLOGY

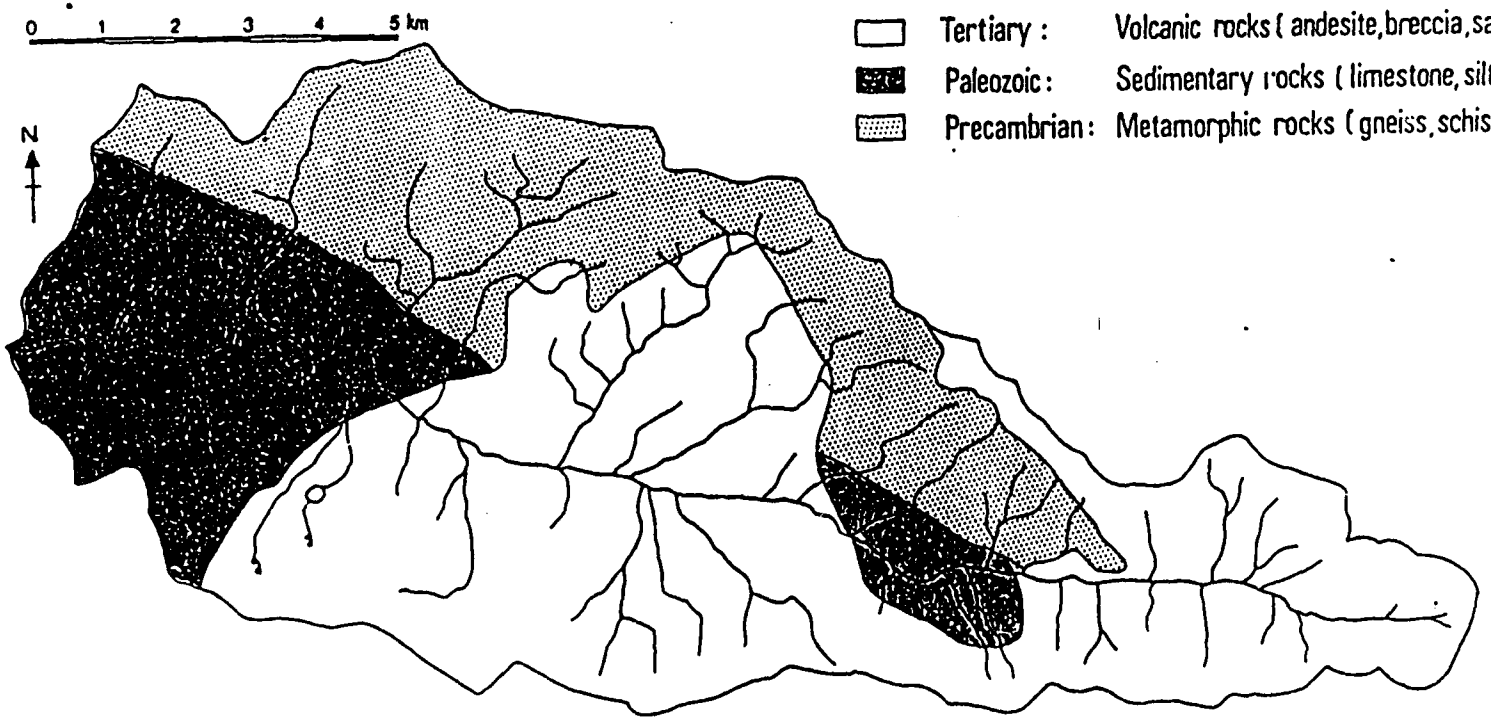

Figure 4.

Figure 5.

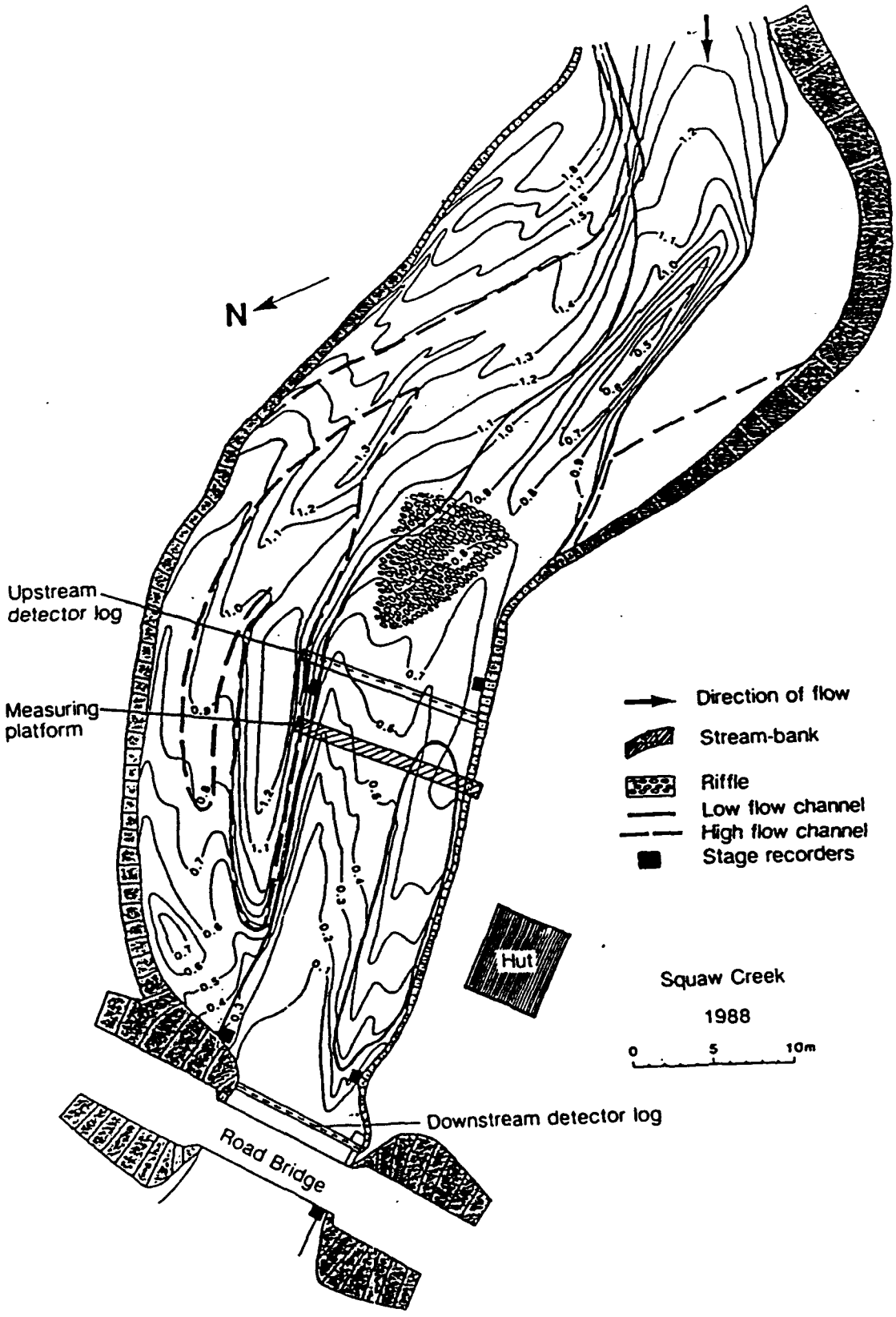
N
Upstream detector log
Measuring platform
Direction of flow
Stream-bank
Riffle
Low flow channel
High flow channel
Stage recorders
Hut
Squaw Creek
1988
0 5 10m
Downstream detector log
Road Bridge

Figure 6.

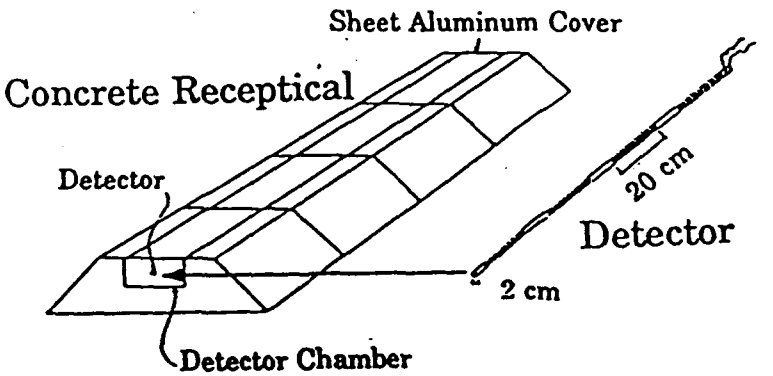

Schematic diagram of 1981 detector (after Custer & Ergenzinger, 1983)

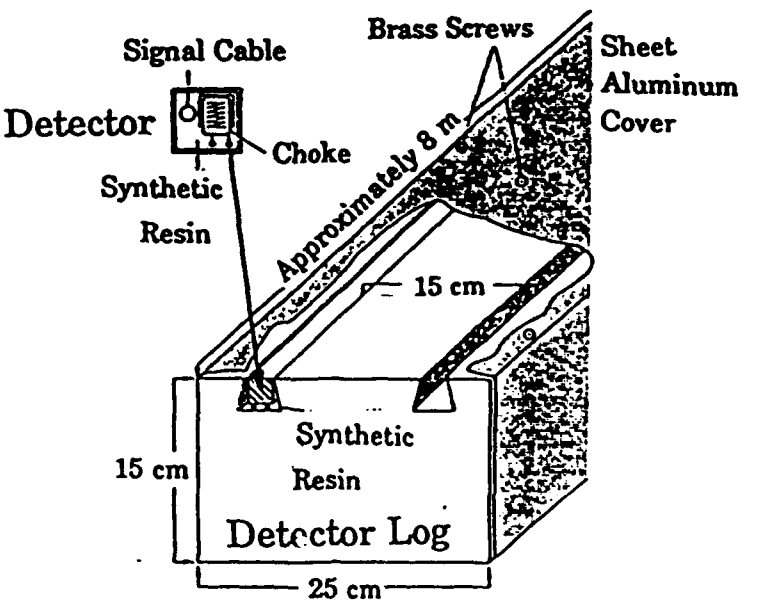

Schematic diagram of the 1986 detector (from Spieker & Ergenzinger, 1990)

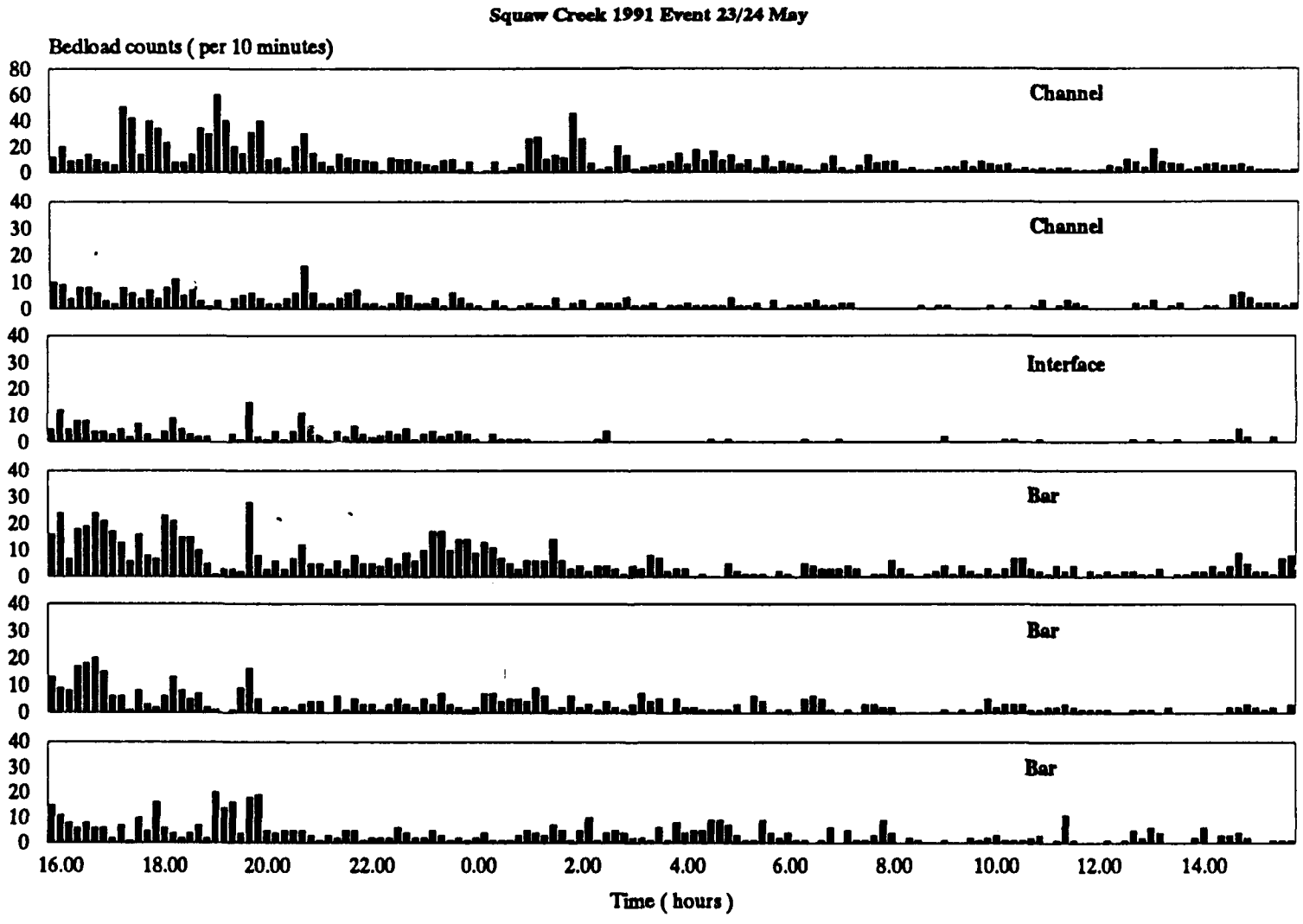
Squaw Creek 1991 Event 23/24 May
Bedload counts (per 10 minutes)
Channel
Channel
Interface
Bar
Bar
Bar
16.00
18.00
20.00
22.00
0.00
2.00
4.00
6.00
8.00
10.00
12.00
14.00
Time (hours)

Figure 7.

Figure 8.

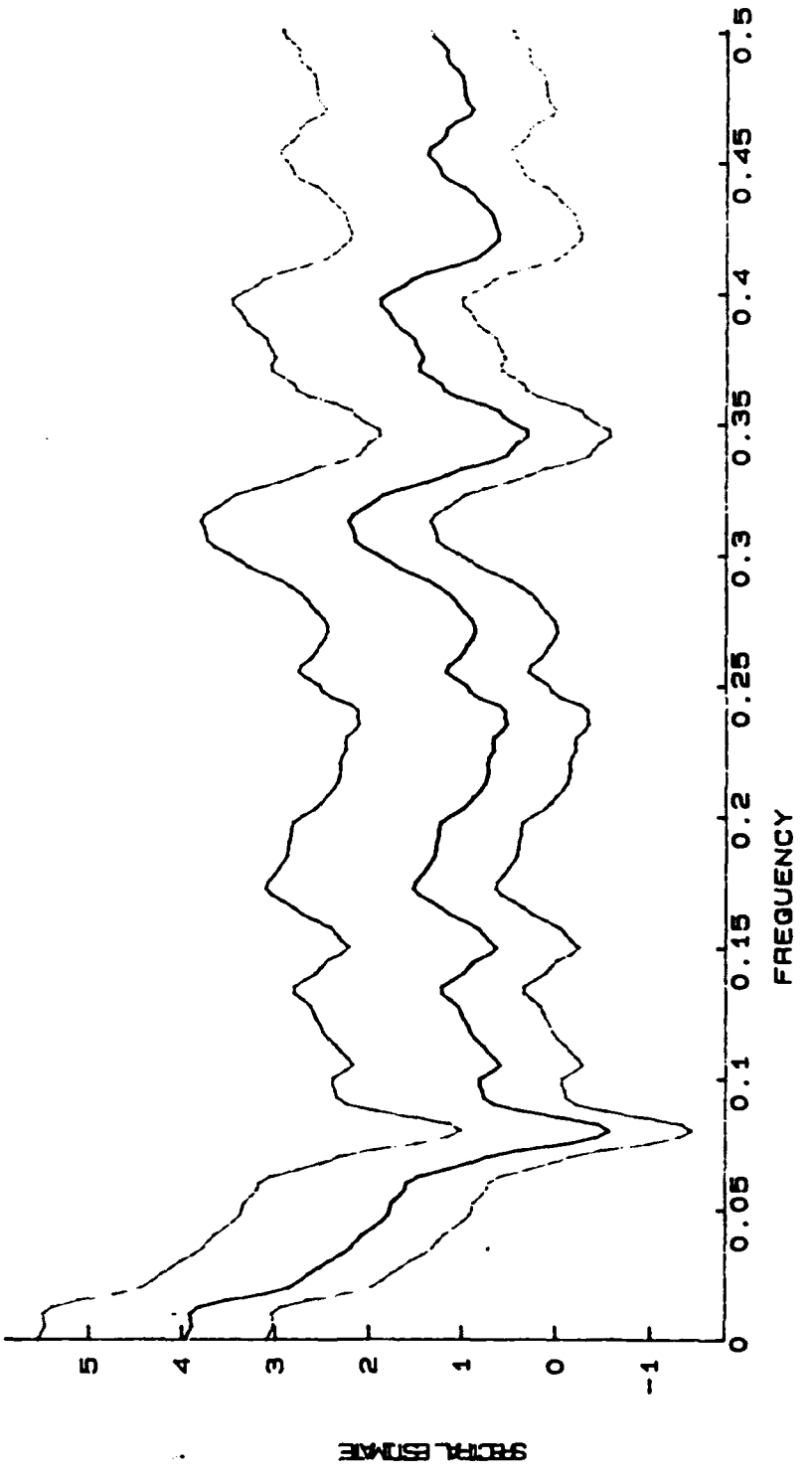
SPECTRAL ESTIMATE
5
4
3
2
1
0
-1
0
0.05
0.1
0.15
0.2
0.25
0.3
0.35
0.4
0.45
0.5
FREQUENCY

Figure 9.

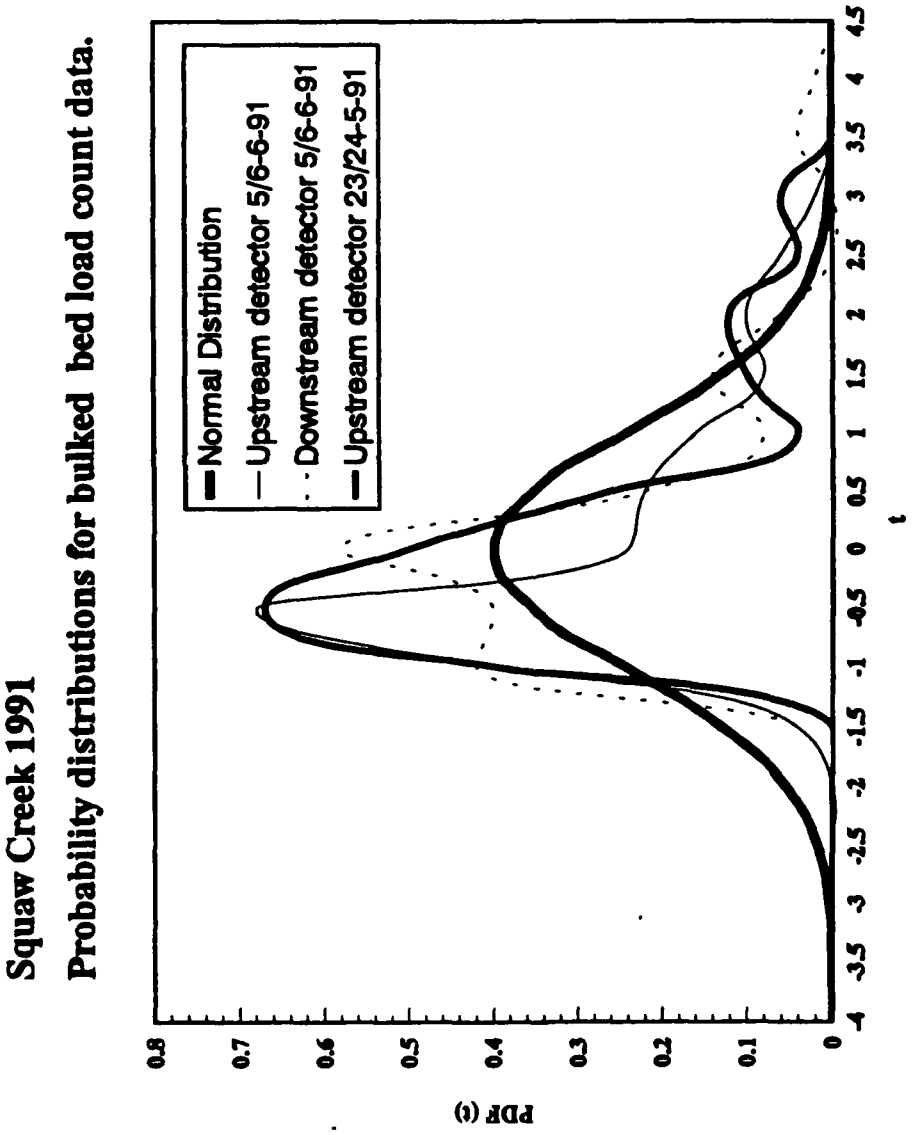
Squaw Creek 1991
Probability distributions for bulked bed load count data.
Normal Distribution
Upstream detector 5/6-6-91
Downstream detector 5/6-6-91
Upstream detector 23/24-5-91
PDF (t)
t
0.8
0.7
0.6
0.5
0.4
0.3
0.2
0.1
0
-4
-3.5
-3
-2.5
-2
-1.5
-1
-0.5
0
0.5
1
1.5
2
2.5
3
3.5
4
4.5

Figure 10.

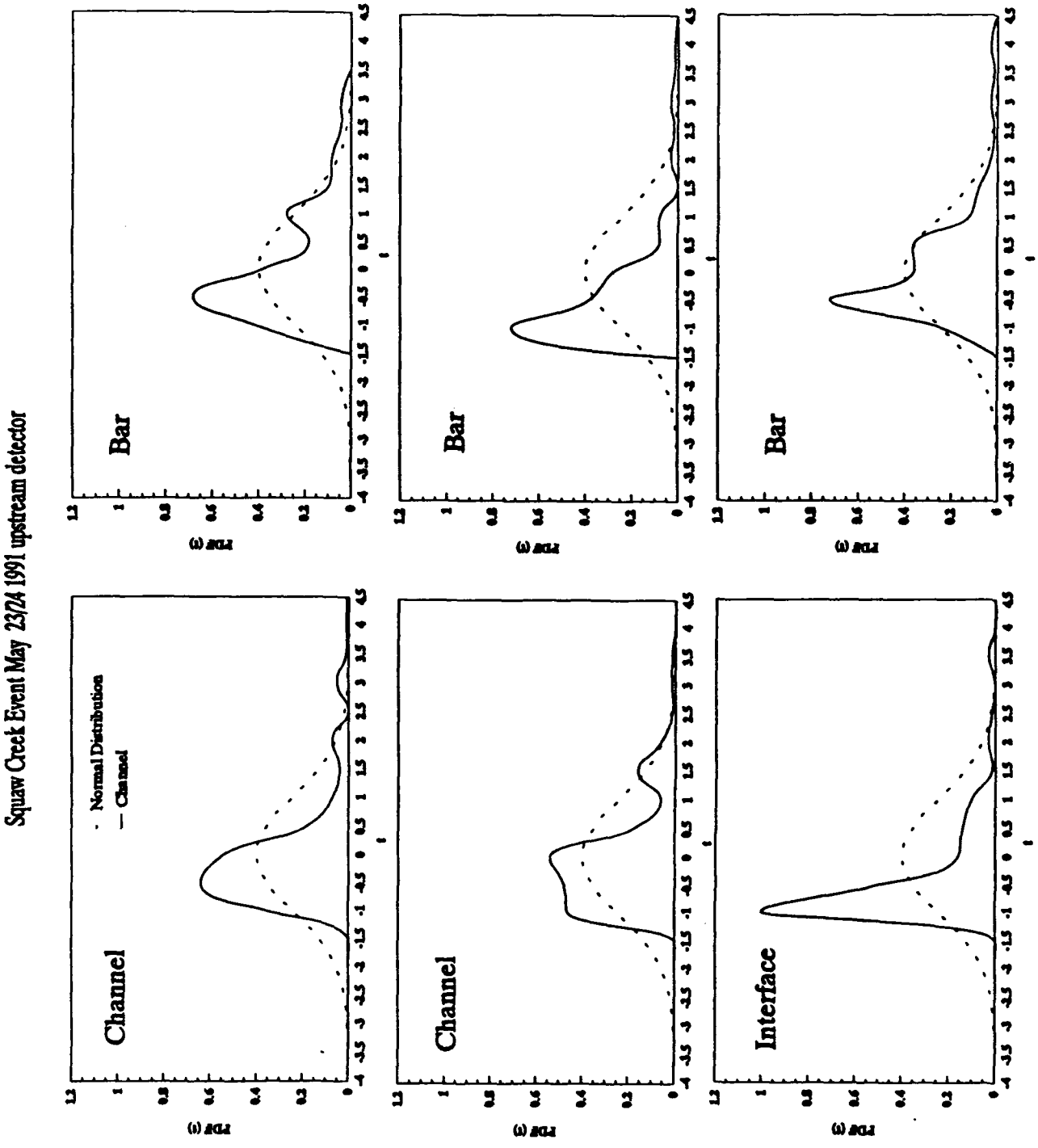
Squaw Creek Event May 23/24 1991 upstream detector
Normal Distribution
Channel
Channel
Bar
Channel
Bar
Interface
Bar
PDF (f)
f

Figure 11.

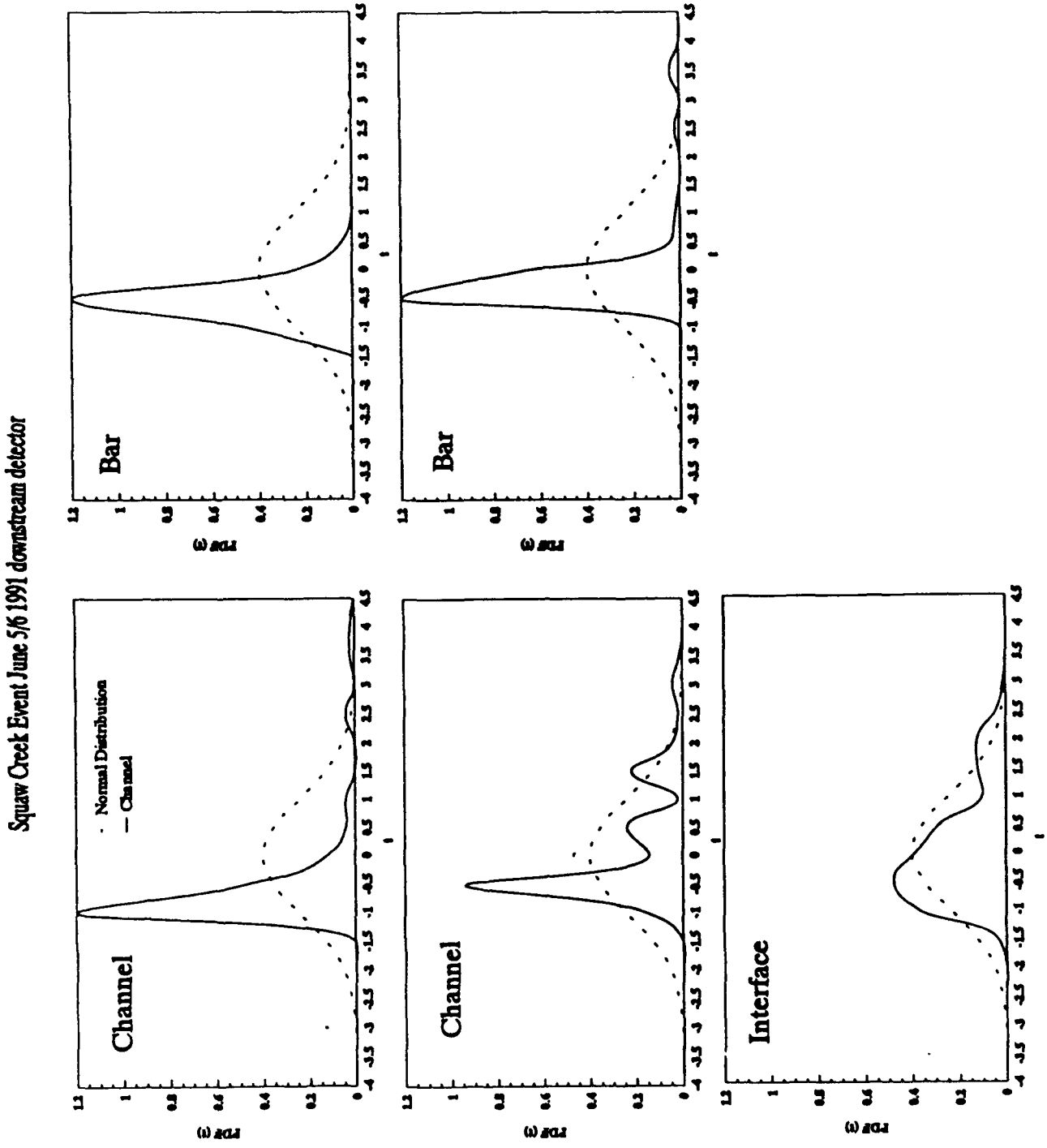
Squaw Creek Event June 5/6 1991 downstream detector
Normal Distribution
Channel
Channel
Bar
Channel
Bar
Interface

Figure 12.

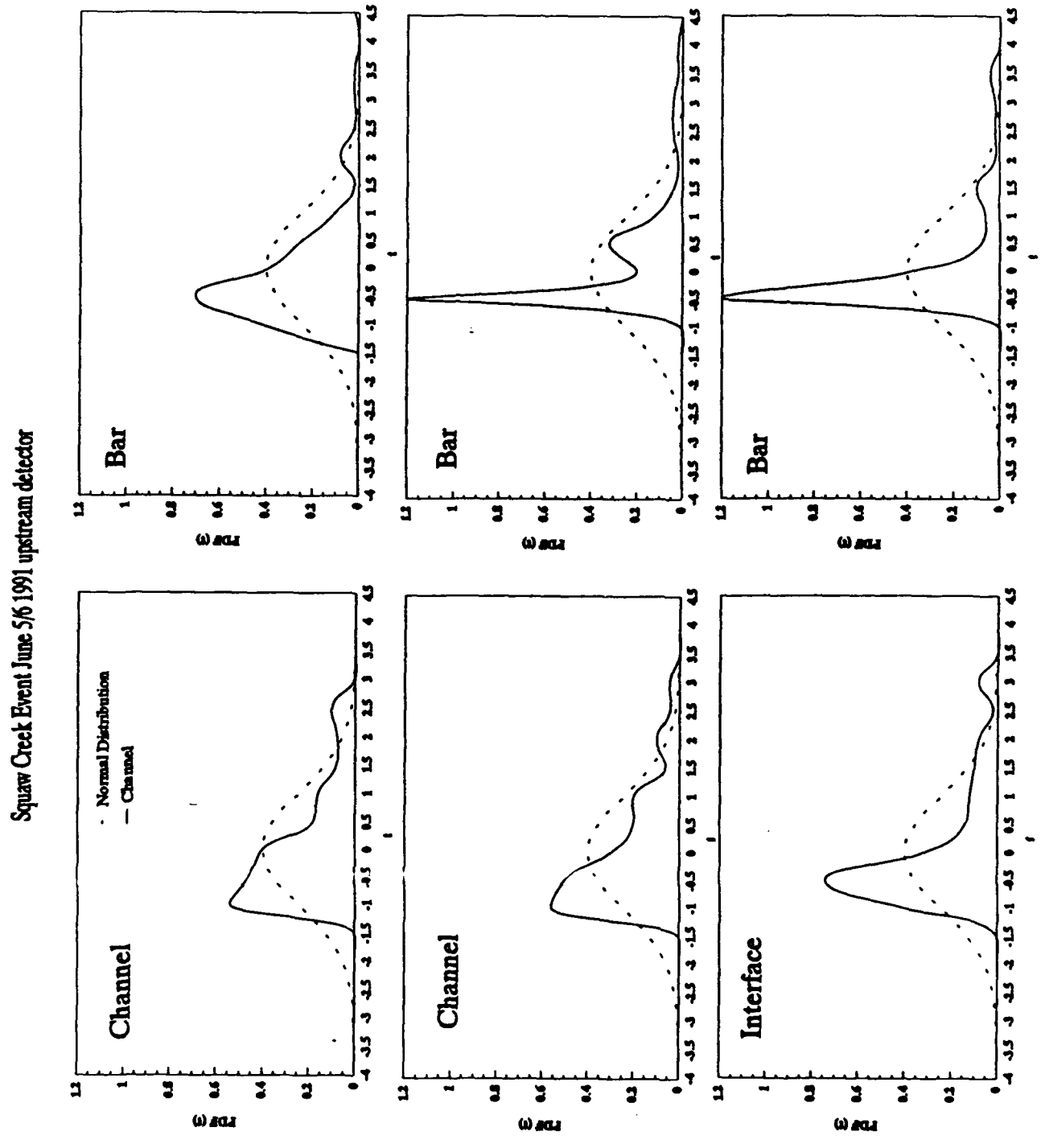
Squaw Creek Event June 5/6 1991 upstream detector
Normal Distribution
Channel
Channel
Channel
Bar
Bar
Bar
Interface
PDF (f)
f

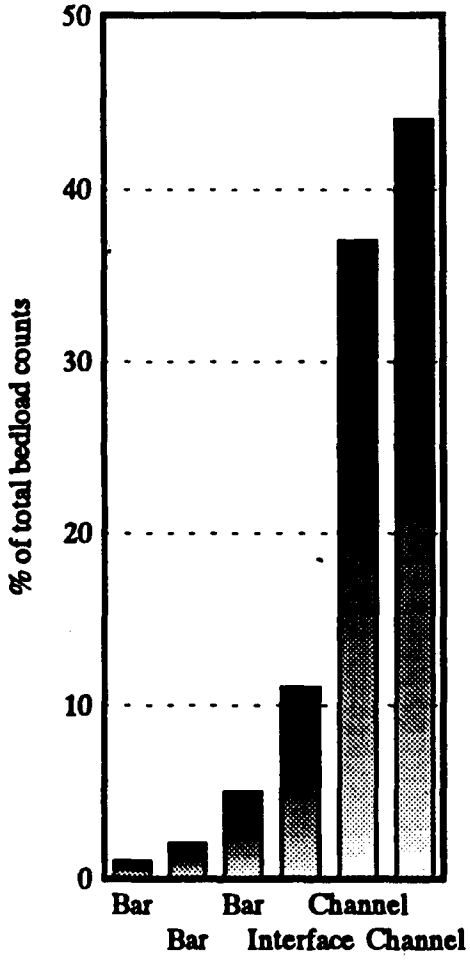

Percentage of bedload counts on upstream detector event 5/6th June 1991

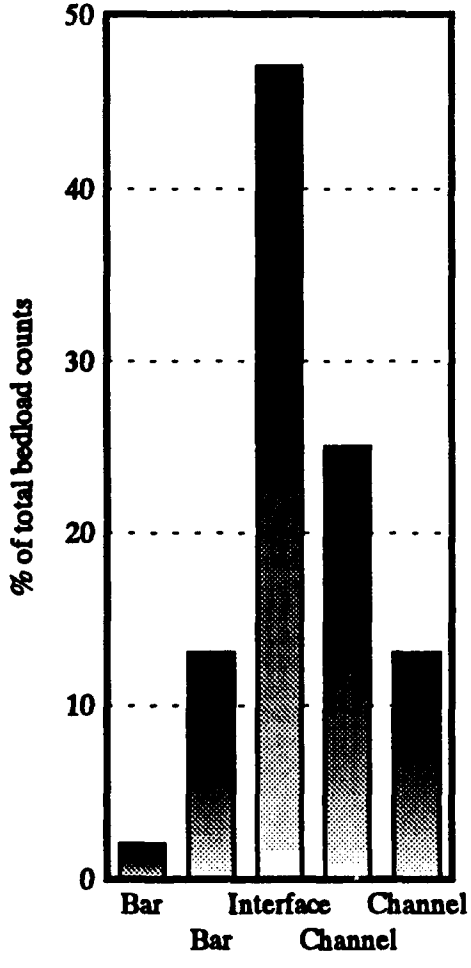

Percentage of bedload counts on downstream detector event 5/6th June 1991

Figure 13.

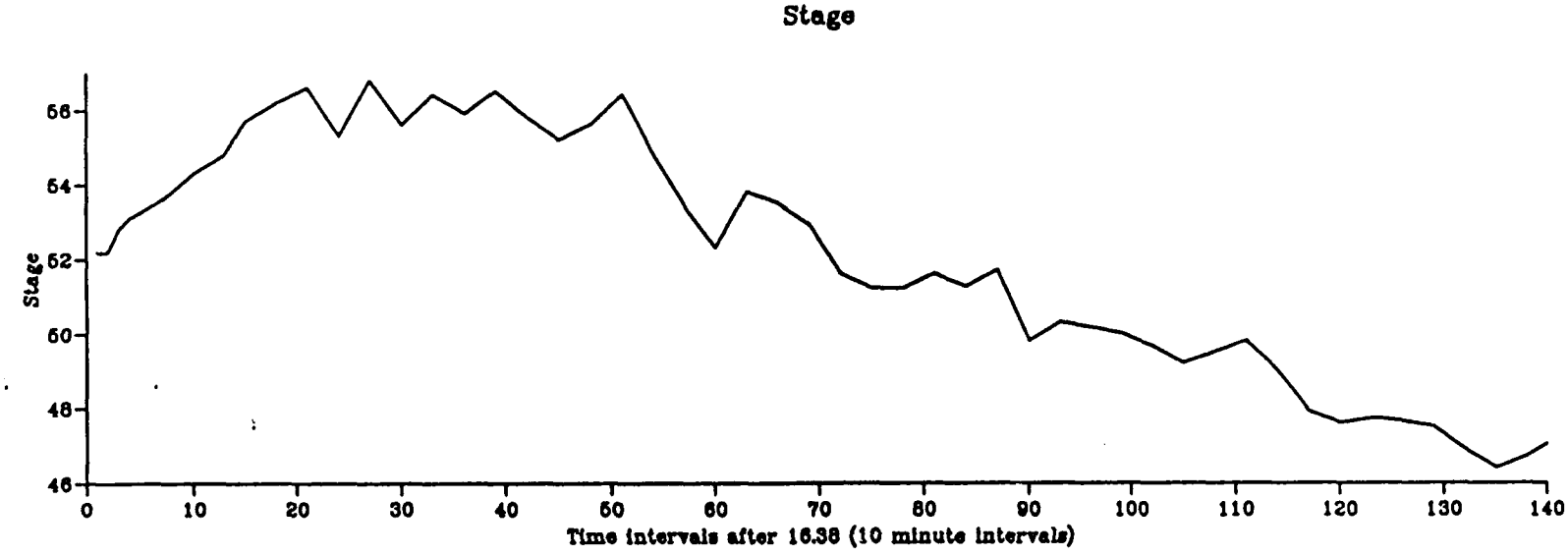
Stage
Stage
56
54
52
50
48
46
0
10
20
30
40
50
60
70
80
90
100
110
120
130
140
Time intervals after 16.38 (10 minute intervals)

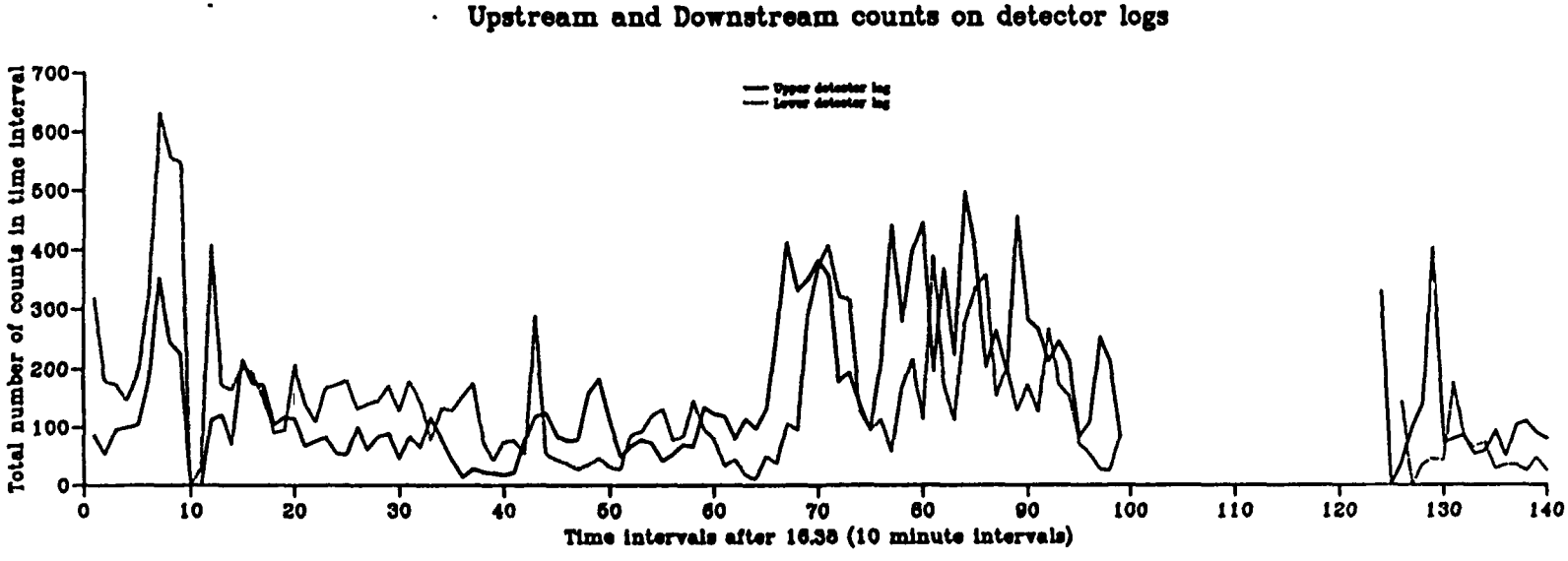
Upstream and Downstream counts on detector logs
Total number of counts in time interval
700
600
500
400
300
200
100
0
0
10
20
30
40
50
60
70
80
90
100
110
120
130
140
Time intervals after 16.38 (10 minute intervals)

Figure 14.

Figure 15.

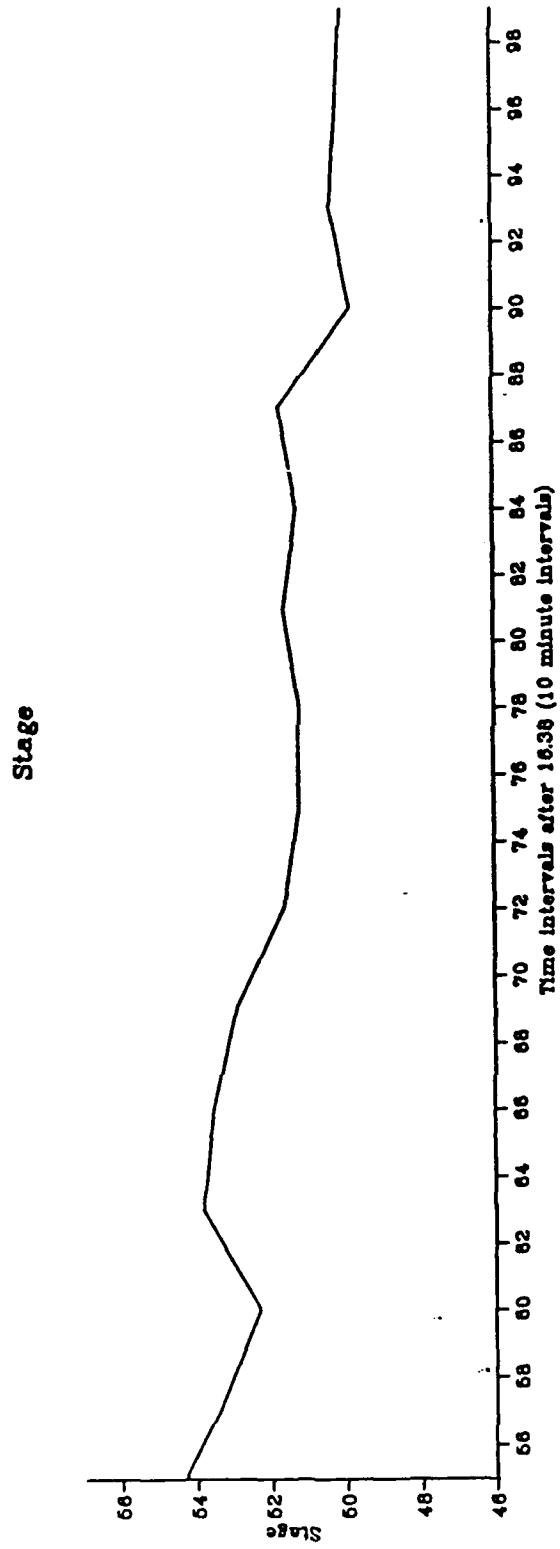
Stage
Stage
Time intervals after 16:30 (10 minute intervals)

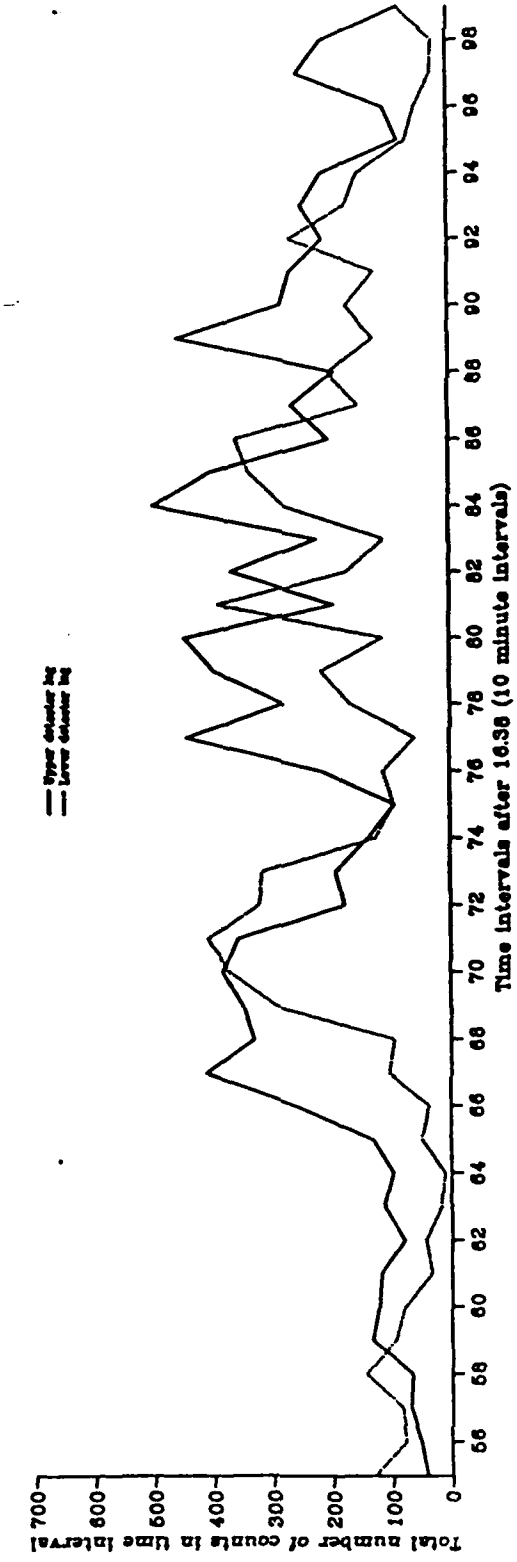
Upstream and Downstream counts on detector logs
Total number of counts in time interval
Time intervals after 16:30 (10 minute intervals)

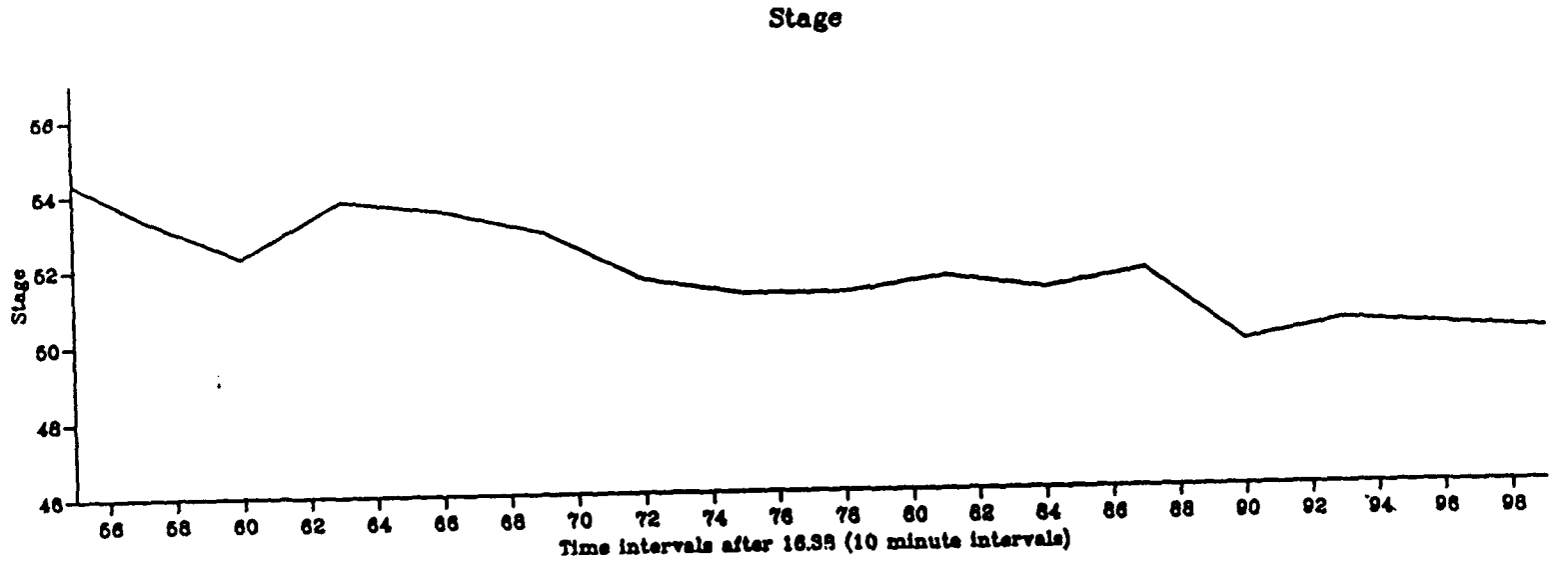
Stage
Stage
66
64
62
60
58
56
56 58 60 62 64 66 68 70 72 74 76 78 80 82 84 86 88 90 92 94 96 98
Time intervals after 16.38 (10 minute intervals)

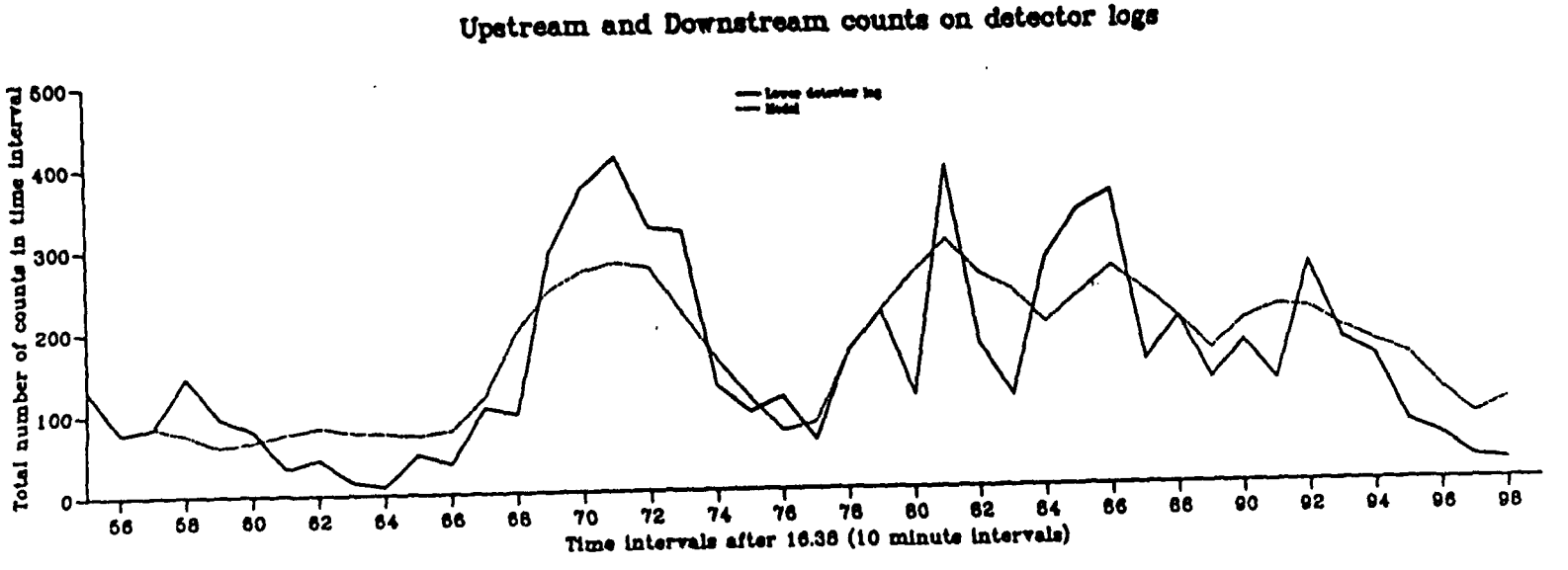
Upstream and Downstream counts on detector logs
Total number of counts in time interval
500
400
300
200
100
0
56 58 60 62 64 66 68 70 72 74 76 78 80 82 84 86 88 90 92 94 96 98
Time intervals after 16.38 (10 minute intervals)

Figure 16.

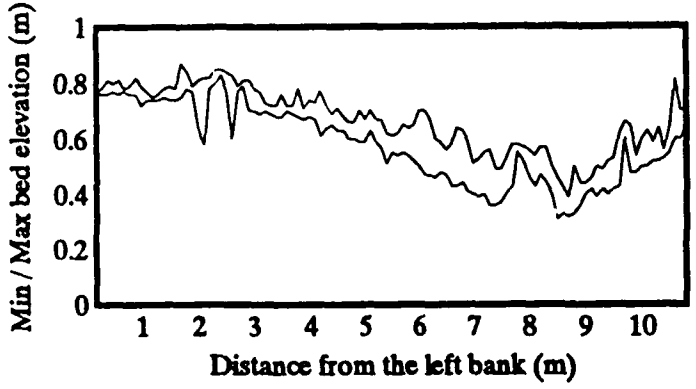

Maximum and minimum bed elevation at upstream section event 23/24 May 1991

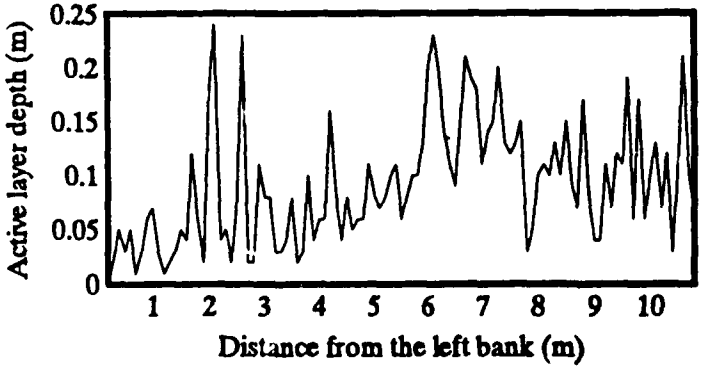

Active layer thickness across upstream section event 23/24 May 1991

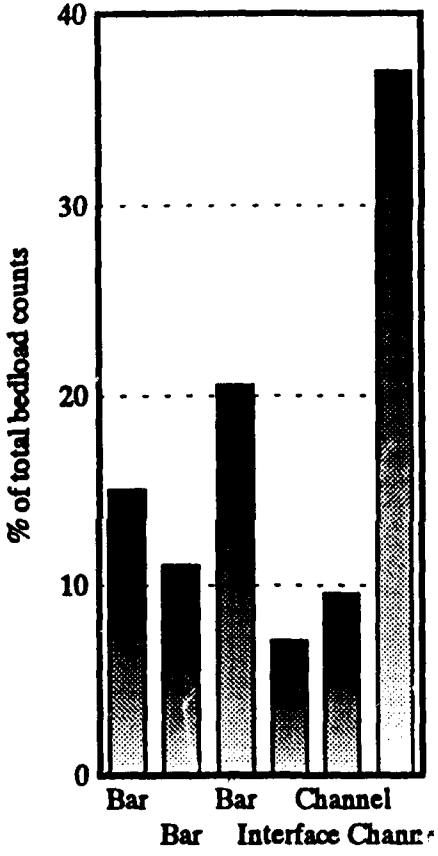

Percentage of bedload counts on upstream detector event 23/24 May 1991

Figure 17.

Figure 18.

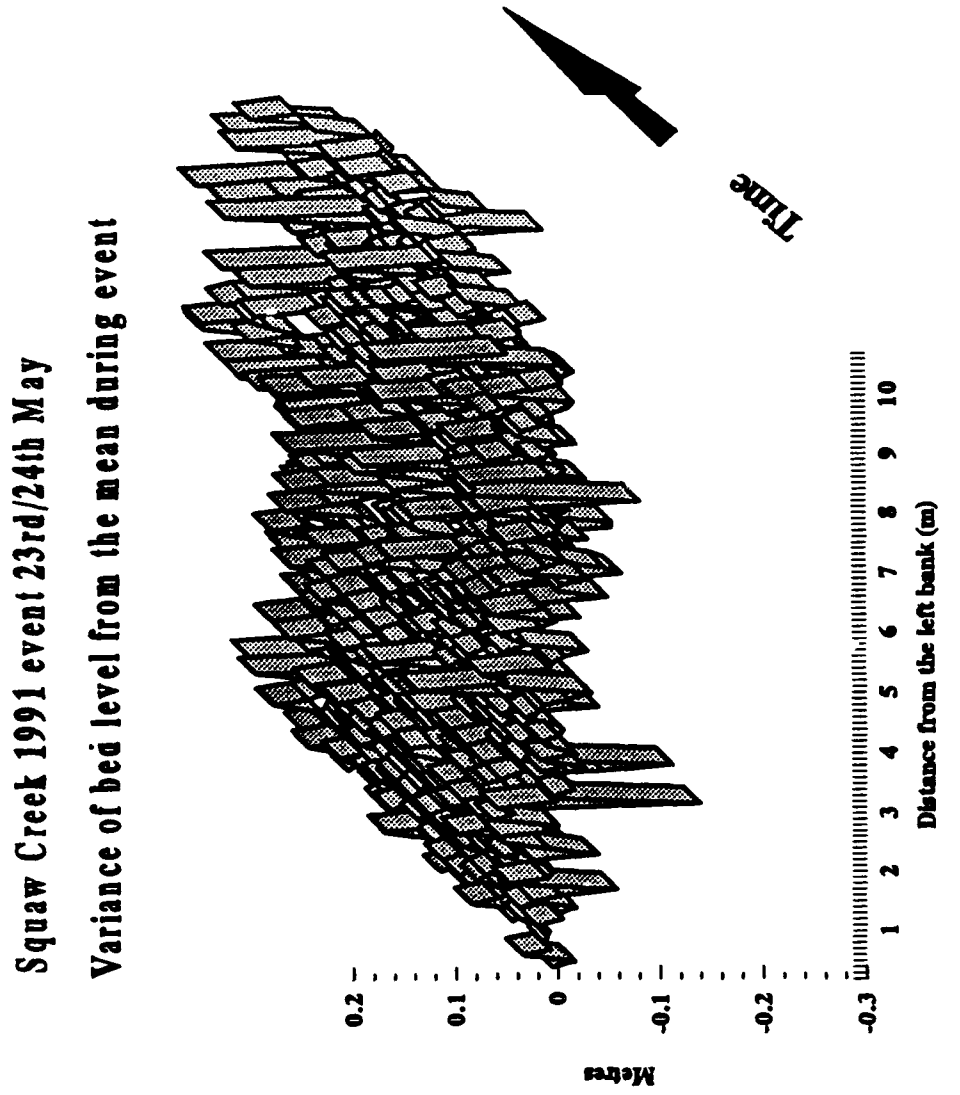
Squaw Creek 1991 event 23rd/24th May
Variance of bed level from the mean during event
Time
Meters
0.2
0.1
0
-0.1
-0.2
-0.3
1 2 3 4 5 6 7 8 9 10
Distance from the left bank (m)

Figure 19.

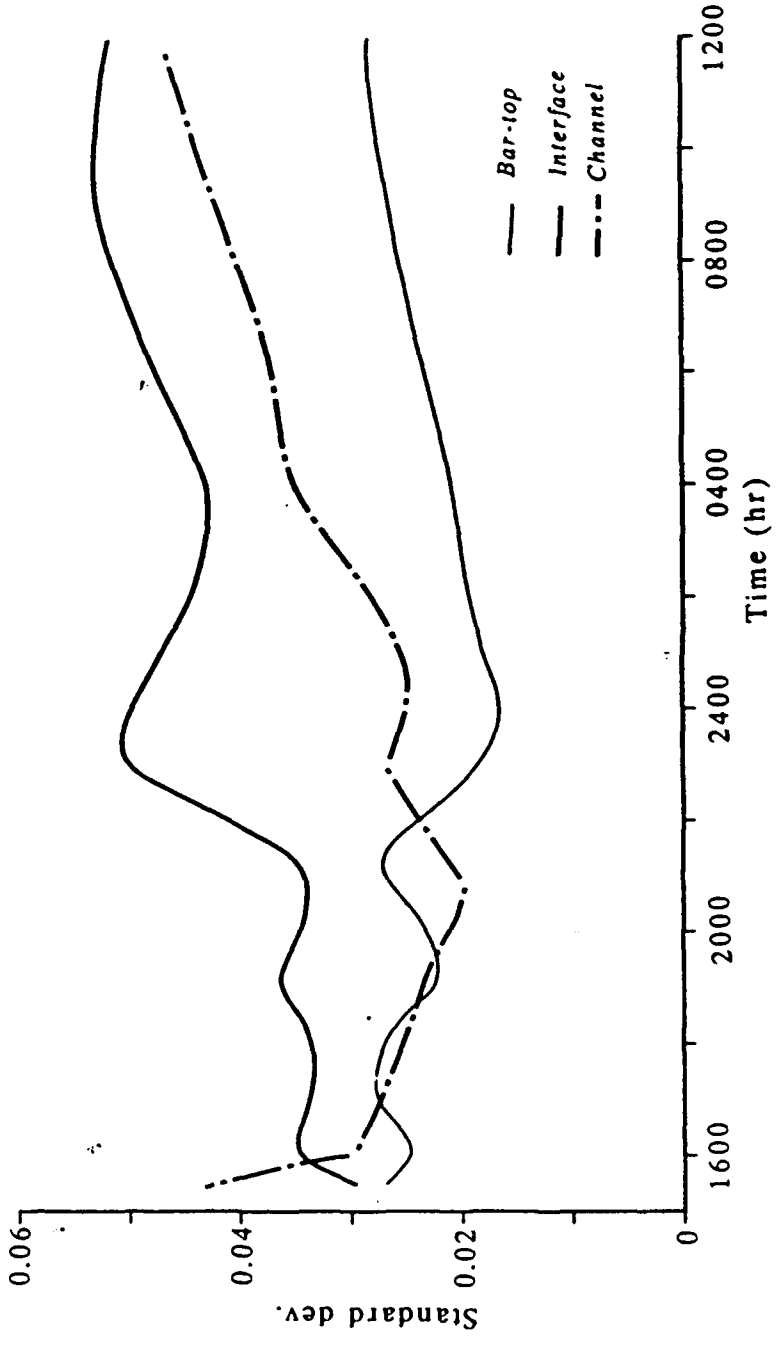
Bar-top
Interface
Channel
Standard dev.
0.06
0.04
0.02
0
1600
2000
2400
0400
0800
1200
Time (hr)

Figure 20.

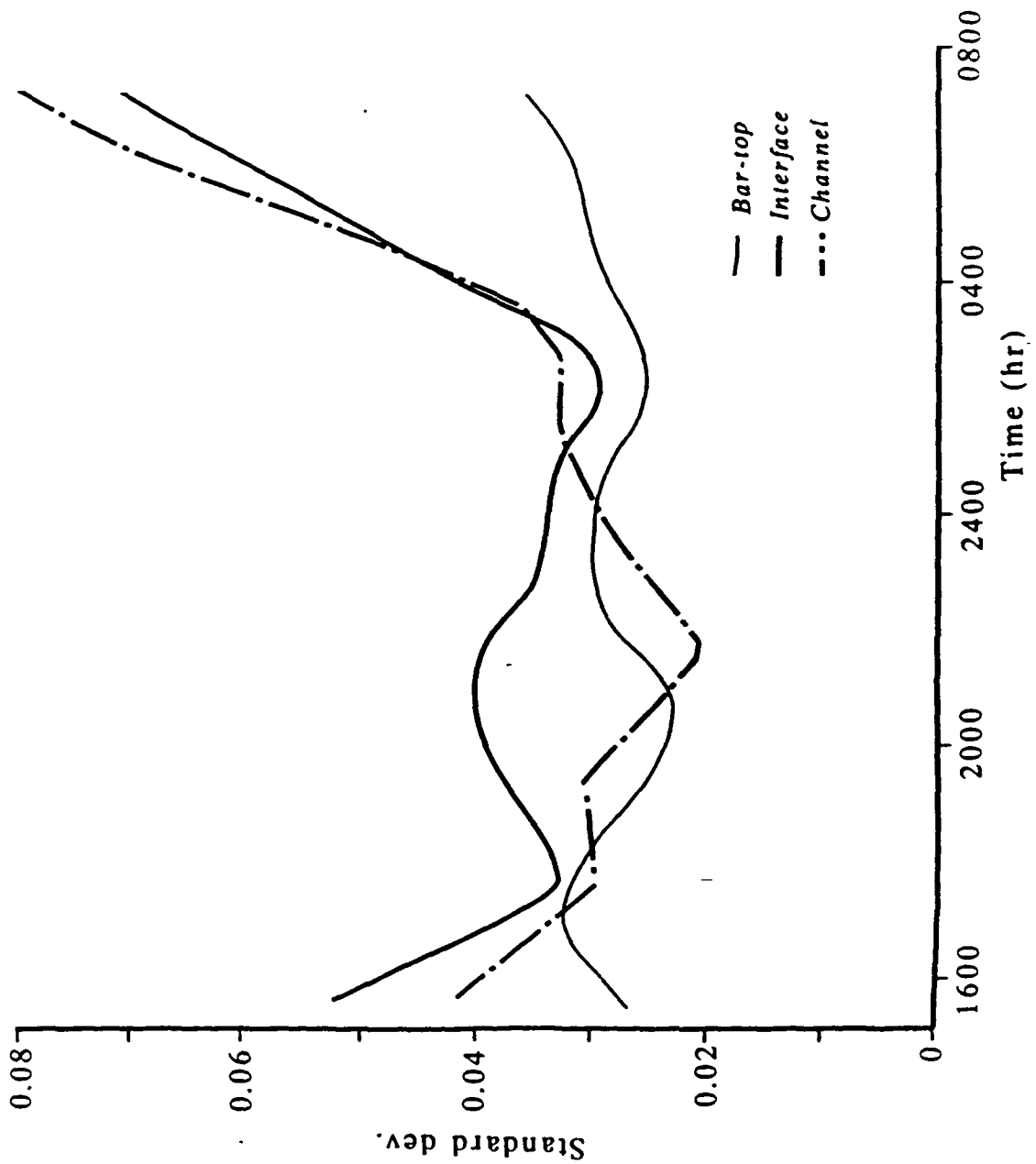
Standard dev.
0.08
0.06
0.04
0.02
0
1600
2000
2400
0400
0800
Time (hr)
Bar-top
Interface
Channel

Figure 21.

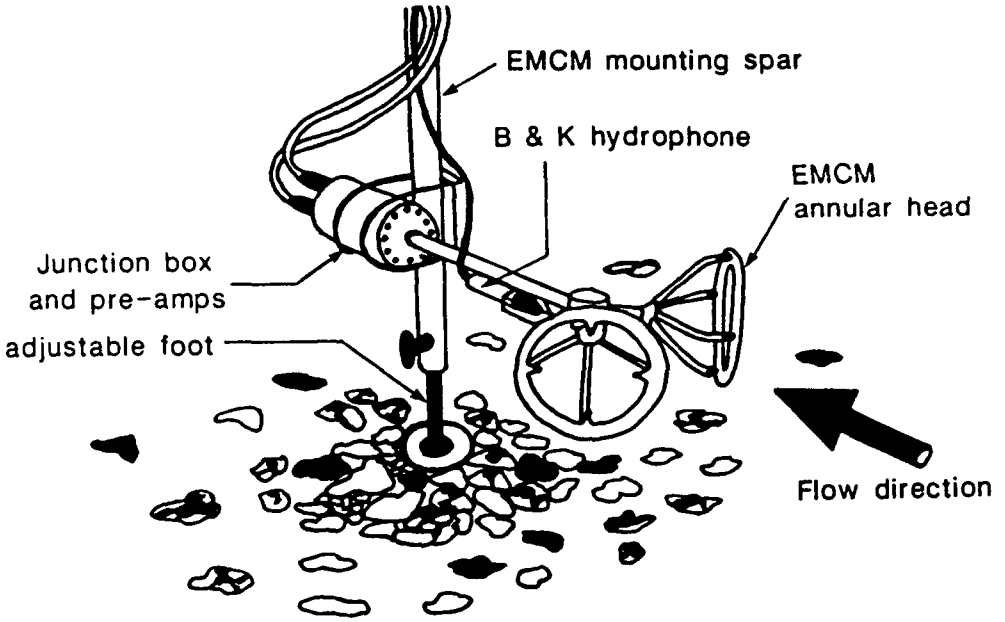
EMCM mounting spar
B & K hydrophone
EMCM
annular head
Junction box
and pre-amps
adjustable foot
Flow direction

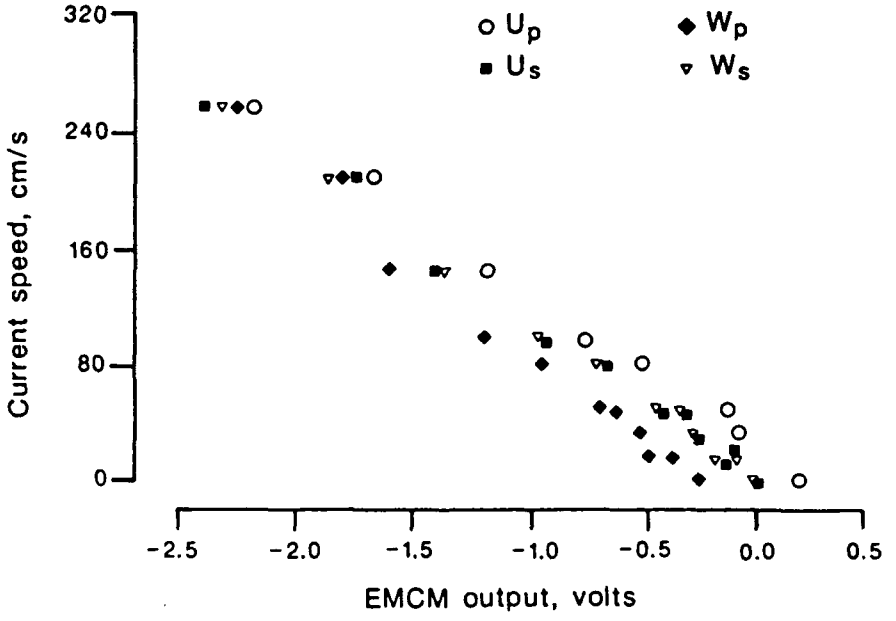
320
240
160
80
0
Current speed, cm/s
o Up
■ Us
◆ Wp
▿ Ws
-2.5
-2.0
-1.5
-1.0
-0.5
0.0
0.5
EMCM output, volts

Figure 22.

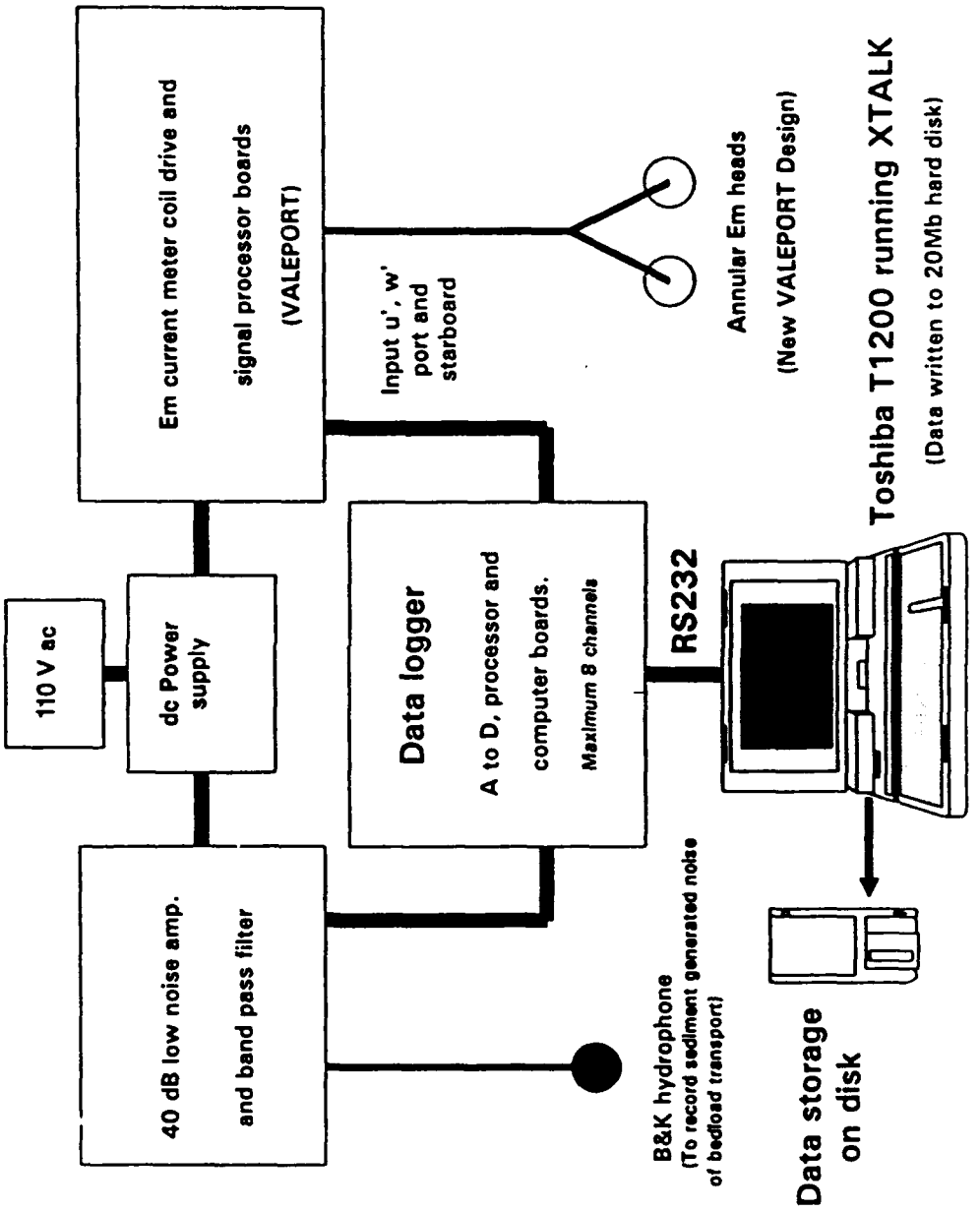
Em current meter coil drive and
signal processor boards
(VALEPORT)
Input u', w'
port and
starboard
Annular Em heads
(New VALEPORT Design)
Toshiba T1200 running XTALK
(Data written to 20Mb hard disk)
110 V ac
dc Power
supply
Data logger
A to D, processor and
computer boards.
Maximum 8 channels
RS232
40 dB low noise amp.
and band pass filter
B&K hydrophone
(To record sediment generated noise
of bedload transport)
Data storage
on disk

Figure 23.

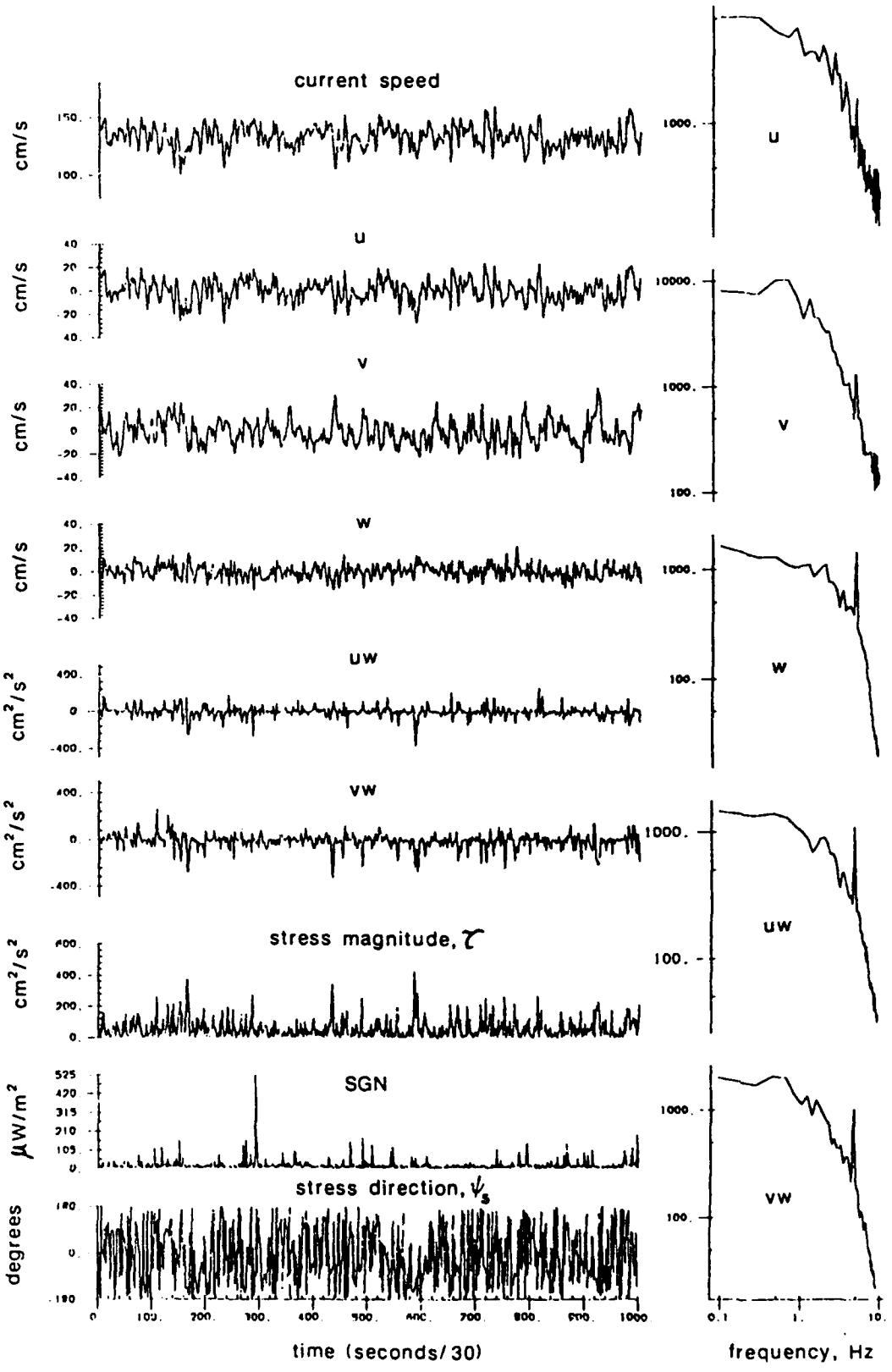
current speed
cm/s
150.
100.
u
cm/s
40.
20.
0.
-20.
-40.
v
cm/s
40.
20.
0.
-20.
-40.
w
cm/s
40.
20.
0.
-20.
-40.
uw
cm²/s²
400.
0.
-400.
vw
cm²/s²
400.
0.
-400.
stress magnitude, τ
cm²/s²
600.
400.
200.
0.
SGN
μW/m²
525
420
315
210
105
0.
stress direction, ψs
degrees
180
0.
-180
0
100.
200.
300.
400.
500.
600.
700.
800.
900.
1000
time (seconds/30)
u
1000.
v
10000.
1000.
100.
w
1000.
100.
uw
1000.
100.
vw
1000.
100.
0.1
1.
10.
frequency, Hz

Figure 24.

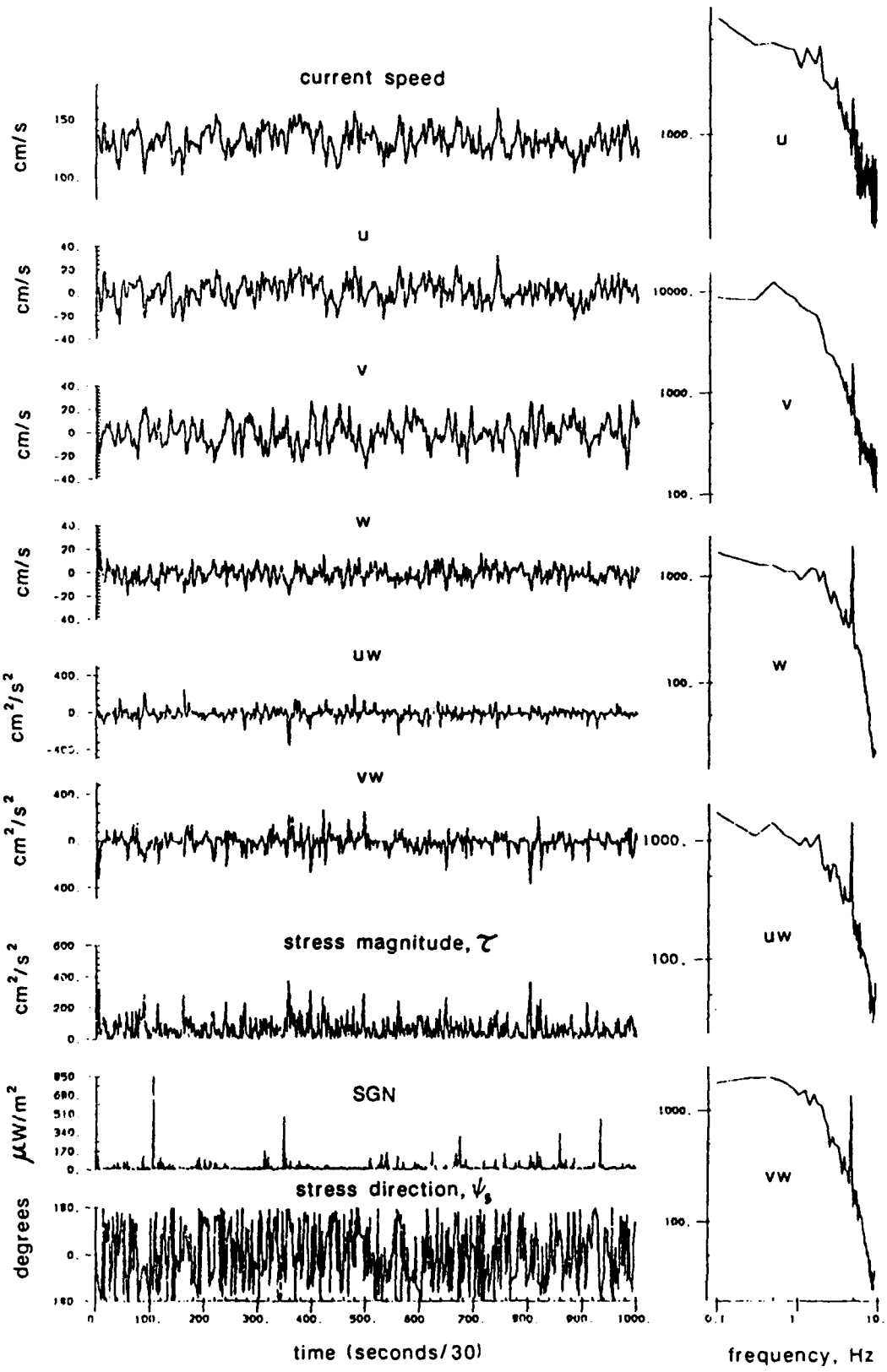
current speed
cm/s
150
100.
u
cm/s
40.
20
0.
-20
-40.
v
cm/s
40.
20.
0.
-20
-40.
w
cm/s
40.
20
0.
-20
40.
uw
cm²/s²
400.
0.
vw
cm²/s²
400.
0.
400.
stress magnitude, τ
cm²/s²
600
400.
200
0.
SGN
μW/m²
850
680.
510
340.
170.
0.
stress direction, ψs
degrees
180.
0.
180
0
100.
200
300.
400.
500.
600
700.
800
900.
1000.
time (seconds/30)
u
1000.
v
10000.
1000.
100.
w
1000.
100.
uw
1000.
100.
vw
1000.
100.
0.1
1
10.
frequency, Hz

Figure 25.

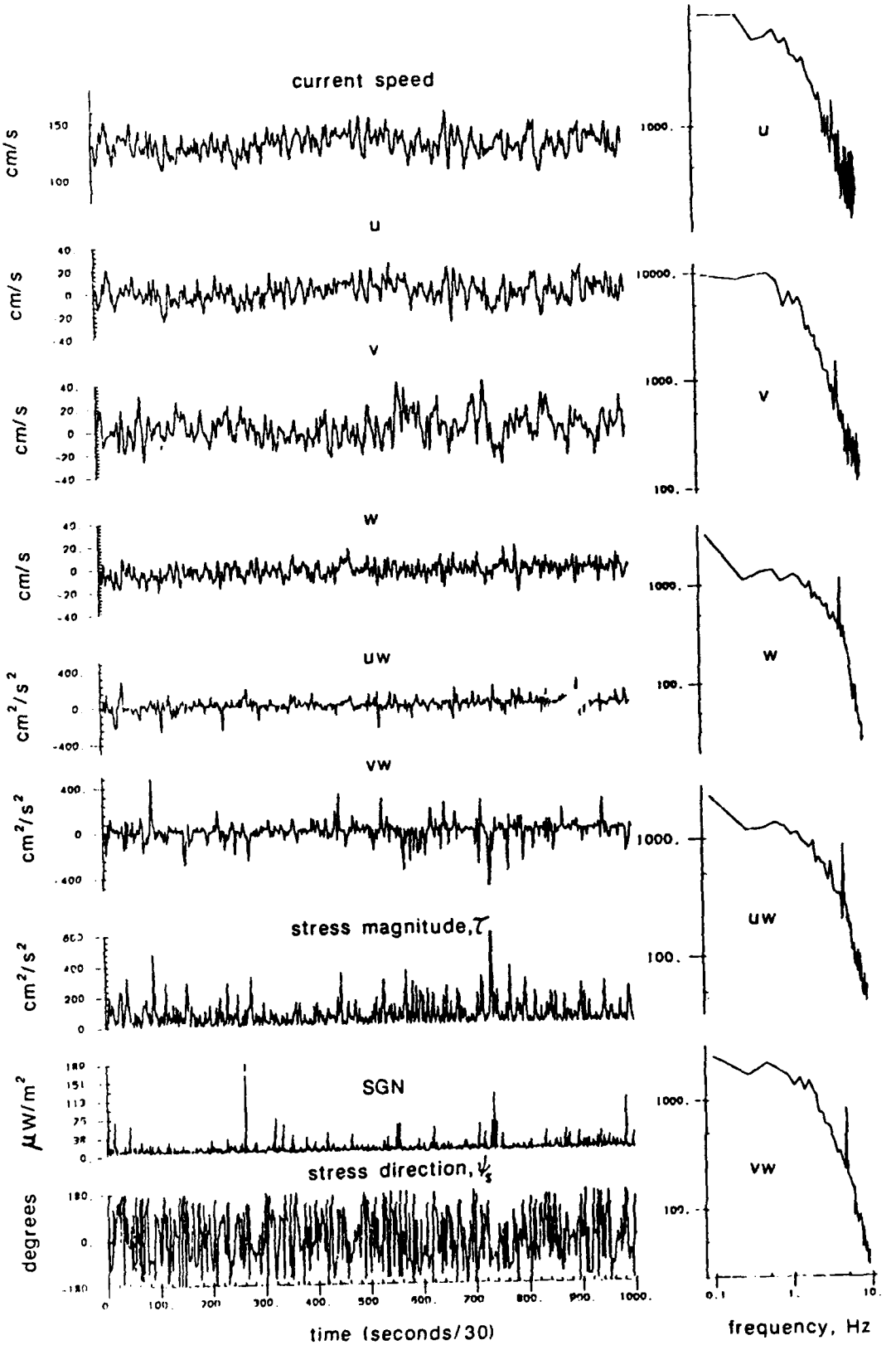
current speed
cm/s
u
v
w
uw
vw
stress magnitude, τ
SGN
stress direction, ψs
degrees
time (seconds/30)
frequency, Hz

Figure 26.

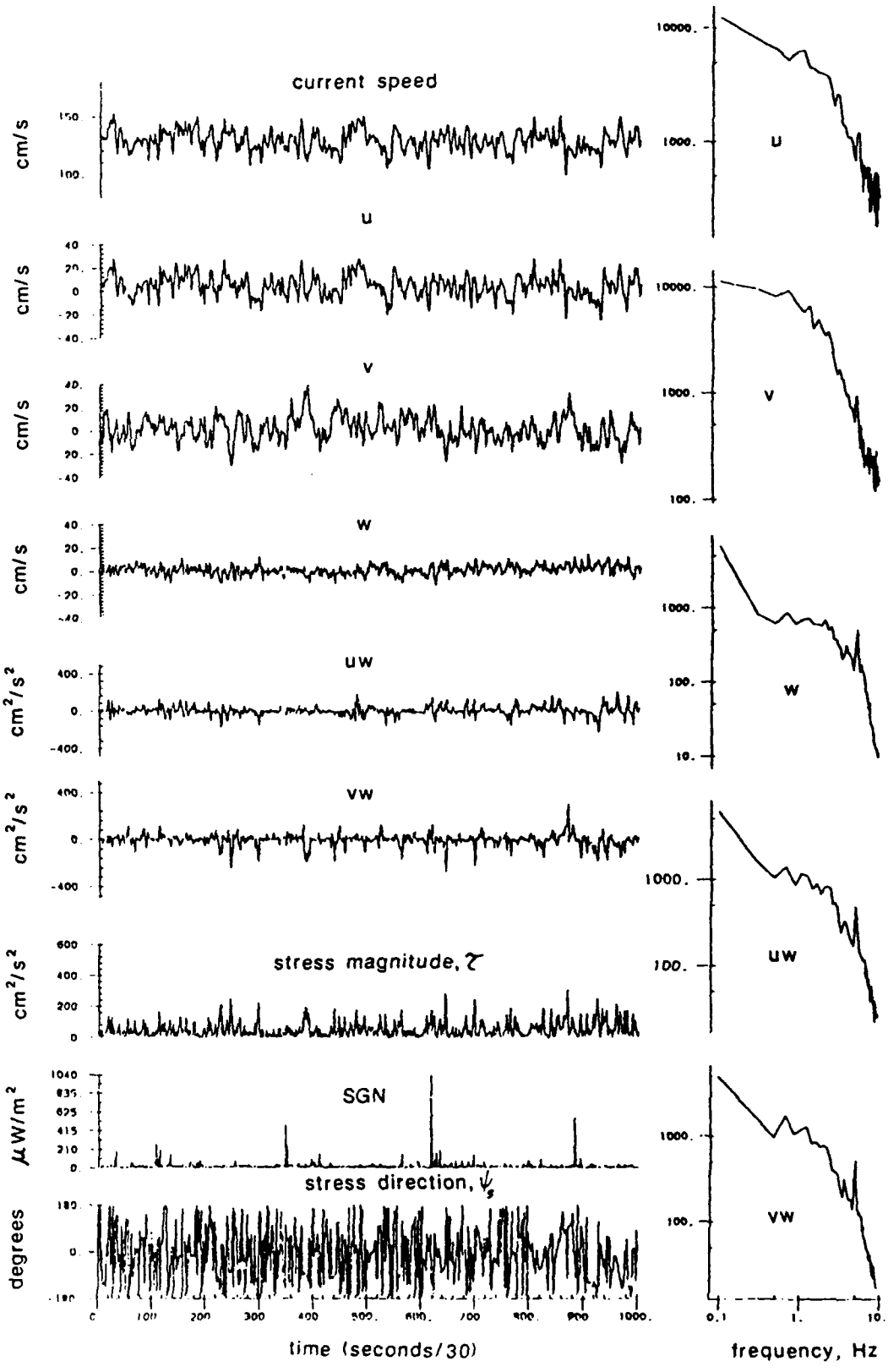
current speed
cm/s
u
v
w
uw
vw
stress magnitude, τ
cm²/s²
SGN
μW/m²
stress direction, ψs
degrees
time (seconds/30)
frequency, Hz

Figure 27.

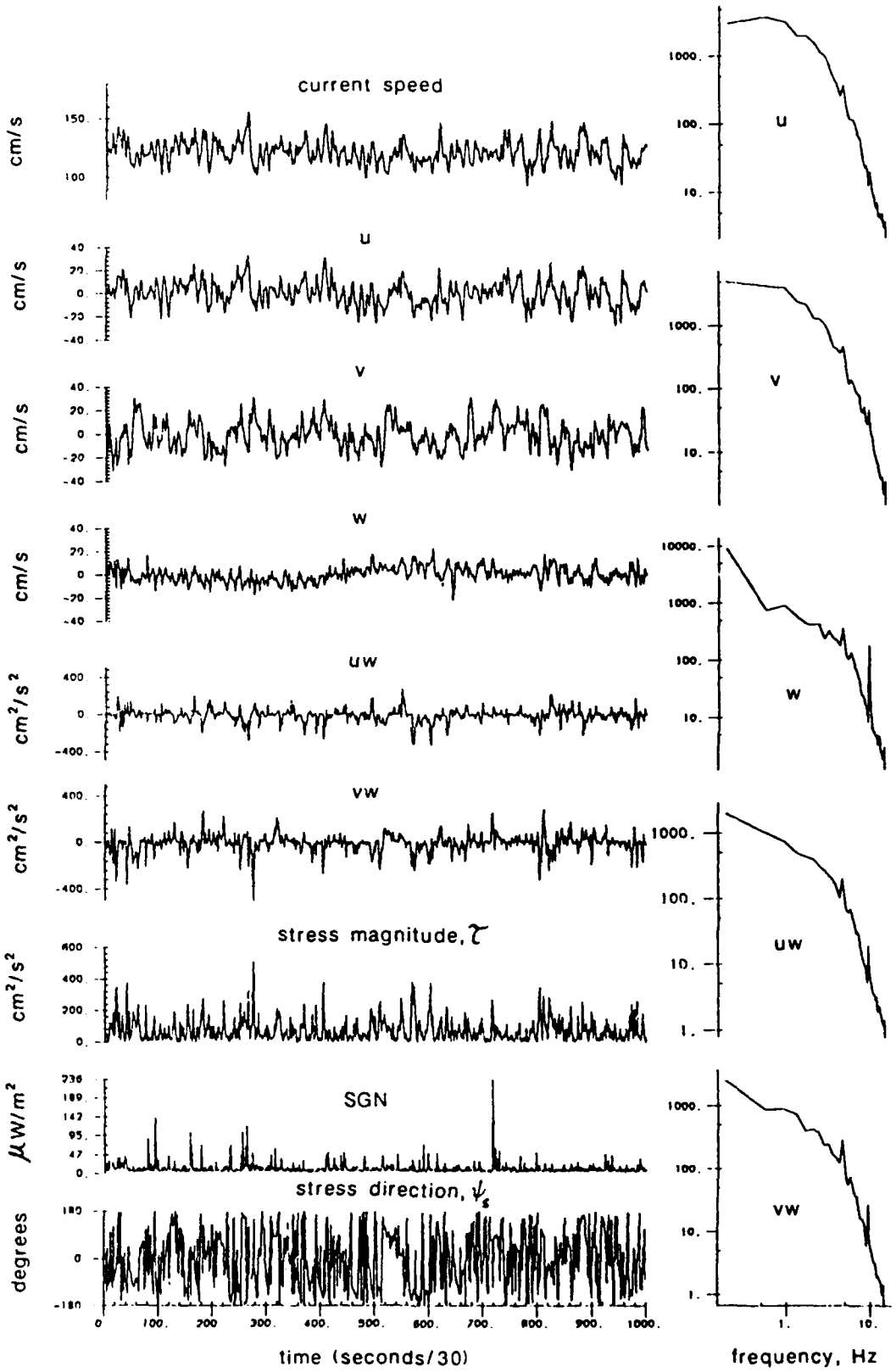
current speed
cm/s
u
v
w
uw
vw
stress magnitude, τ
cm²/s²
SGN
μW/m²
stress direction, ψs
degrees
time (seconds/30)
frequency, Hz

Figure 28.

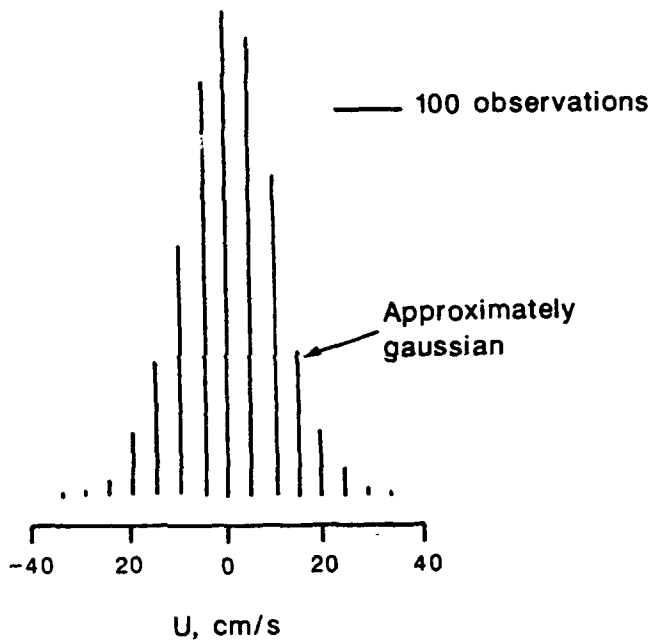

Figure 29.

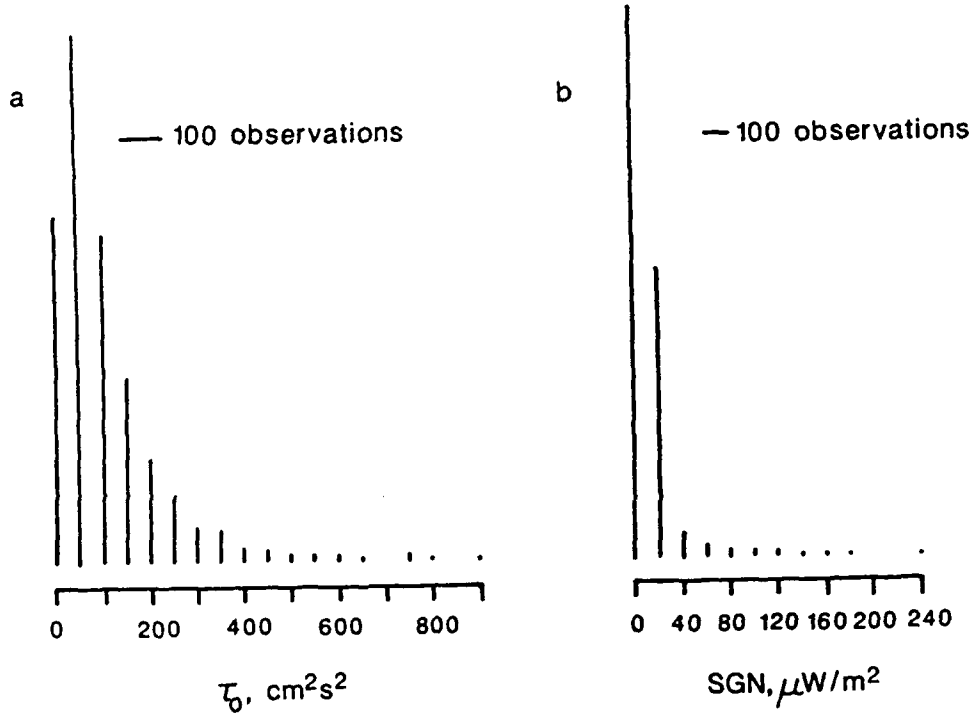
a
— 100 observations
0
200
400
600
800
τ_0, cm^{2}s^2
b
— 100 observations
0 40 80 120 160 200 240
SGN, μW/m^2

Figure 30.

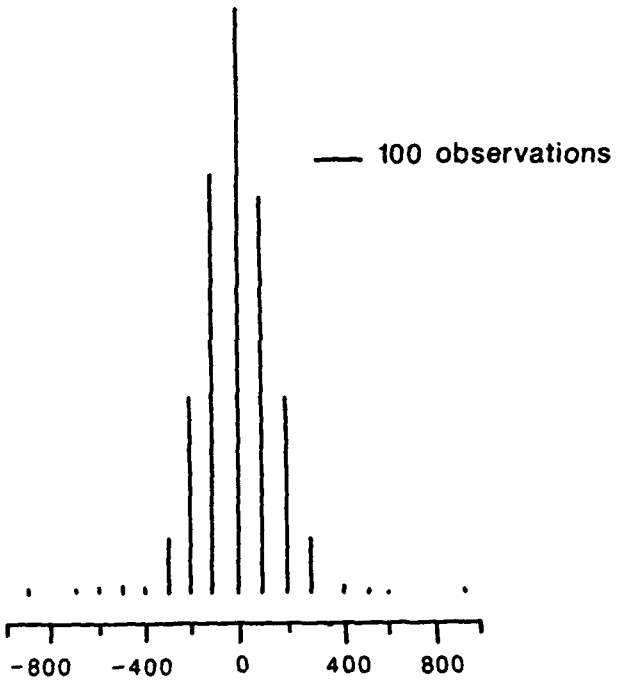

Instantaneous acceleration for U, cm/s^2

Figure 31.

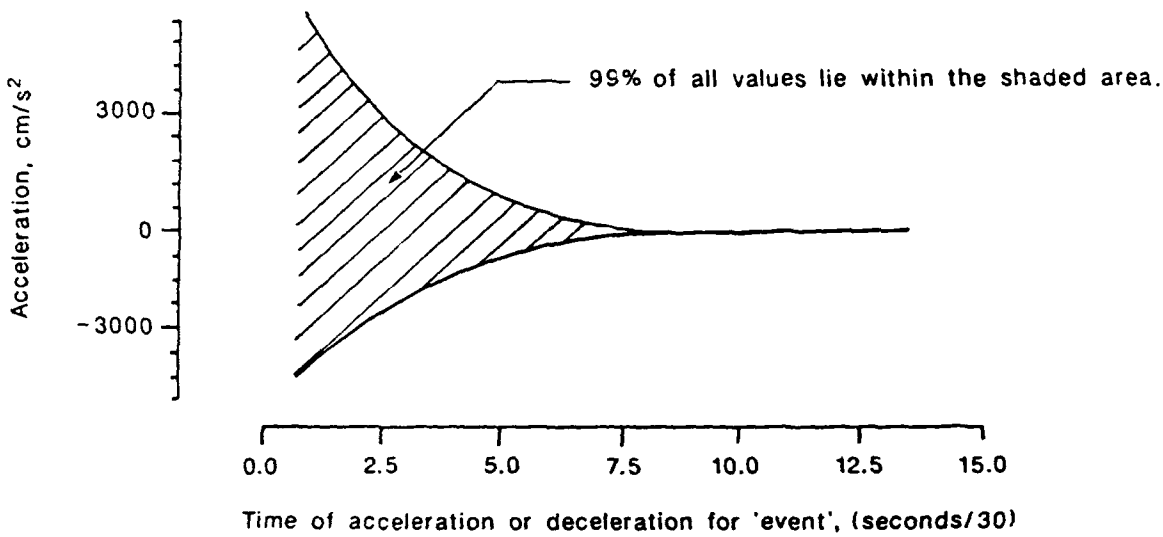
99% of all values lie within the shaded area.
Acceleration, cm/s²
3000
0
-3000
0.0
2.5
5.0
7.5
10.0
12.5
15.0
Time of acceleration or deceleration for 'event', (seconds/30)

Figure 32.

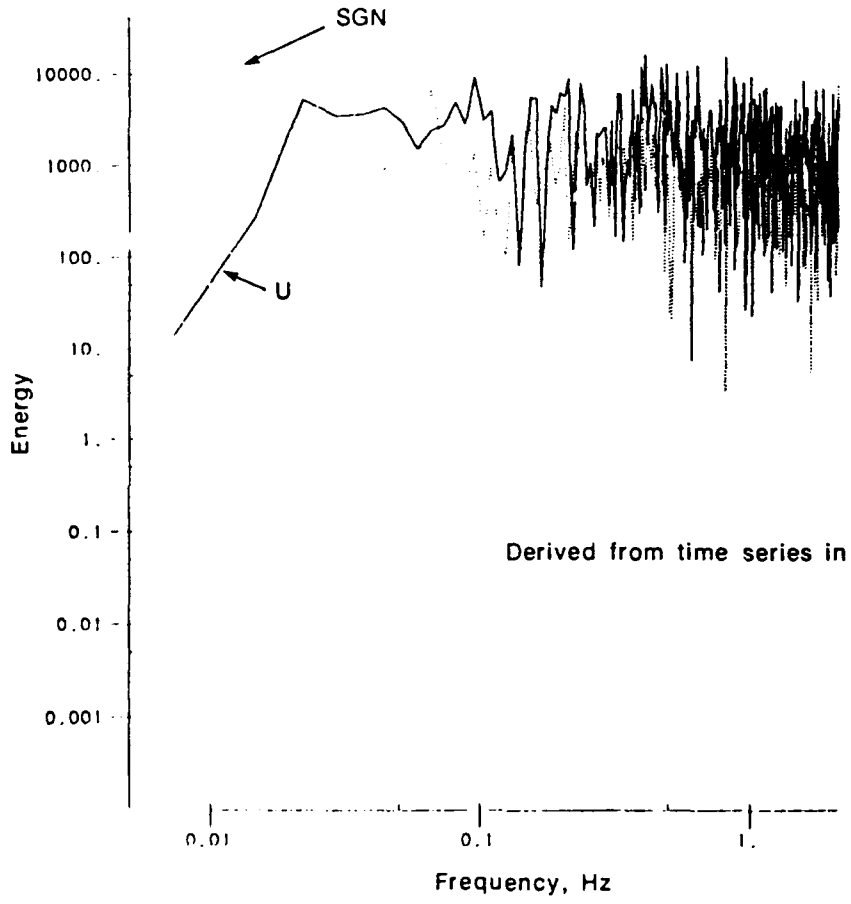

Derived from time series in figure 27

Figure 33.

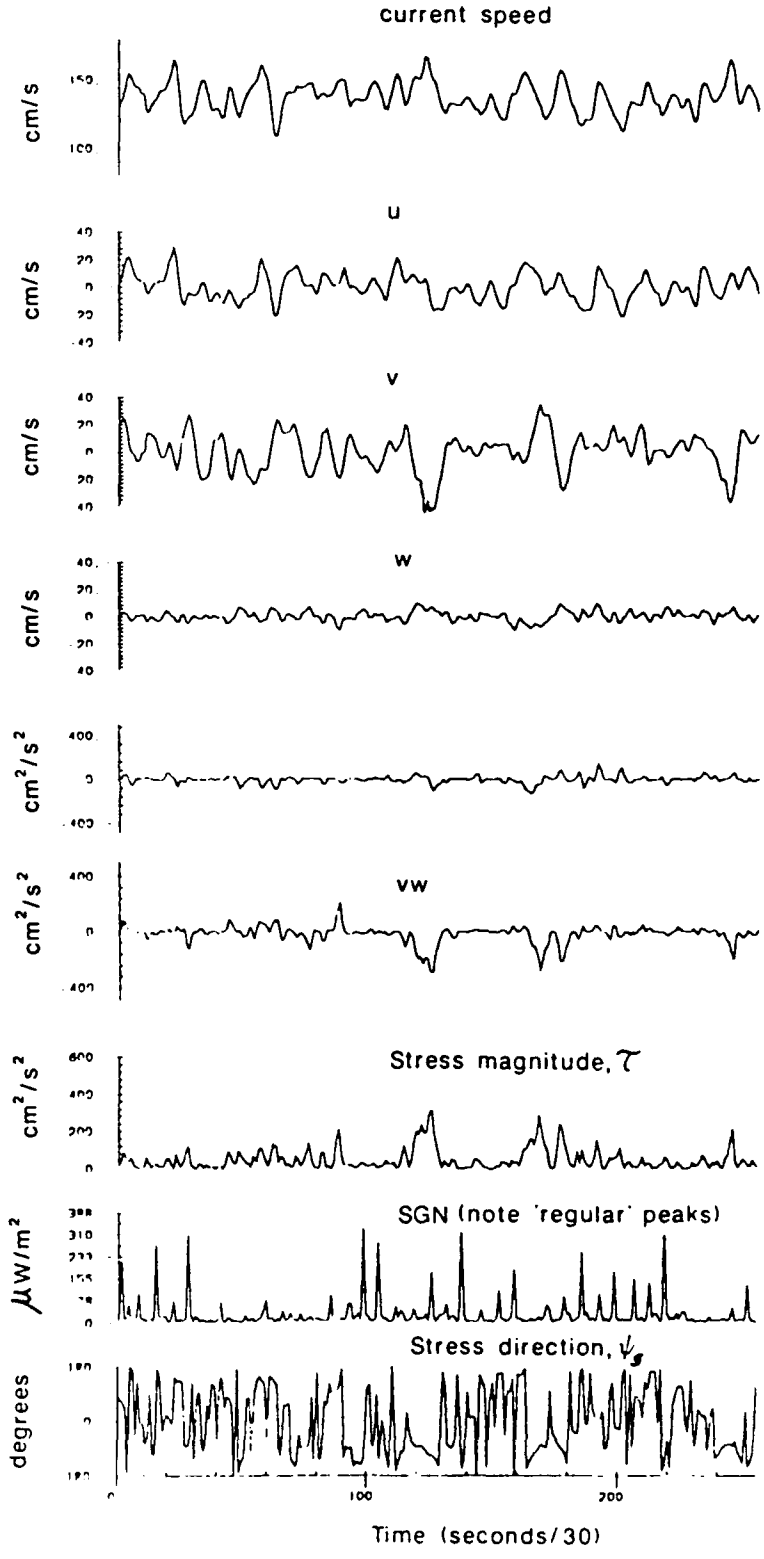
current speed
cm/s
u
cm/s
v
cm/s
w
cm/s
cm²/s²
vw
cm²/s²
Stress magnitude, τ
cm²/s²
SGN (note 'regular' peaks)
μW/m²
Stress direction, ψs
degrees
100
200
Time (seconds/30)

Figure 34.

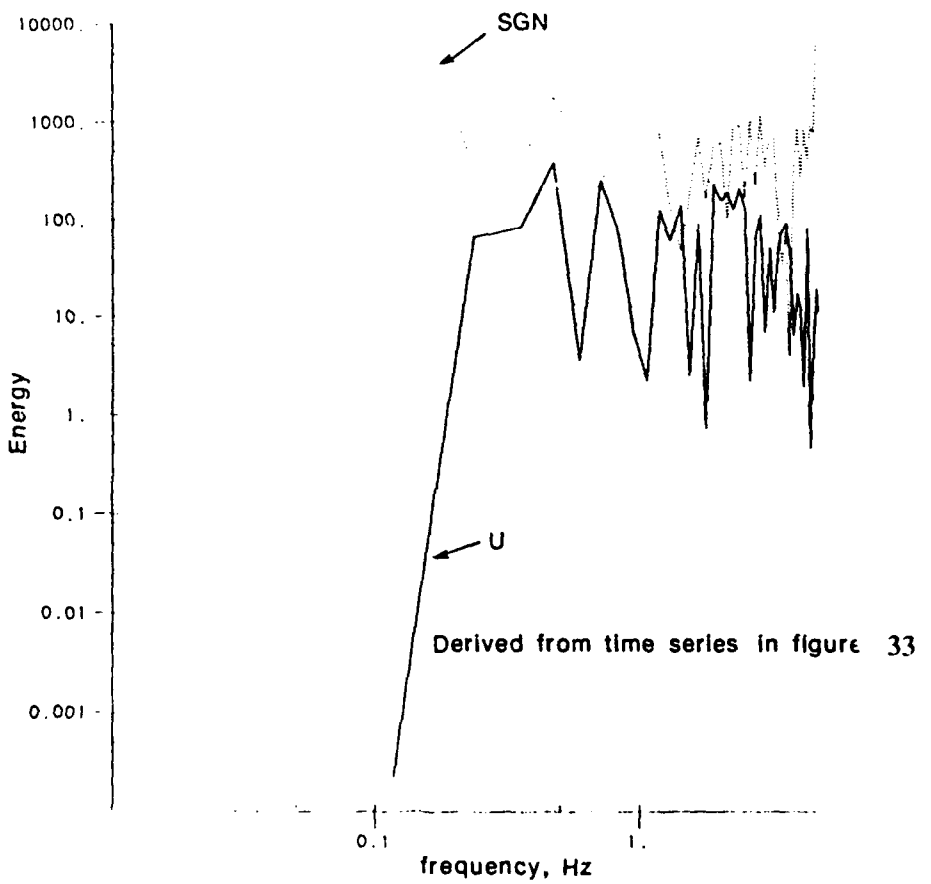
SGN
U
Derived from time series in figure 33
10000.
1000.
100.
10.
1.
0.1
0.01
0.001
Energy
0.1
1.
frequency, Hz

Figure 35.

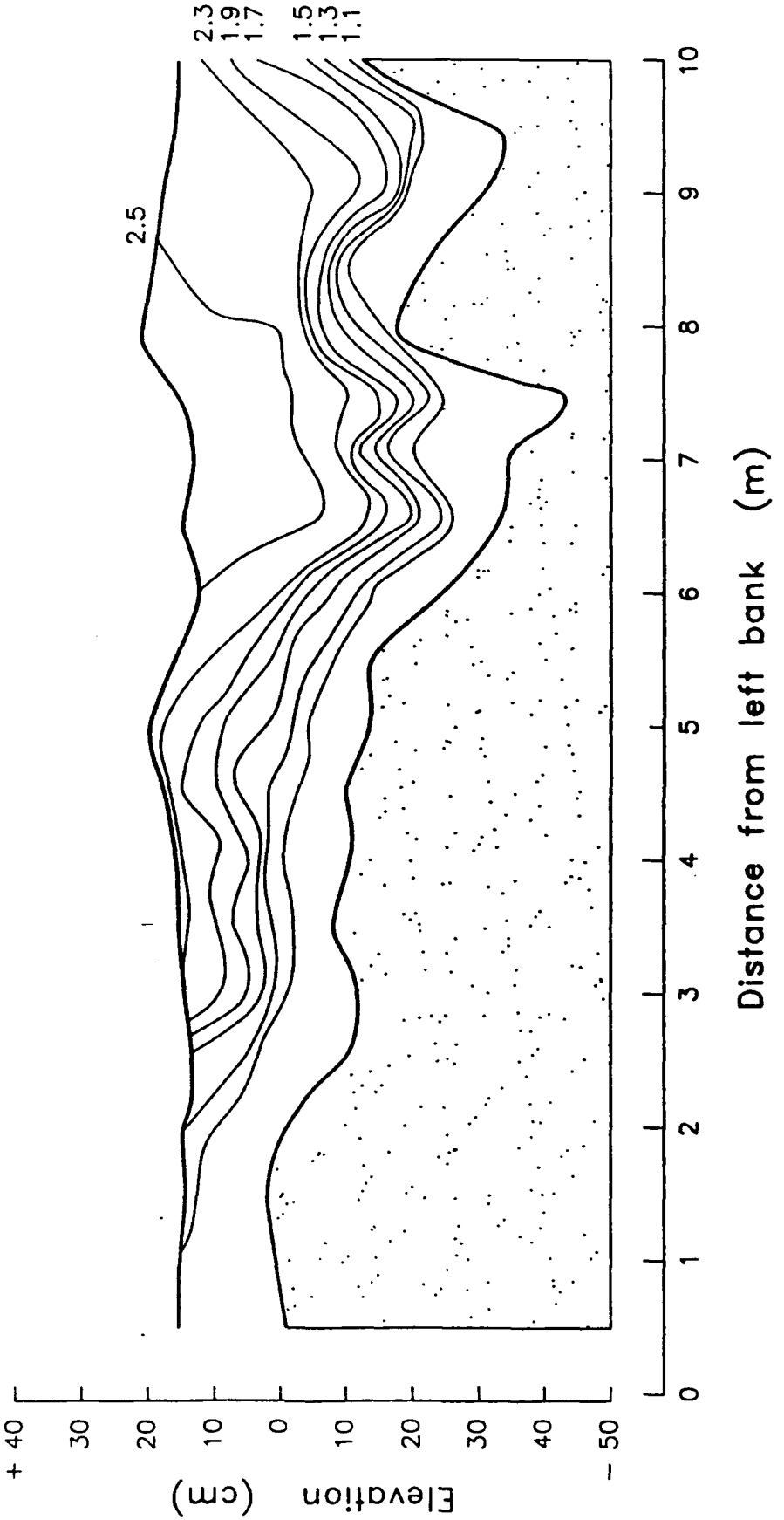
2.3
1.9
1.7
1.5
1.3
1.1
2.5
+ 40
30
20
10
0
10
20
30
40
- 50
Elevation (cm)
0
1
2
3
4
5
6
7
8
9
10
Distance from left bank (m)

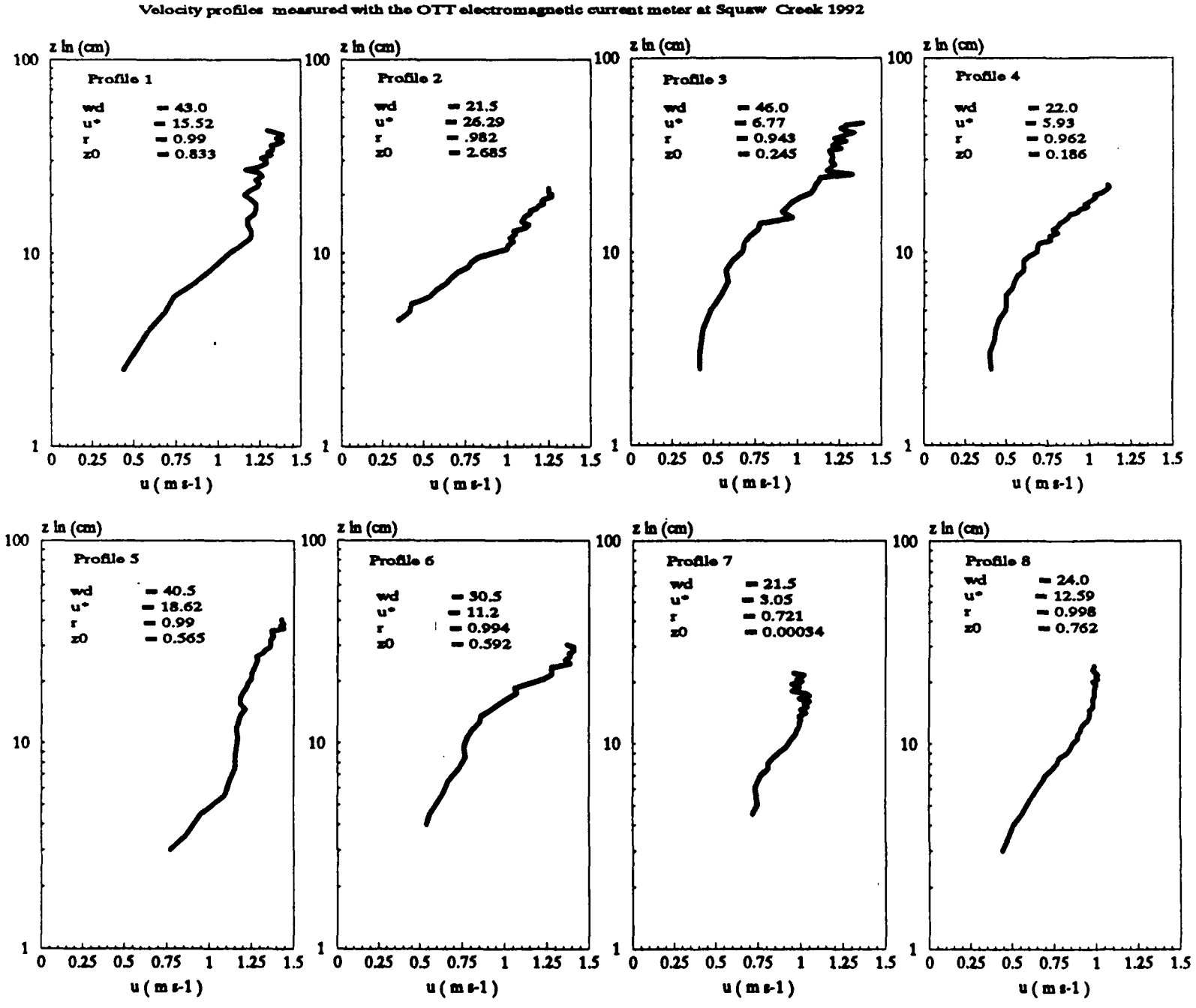
Velocity profiles measured with the OTT electromagnetic current meter at Squaw Creek 1992
z in (cm)
Profile 1
wd = 43.0
u* = 15.52
r = 0.99
z0 = 0.833
Profile 2
wd = 21.5
u* = 26.29
r = .982
z0 = 2.685
Profile 3
wd = 46.0
u* = 6.77
r = 0.943
z0 = 0.245
Profile 4
wd = 22.0
u* = 5.93
r = 0.962
z0 = 0.186
Profile 5
wd = 40.5
u* = 18.62
r = 0.99
z0 = 0.565
Profile 6
wd = 30.5
u* = 11.2
r = 0.994
z0 = 0.592
Profile 7
wd = 21.5
u* = 3.05
r = 0.721
z0 = 0.00034
Profile 8
wd = 24.0
u* = 12.59
r = 0.998
z0 = 0.762
100
10
1
0 0.25 0.5 0.75 1 1.25 1.5
u (m s-1)

Figure 36.

Squaw Creek 1991 event 23rd/24th May

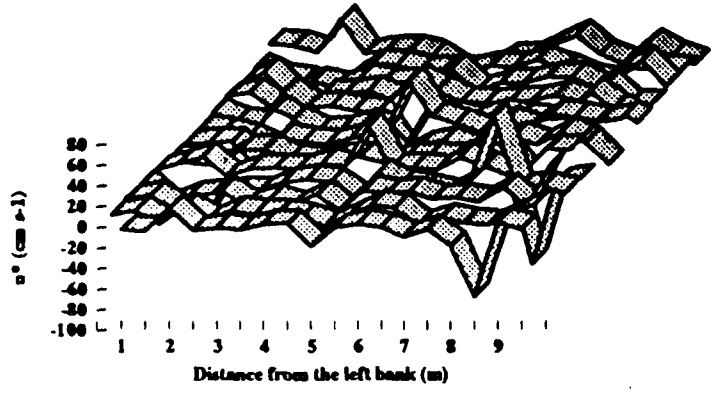

Variance of u* from mean during event

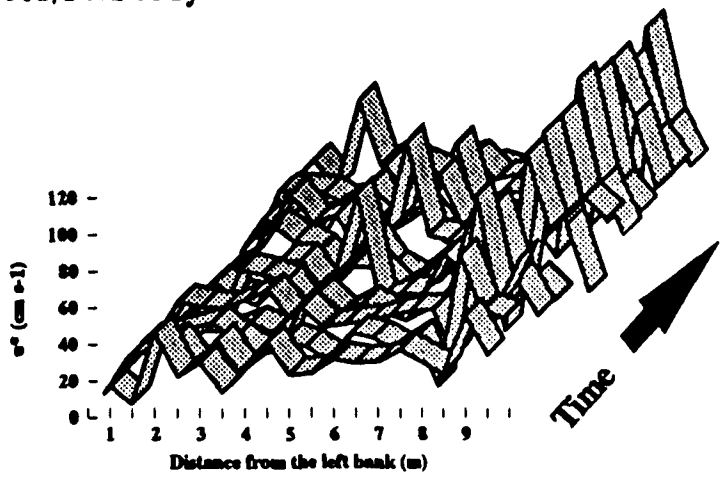

Shear velocity (u*) during event

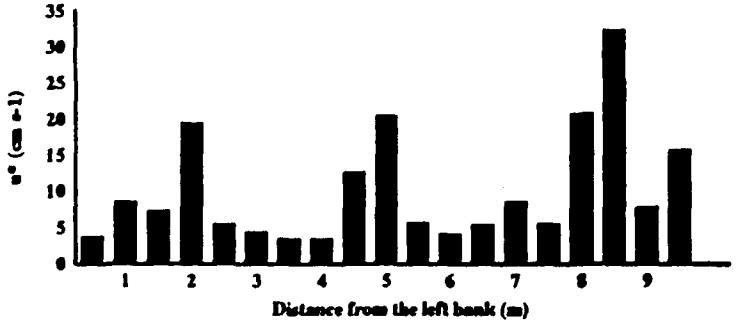

Standard deviation of u* across channel during event

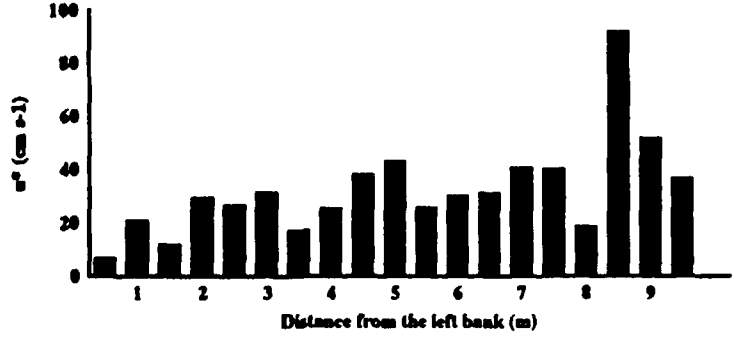

Mean u* at 0.5 m intervals during event

Figure 37.

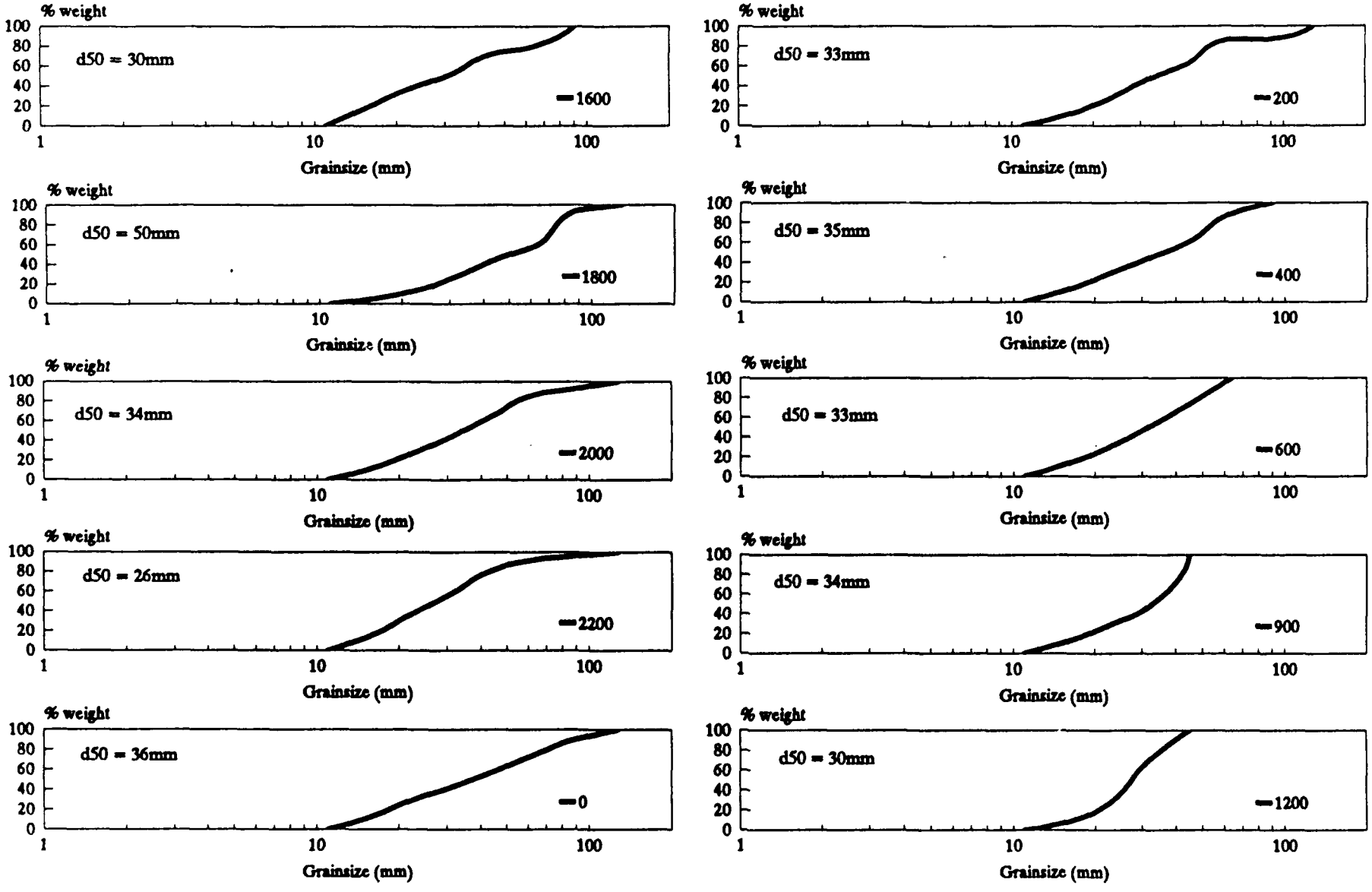
% weight
d50 = 30mm
1600
Grainsize (mm)
% weight
d50 = 33mm
200
Grainsize (mm)
% weight
d50 = 50mm
1800
Grainsize (mm)
% weight
d50 = 35mm
400
Grainsize (mm)
% weight
d50 = 34mm
2000
Grainsize (mm)
% weight
d50 = 33mm
600
Grainsize (mm)
% weight
d50 = 26mm
2200
Grainsize (mm)
% weight
d50 = 34mm
900
Grainsize (mm)
% weight
d50 = 36mm
0
Grainsize (mm)
% weight
d50 = 30mm
1200
Grainsize (mm)

Figure 38.

Figure 39.

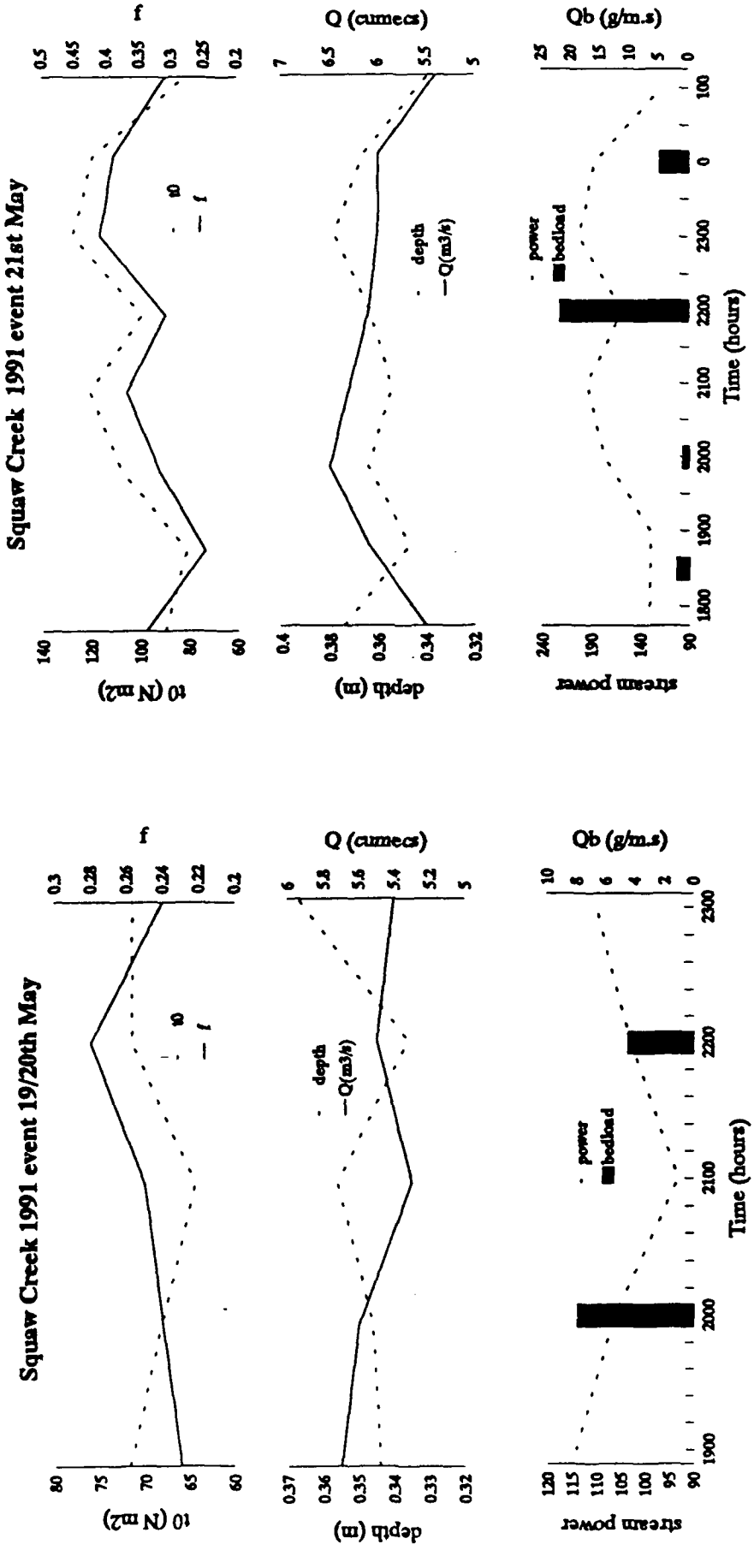
Squaw Creek 1991 event 21st May
Squaw Creek 1991 event 19/20th May
f
Q (cumecs)
Qb (g/m.s)
10 (N m2)
depth (m)
stream power
Time (hours)
power
bedload
depth
Q(m3/s)

Figure 40.

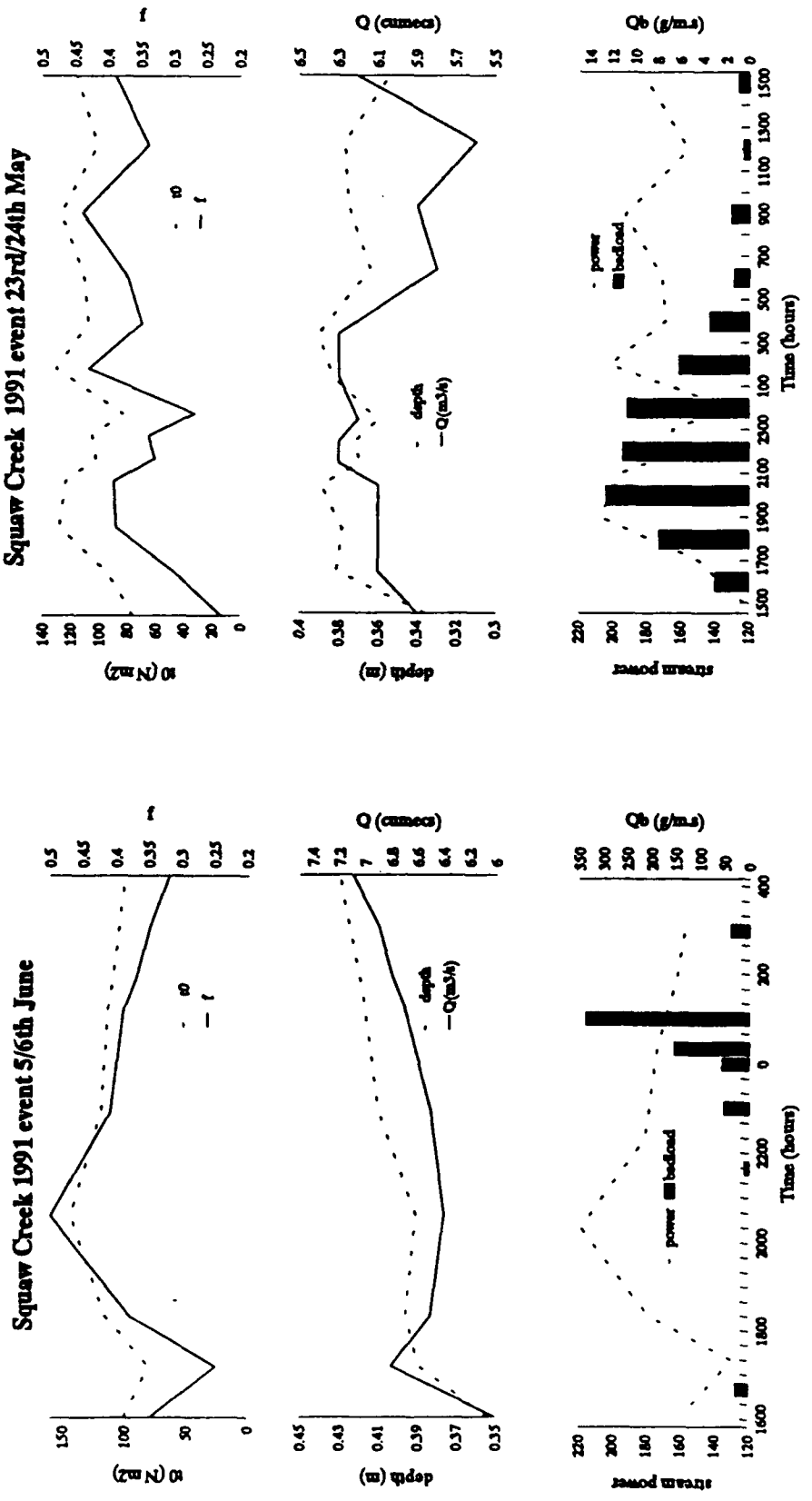
Squaw Creek 1991 event 23rd/24th May
Squaw Creek 1991 event 5/6th June
f
Q (cumecs)
Qb (g/m.s)
t0
f
depth
Q(m3/s)
power
bedload
t0 (N m2)
depth (m)
stream power
Time (hours)

Figure 41.

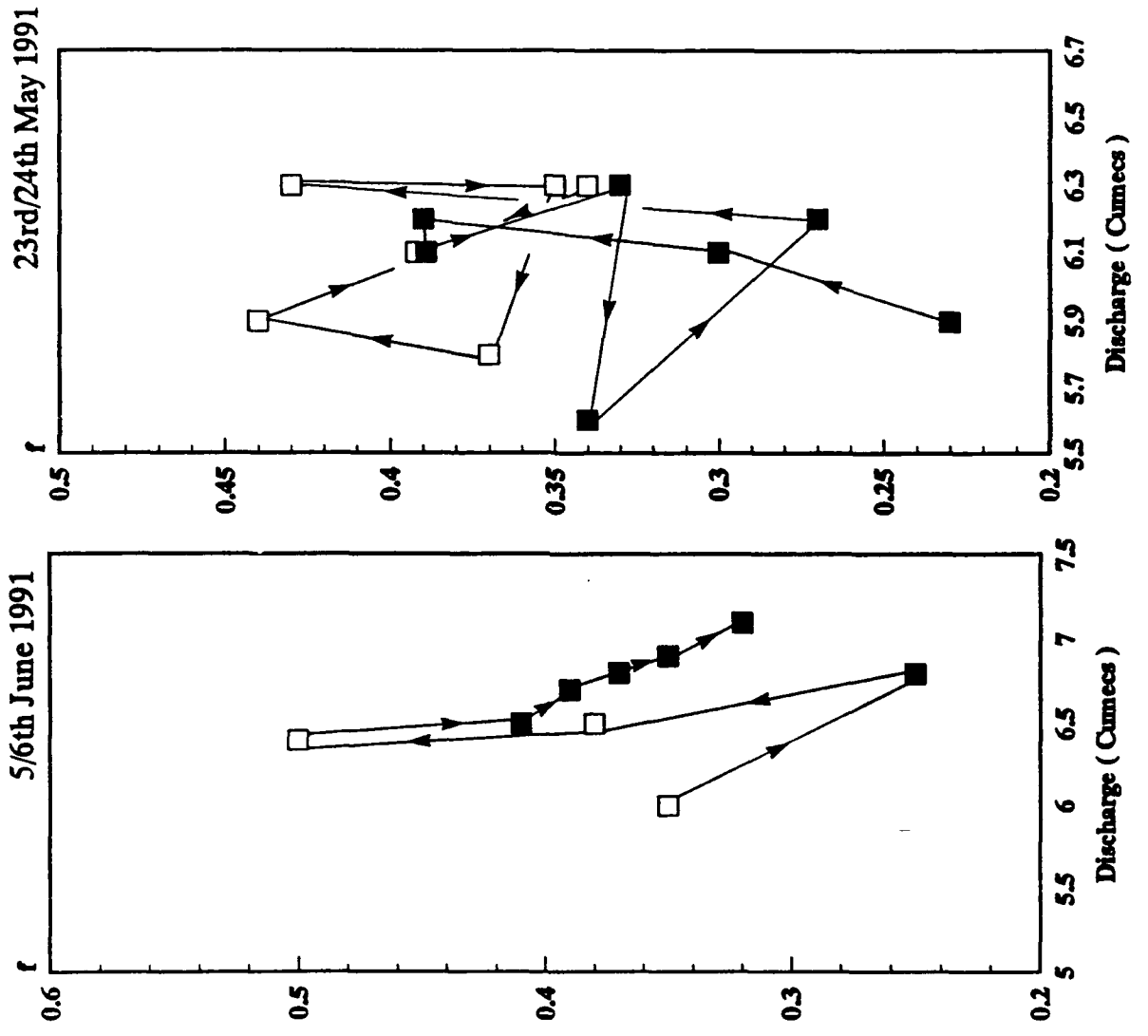
23rd/24th May 1991
f
0.5
0.45
0.4
0.35
0.3
0.25
0.2
5.5
5.7
5.9
6.1
6.3
6.5
6.7
Discharge (Cumecs)
5/6th June 1991
f
0.6
0.5
0.4
0.3
0.2
5
5.5
6
6.5
7
7.5
Discharge (Cumecs)

Figure 42.

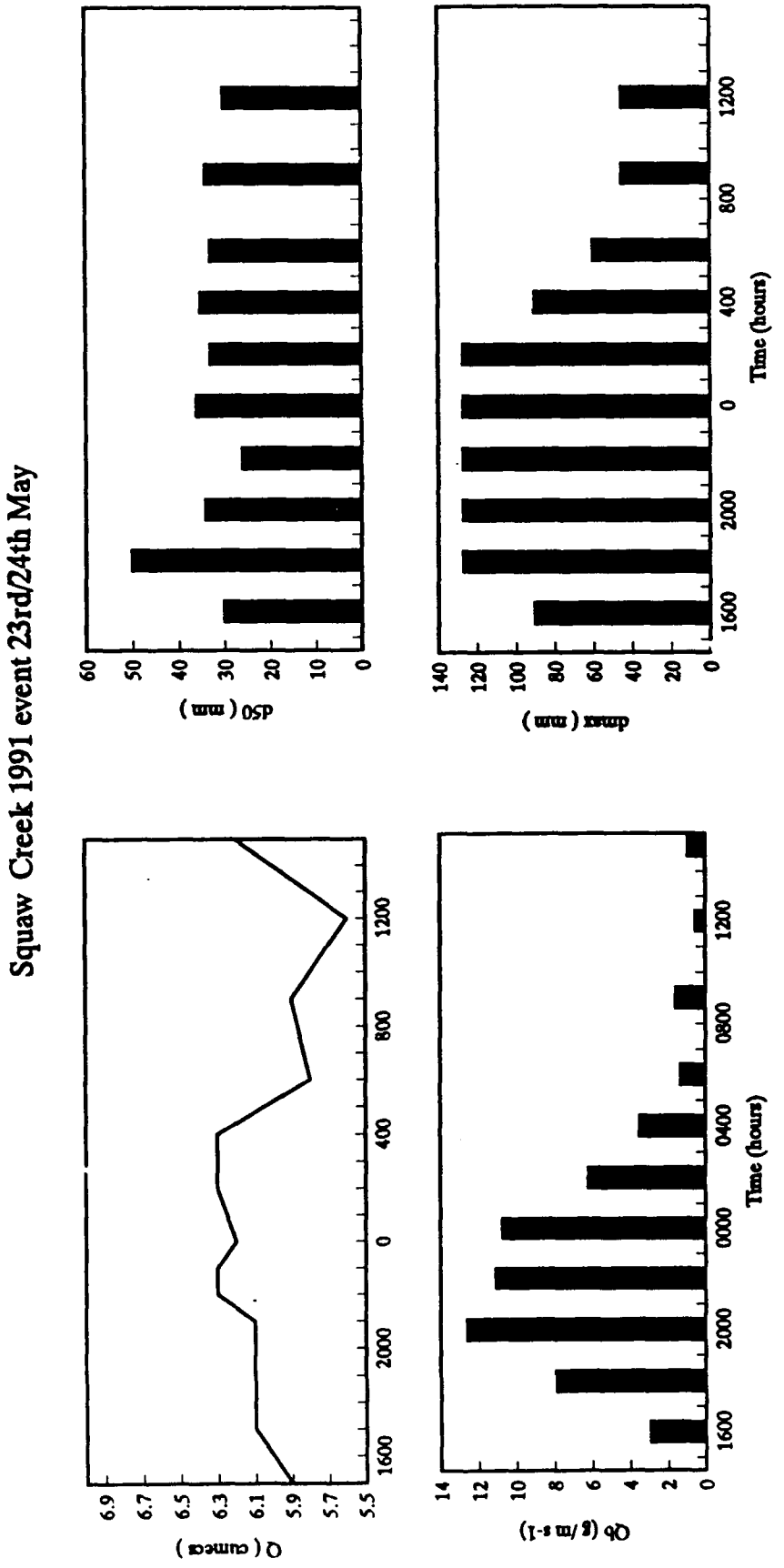
Squaw Creek 1991 event 23rd/24th May
Q (cumecs)
6.9
6.7
6.5
6.3
6.1
5.9
5.7
5.5
1600
2000
0
400
800
1200
Qb (g/m s-1)
14
12
10
8
6
4
2
0
1600
2000
0000
0400
0800
1200
Time (hours)
d50 (mm)
60
50
40
30
20
10
0
dmax (mm)
140
120
100
80
60
40
20
0
1600
2000
0
400
800
1200
Time (hours)

Figure 43.

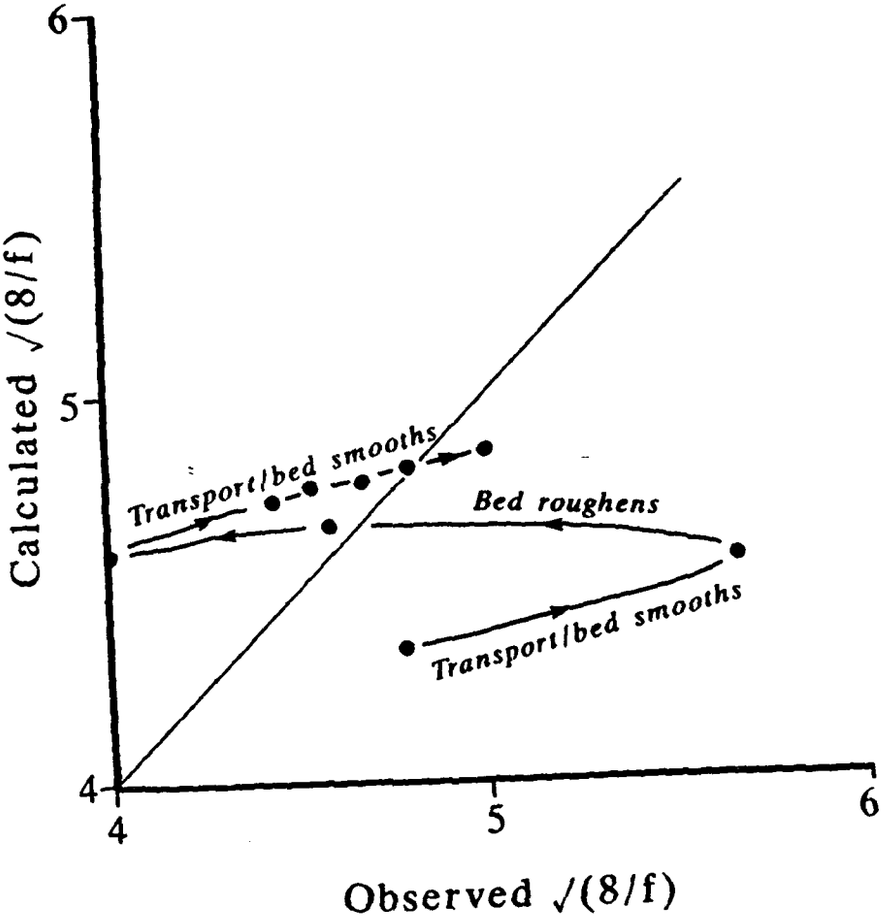
6
5
4
4
5
6
Calculated √(8/f)
Observed √(8/f)
Transport/bed smooths
Bed roughens
Transport/bed smooths